Design and Modeling of a Micro Vibration-Based Power Generator

CHAN Ming-Ho Gordon

A Thesis Submitted in Partial Fulfilment of the Requirements for the Degree of

Master of Philosophy

in

Mechanical and Automation Engineering

June 2000

ABSTRACT

This paper presents the design, analysis and experimental results of a vibration-induced power generator with total volume less than one cm^3. The power generated by the micro generator is studied as a function of generator dimensions and other governing parameters. Analytical equations are developed and experiment results on the fabricated generator structure are compared with those obtained with three-dimensional Finite Element Analysis (FEA). Resonating structure formed by a rare earth permanent magnet and laser micromachined copper springs vibrating at 90Hz is recorded to generate 3V AC (peak-to-peak) with less than 200μm input vibration amplitude. The ultimate goal of this project is to develop a micro sized electric power generator which is capable of producing enough voltage to drive a low-power IC circuit systems or micro sensors for robotics and automation applications.

Abstract of thesis entitled "Design and Modeling of a Micro Vibration-Based Power Generator" submitted by Chan Ming-Ho Gordon for the degree of Master of Philosophy at The Chinese University of Hong Kong in June 2000.

摘 要

這篇文章展示了一台以機械震動作爲能源的微型發電組件，該發電機的體積少於一立方厘米。影響發電機的變數，均被作出分析，從而增加和改善發電機的效能。本文展示了發電機系統的分析方程式和實驗結果，並使用三維有限原素分析法（Finite Element Analysis － FEA）改善發電機的設計。透過實驗結果和電腦模擬結果的比較，初步的發電機原型已經被研製出來。發電機原型的震動組件包含一顆強力永久磁石和激光切割出來的銅質彈簧。在少於二百微米震幅輸入（90Hz）的情況下，該發電機仍然能夠產生 3V（p-p）的交流電壓。這項研究的最終目標，在於成功研製出一台能夠產生足夠電壓以推動低能量 IC 電路系統的微型發電組件。該發電機最終可以爲機械人或自動化領域用作推動微型傳感器之用。

Abstract of thesis entitled “Design and Modeling of a Micro Vibration-Based Power Generator” submitted by Chan Ming-Ho Gordon for the degree of Master of Philosophy at The Chinese University of Hong Kong in June 2000.

ACKNOWLEDGEMENT

First of all, I would like to thank express my acknowledge to my supervisor, Prof. Wen J. Li for teaching me and introducing me to the field of micro devices. I am profoundly grateful to him especially for his patience and kindness in the past three years. Secondly, I would like to give my deepest gratitude to my partners, Neil Ngai and Terry Ho. This research would not be a success without their continuous efforts. Thirdly, I would like to thank my dear fellows, Pak Wong and Samuel Tsang. Their contributions in experimental and theoretical studies did serve as a guideline to me during my research. Finally, I would like to thank all my AML fellows, Antony, Michael, Fong Fong, Winston and Julia, whom I have enjoyed so many pleasurable moments with for long.

TABLE OF CONTENTS

LIST OF TABLES

LIST OF FIGURES

LIST OF SYMBOLS

F	Generator input force
y	Generator input displacement
z	Mass displacement relative to coil
V	Voltage output at load resistor
f_e	Feedback electromechanical force
m	Mass of magnet
d	Mechanical damping coefficient
k	Spring constant of springs
B	Magnetic field strength of magnet
l	Length of wire coil
R	Load resistance
L	Coil inductance
R_c	Coil resistance
Y_0	Generator input displacement amplitude
P	Average power output
ω	Input vibration frequency
ω_n	Natural frequency of the resonator structure
ζ_m	Mechanical damping ratio
ζ_e	Electrical damping ratio
ζ	Total damping ratio of the system
V_0	Peak voltage output
P_{input}	Power input
l_s	Length of spring
t_s	Thickness of spring
w_s	Width of spring
σ_{max}	Maximum tensile stress
τ_{max}	Maximum shear stress
E	Young's modulus
I	Moment of inertia
z_0	Maximum mass deflection relative to coil
F_0	Generator input force amplitude
$F_{magnetic}$	Electromagnetic force generated in a solenoid coil
S_m	Surface area of cross section of the solenoid
μ_0	Free space permeability (4πE-7 H/m)
N	Number of turns of conductor in a solenoid

A	Cross section area of solenoid

CHAPTER 1 INTRODUCTION

1.1 BACKGROUND ON MICRO POWER SUPPLY

1.1.1 Brief Introduction

There has been much work done towards realising practical micro sensor systems with reasonable cost and high performance using different operating principles for a variety of applications such as medical, automotive, manufacturing, household applications. These efforts have been focused mainly on distributed systems with their own integrated power supply due to the complexity of interconnection, reduction of electronic noise and control system complexity. However, while shelf life or replacement accessibility is limiting factor, replaceable chemical battery and rechargeable power supply may not be the optimal choice.

Williams *et al.* proposed the idea of vibration based micro electric generator and performed a series of theoretical and feasibility studies in 1996 [1] [2]. Shearwood and Yates reported a root-mean-square (RMS) power output of 0.3μW at a resonant frequency of 4.4kHz from a 3mm×3mm miniature generator fabricated in 1997 [3]. In 1998, Amirtharajah and Chandrakasan reported the success of operating a digital system, which contained an ultra-low power controller and a low power subband filter DSP load circuit, from power generated by a vibration based generator in *macro* scale [4] [5].

With the use of microelectromechanical systems (MEMS) technology, we propose to

build a mechanically based integrated miniature power generator, which transforms the kinetic vibration energy from the immediate environment to electrical energy usable by a low power CMOS circuit system or MEMS sensor system. The successful development of an efficient integrated mechanical power supply will potentially benefit numbers of applications such as vibration monitoring of manufacturing equipment, implanted medical devices, mobile communication systems, free moving micro robotic systems and space based MEMS components.

In this work, an analysis of the factors governing the behaviour and performance of a micro vibration based power generator is presented. Finite Element Analysis (FEA) is carried out to simulate the response of individual designs during development because it offers an informational but efficient testing of the real system. Information such as resonant frequency and spring constant of individual design cannot be easily obtained without comprehensive experiments. However, preparations of prototypes including CAD modeling, fabrication and setup for experiments usually takes significant time and resources. With the use of the Finite Element Analysis, the design period may be shorten by the fact that individual designs can be tested and modified with computer simulation before actual fabrication. Moreover, for design with complex structure, Finite Element Analysis is able to provide information, such as numerical stress distribution, which can hardly be obtained by experiments. The simulation results from Finite Element Analysis are compared with those obtained from laboratory experiments and the final design is expected to be improved by means of repeated simulations and testing. Figure1 indicates a flow diagram of the design process of the micro generator. A fully integrated alternative to traditional micro power sources, which life span, energy capacity and replacement are of concern, is expected in the visible future.

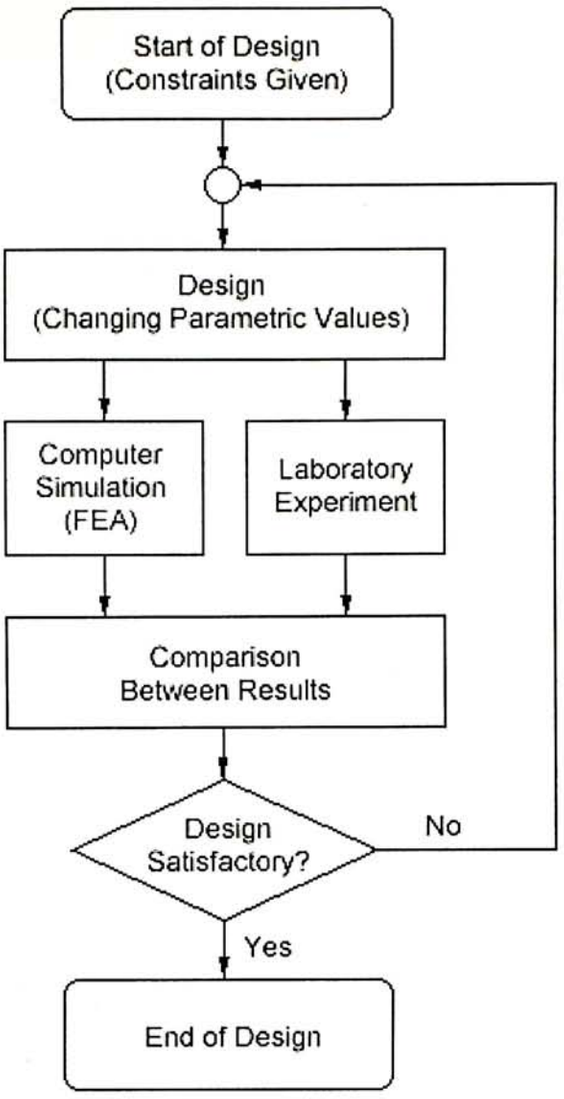

Figure 1. Flow diagram of design process.

1.1.2 Proposed Applications of Micro Power Supplies

The proposed micro generator may benefit the applications of MEMS or low power CMOS devices based on its size, energy capability and integration. The proposed generator sizes less than $1cm^3$. In applications such as mini robot applications and MEMS devices, where space factor is critical, micro power supply from mechanical energy may be an option.

In 1992, Seiko Epson developed an autonomous mobile robot with $1cm^3$ volume size based on the conventional watch production technology. A high capacity condenser of 6mm diameter, 2mm thickness and 0.33F electric capacity was used as the energy source such that the micro robot was able to move about five minutes for 30 seconds charge. With such relatively small energy consumption, a micro vibration based generator may be a substitute of conventional rechargeable batteries.

Vibration based generator contains virtually unlimited energy, which is essential in embed or isolated systems such as space applications. Besides, the use of MEMS technology makes it possible for the proposed generator to integrate with conventional MEMS circuit. The proposed micro generator has been successfully tested as a power source of a radio frequency transmission device by the *Advanced Microsystems Laboratory* group in *The Chinese University of Hong Kong.*

1.1.3 Comparison Among Different Power Sources

Various integrated micro power supplies have been proposed recently. Matsuki *et al.* used an energy coupling method to remotely induce voltages and currents on-chip by an external magnetic field in 1988 [6]. Kiely *et al.* built a miniature thermoelectric generator, which could generate electricity under temperature gradient, in 1991 [7]. Rashidian and Allen demonstrated the use of electric field in dielectric loss heating by driving an electrothermal micro actuator with high frequency electric field remotely in 1993 [8]. Bates *et al.* developed a rechargeable thin-film lithium micro-battery, which serves as a self-contained on-board power supply for micro devices in 1993 [9]. Lee *et al.* built a miniaturised high-voltage solar cell array as an on-board power supply

for an electrostatically driven silicon mirror in 1994 [10] [11]. In 1997, Koeneman *et al.* presented a comprehensive study on the feasibility of different types of micro power supplies for MEMS and concluded that chemical microbatteries, elastic strain energy, magnetic fields and electric fields are the most practical forms of energy storage [12]. Some possible energy sources and their corresponding applications are listed in Table 1.

Sources of energy	Year	Examples
Electromagnetic field	1959	Non-invasive pacemaker battery recharging [13].
	1988	Voltage induction by external magnetic field in medical applications [6].
	1997	Radio frequency powered identification tags [14].
	1997	Inductively powered smart cards [15].
Gravitational energy	1991	Electronic wristwatch with generator [16].
Thermal energy	1991	Miniature thermoelectric generator was used to generate electricity by temperature gradient [7].
Electric field	1993	Electrothermal micro actuator was driven by high frequency electric field [8].
Chemical energy	1993	Rechargeable thin-film lithium micro-battery [9].
Solar energy	1994	High voltage solar cell array as power supply of electrostatic silicon mirrors [10] [11].
Human motion	1996	Human powered wearable computing [17].
Fluid flow	-	-
Acoustic energy	-	Super sonic wave used as driving force of micro objectives. [18]

Table 1. List of possible ambient energy sources.

Even though conventional chemically based rechargeable or replaceable micro batteries are widely employed in current MEMS devices, they may suffer from defects such as finite capacity and shelf life. Batteries which contain chemicals hazardous to health are not suitable for medical applications such as implanted medical devices. In isolated or permanent systems such as embedded MEMS devices and space based MEMS, where real-time recharging or replacement of batteries becomes difficult, chemical battery may not be the optimal choice. There are also many applications where light, thermal, electrical or magnetic energies are not practical or available. Therefore, we propose a new micro power supply which generates electricity from ambient mechanical vibrations.

A summary of energy densities for MEMS energy storage conducted by Koeneman *et al.* [12] is reprinted in Table 2. It is noticed that mechanical vibration based energy (elastic strain energy) is reported to be a satisfactory form of energy storage in general cases when combustion, heat and chemical cells are not allowed.

Storage Method	Energy Density (J/L)	Parameters
Fission Fuel	1.5×10^{12}	U235
Combustion Reactions	3.5×10^{7}	gasoline
Electrochemical Cell	2.1×10^{6}	Li – aV_2O_5
Heat Capacity	8.4×10^{5}	Water, ΔT=20K
Latent Heat	1.0×10^{5}	Refrigerant 11
Fuel Cell	6.5×10^{3}	$H_2 - O_2$, 1atm
Elastic Strain Energy	6.4×10^{3}	Spring steel
Kinetic (translational)	3.3×10^{3}	Lead, v=24m/s
Magnetic Field	9.0×10^{2}	B = 1.5T
Electric Field	4.0×10^{2}	E = $3x10^{8}$V/m
Pressure Differential	7.0×10^{1}	1atm, V_0/V_f=2
Kinetic (rotational)	2.0×10^{0}	Pb, 3600rpm, d=4500μm
Gravitational Potential	5.0×10^{-1}	Lead, h=4500μm

Table 2. Summary of energy densities for energy storage. [12]

Minimisation of power consumption is the current trend in very large scale integration (VLSI) circuit design, aiming to extend battery life in portable systems and remove heat in relatively large systems. It was predicated that the power consumption of sensor systems might be reduced to tens to hundreds of micro-watt [4]. Coupling with this recent advent in low power MEMS sensors, MEMS integrated mechanical power generators with life span far greater than its chemically based counterparts may be an option in diverse sensor and circuit applications in the coming future.

1.2 LITERATURE SURVEY

Shearwood and Yates developed an electromagnetic micro generator, which consisted of a planar gold pick-up coil and a rare-earth SmCo magnet attached on a flexible polyimide membrane of diameter 2mm, in 1997 [3]. They reported a non-linear spring stiffening effect, which limited the power that could be generated from the device, at certain vibration amplitudes. A maximum RMS power of 0.3μW was reported at a resonant frequency of 4.4kHz. However, no structural optimisation or integration of the micro generator to any circuit system was reported. Figure 2 indicates the schematic diagram of the micro generator.

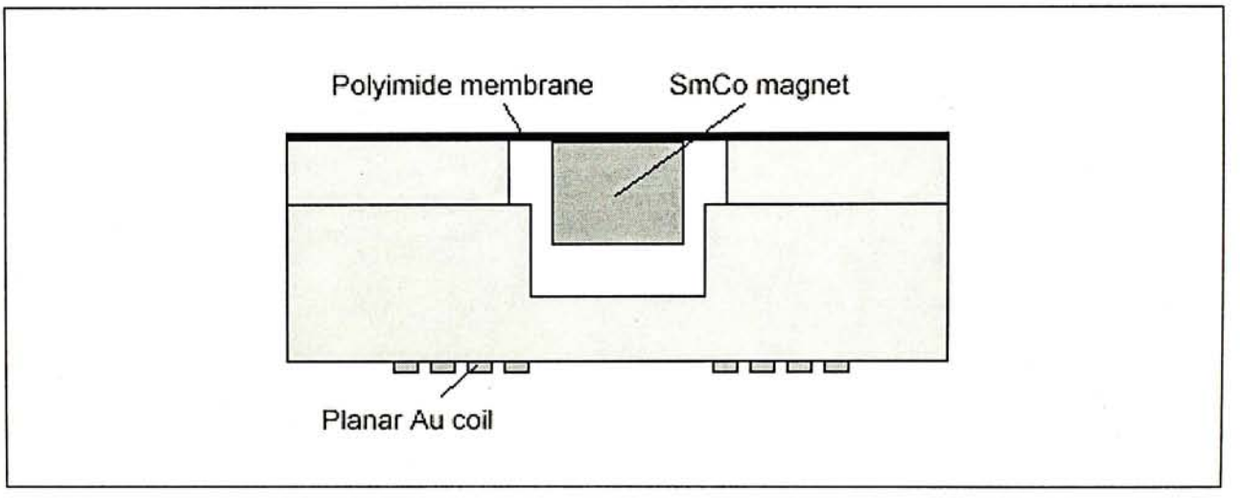

Figure 2. Schematic diagram of micro generator developed by Shearwood and Yates in 1997 [3].

Amirtharajah and Chandrakasan successfully used a *macro* scaled (500mg mass) vibration based electromagnetic power generator to drive a signal processing circuitry in 1998 [4] [5]. They integrated an ultra-low power controller to regulate the generator voltage, and a low power subband filter DSP load circuit on a CMOS chip, which consumed 18μW of power. It was reported that 400μW of power could be

generated by the *macro* generator and 500kHz self-powered operation of the subband filter corresponded to a level of performance suitable for sensor applications. At a 500kHz clock frequency, 23ms of valid DSP operation could be generated by a single generator excitation.

Nearly all the previous studies mentioned aimed to the same target – to develop a self-generated power source for low power circuit. However, by far no one has ever published a work combining a MEMS resonating system and a low-power circuit system with optimised mechanical structures for specific applications In this paper, a micro mechanical vibration based power generator is developed to study the feasibility of power generation with very low frequency, e.g. human walking and running.

CHAPTER 2 MICRO POWER GENERATOR WITH COPPER SPRINGS

2.1 POWER PRODUCTION FROM MECHANICAL VIBRATIONS: SYSTEM ANALYSIS

A mechanical drawing of the electromagnetic micro generator under study is shown in Figure 3. The device consists of a permanent magnet of mass m and magnetic field strength B, two silicon springs with the total spring constant k, and a wire coil of length l. The two ends of each spring are attached to the permanent magnet and a silicon frame, which is connected to the rigid housing of the device, respectively, forming a mass-spring resonator structure. The wire coil is fixed on the rigid housing of the device. Whenever the rigid housing is vibrated, the magnet will move relatively to the housing and the wire coil. This relative movement of magnet to the coil results in the varying amount of magnetic flux passing through the coil. According to the Faraday's Law of electromagnetic induction [19], which states that the electromotive force induced is equal to minus the rate of change of the flux linkage when the magnetic flux passing through an area enclosed by a loop changes, a voltage is induced on the coil.

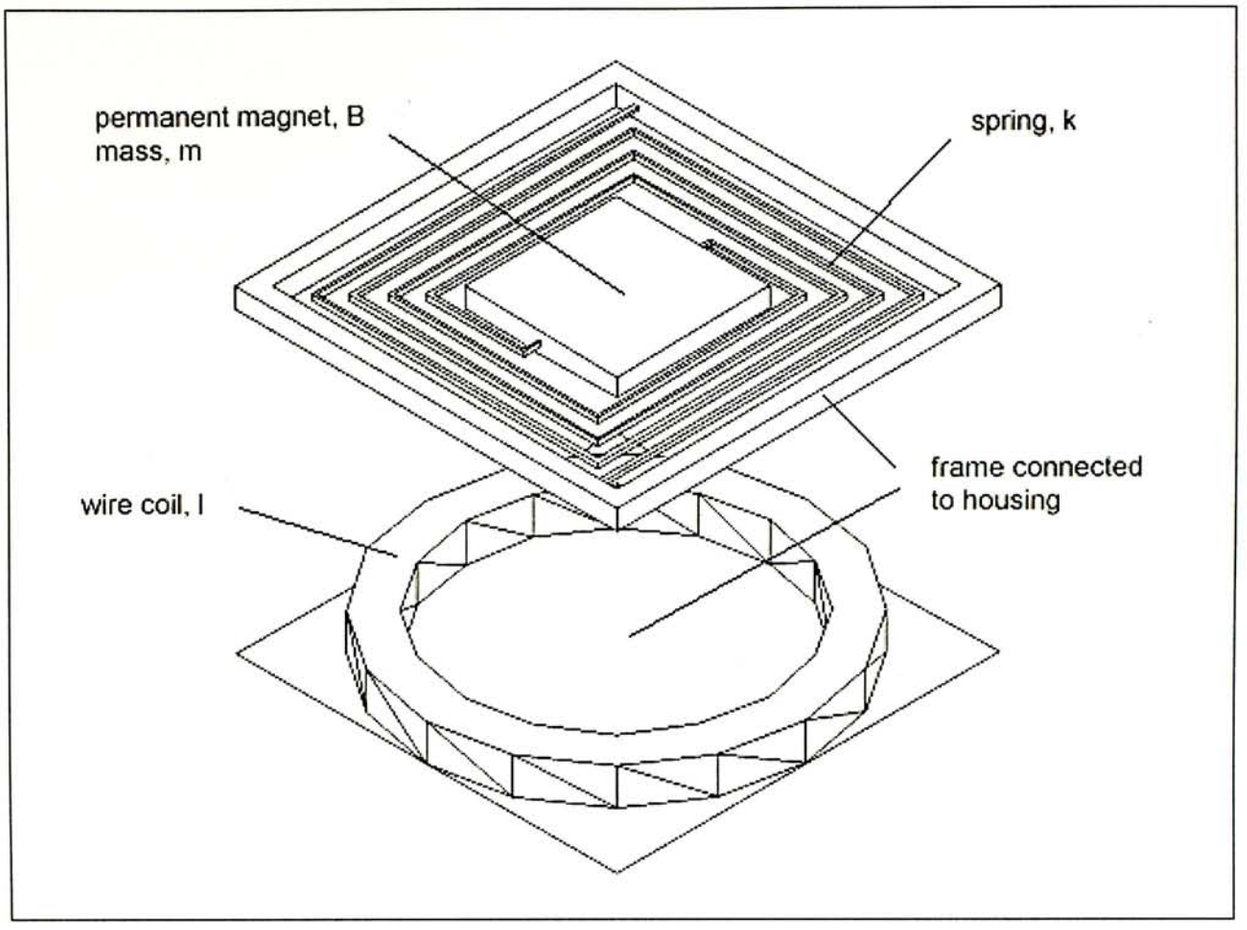

Figure 3. Conceptual illustration of micro generator.

A schematic diagram of the micro generator system is shown in Figure 4. The displacement of the generator is given by *y(t)* and the relative displacement of the magnet to the wire coil is indicated as *z(t)*. The springs of the generator are lumped into one with spring constant *k* and the mechanical damping due to air resistance and friction is represented by a damper with damping coefficient *d*. The wire coil is represented as an inductor with inductance *L* and a resistor with resistance R_c. The voltage induced in the coil is served as the electrical output of the generator and the power input of the load circuit. For the sack of simplification, the load circuit is represented by a single resistor with resistance *R* in the diagram.

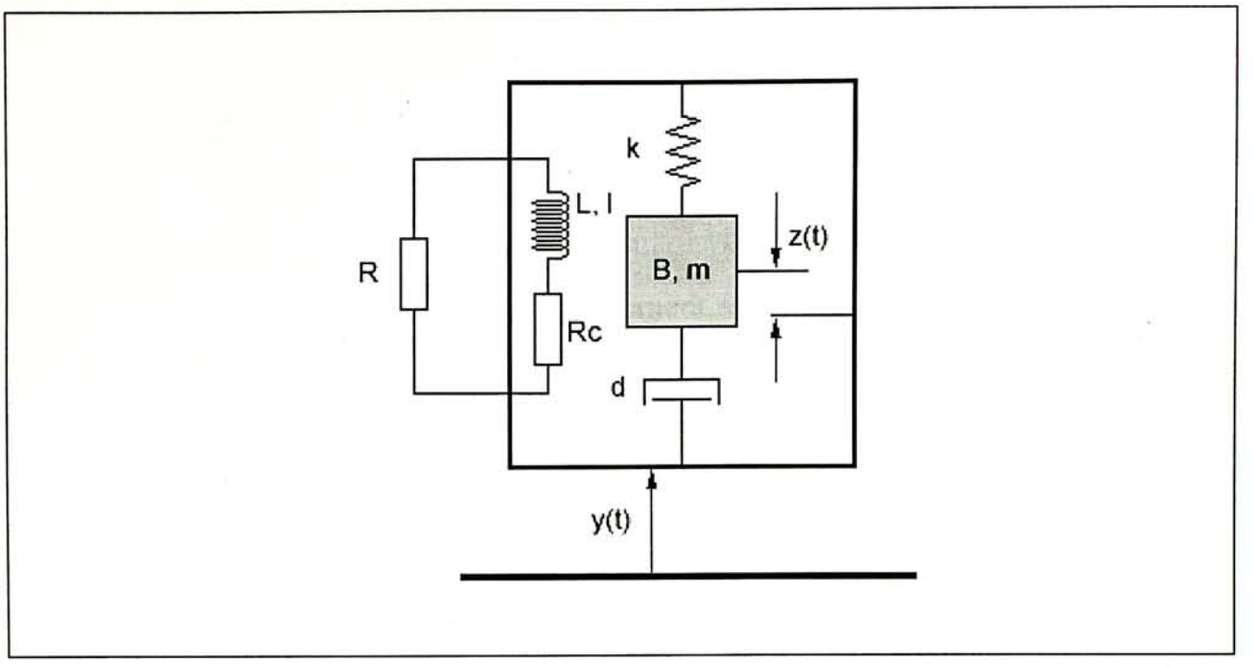

Figure 4. Schematic diagram of micro generator system.

Figure 5 indicates the block diagram of the linearized model of the micro generator system and a summary of the system parameters is shown in Table 3. A mechanical input force is fed into a second-order mechanical mass-spring system corresponding to the resonator structure formed by the magnet and the silicon springs. The output of the mechanical system, displacement of the magnet relative to the coil, is then fed into the first-order electrical system corresponding to the *LR* circuit formed by the load resistor in series with the wire coil. The current induced in the coil by the mechanical excitation generates a feedback electromechanical force, f_e, which, in turn, damps the motion of the magnet. A comprehensive proof of formulas is given in Appendix A.

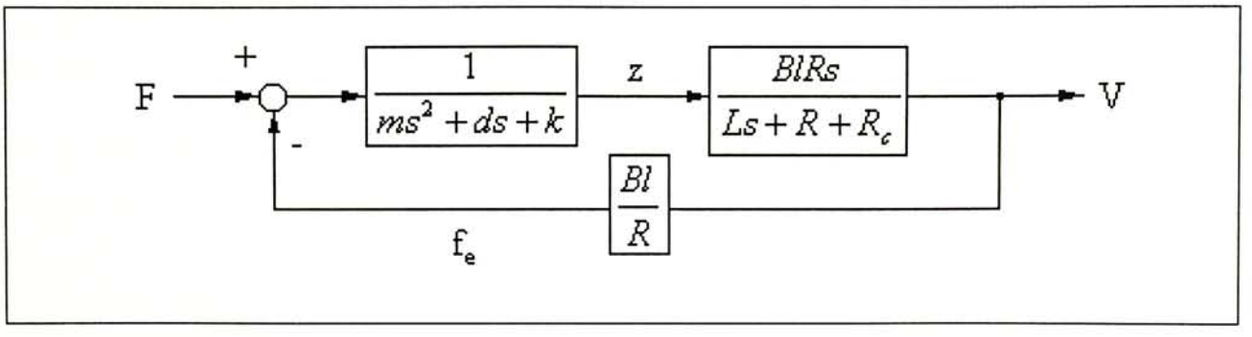

Figure 5. Block diagram of micro generator [4].

Parameter	Description
F	Generator input force
y	Generator input displacement
z	Mass displacement relative to coil
V	Voltage output at load resistor
f_e	Feedback electromechanical force
m	Mass of magnet
d	Mechanical damping coefficient
k	Spring constant of springs
B	Magnetic field strength of magnet
l	Length of wire coil
R	Load resistance
L	Coil inductance
R_c	Coil resistance

Table 3. System parameter summary of micro generator studied.

The overall transfer function from input force to output voltage has been previously derived [4] and is given by the expression:

$$\frac{V(s)}{F(s)} = \frac{BlRs}{(Ls + R + R_c)(ms^2 + ds + k) + (Bl)^2 s} \tag{1}$$

However, as reported by Amirtharajah and Chandrakasan [4], the electrical pole is, in general, much faster than the mechanical dynamics for the vibration cases of interest. The inductance of the wire coil is small while comparing to the load resistance of the output circuit, resulting in a fast electrical pole. If the mechanical constants are chosen such that the resonant frequency of the micro generator system is closed to the expected input vibration frequency, which is usually much smaller than the electrical

resonant frequency, it will be reasonable to ignore the electrical pole. The linearized model of generator system is simplified to a damped second-order system. Moreover, it is noticed that the resistance of the wire coil is much smaller than the load resistance in most cases. By assuming that both L and R_c are zero, the system transfer function may be rewritten as the expression:

$$\frac{V(s)}{F(s)} = \frac{Bls}{(ms^2 + ds + k) + \frac{(Bl)^2}{R}s} \tag{2}$$

Supposed that the generator is driven by a sinusoidal excitation $y(t)=Y_0 sin(\omega t)$, the average output power in steady state of the micro generator system is then given by the expression:

$$P = \frac{m\zeta_e Y_0^2 \left(\frac{\omega}{\omega_n}\right)^3 \omega^3}{\left[1-\left(\frac{\omega}{\omega_n}\right)^2\right]^2 + \left(2\zeta\frac{\omega}{\omega_n}\right)^2} \tag{3}$$

where ω is the input vibration frequency, ω_n is the natural frequency of the resonator structure, ζ_m is the mechanical damping ratio, ζ_e is the electrical damping ratio, and ζ is the total damping ratio of the system.

$$\omega_n = \sqrt{\frac{k}{m}} \tag{4}$$

$$\zeta_m = \frac{d}{2\sqrt{mk}} \tag{5}$$

$$\zeta_e = \frac{(Bl)^2}{2R\sqrt{mk}} \tag{6}$$

$$\zeta = \zeta_m + \zeta_e \tag{7}$$

If the micro generator is operated at resonance, the output power of the system will be maximised. The value of the average output power at resonance is given as [1]:

$$P = \frac{m\zeta_e Y_0^2 \omega_n^3}{4\zeta^2} \tag{8}$$

Hence, the peak voltage output of the generator system at resonance can be expressed as [1]:

$$V_0 = \frac{BlY_0\omega_n}{2\zeta} \tag{9}$$

Now, the power input is given by the product of input force, $F(t)=mY_0\omega^2 sin(\omega t)$, and velocity, $y'(t)= \omega Y_0 cos(\omega t)$.

$$P_{input}(t) = \frac{mY_0^2\omega^3}{2}\sin(2\omega t)$$
$$P_{input} = \frac{mY_0^2\omega^3}{2} \tag{10}$$

2.2 DESIGN OF MICRO RESONATING SPRING

2.2.1 Design Objective

As predicted by Amirtharajah *et al.* [4], the power consumption of sensor systems would be reduced to tens to hundreds of microwatt. Given the equations derived in the previous section, an interesting question is asked, "What is the smallest generator possible which can generate 1V for a system consuming 30μW of power at an frequency between 2 to 10Hz (i.e. human walking or running) using conventional MEMS technology?" With the use of Finite Element Analysis (FEA), we would like to explore the feasibility of an integrated micro power generator structure for particular need. While an objective application is clear, a variety of factors and governing parameters are limited in designing the micro generator. Some of the major criteria of the design objective are stated in Table 4.

Parameter	Criterion
Size of Structure	Less than 1cm x 1cm
Input Frequency	About 10Hz
Width of Springs	Larger than 100μm
Voltage Output	About 1V
Power Output	About 30μW

Table 4. Design objectives in designing micro vibration based power generator.

In general, the criteria listed in Table 4 provides us a guideline of which design parameters can be altered and which cannot at the expense of limited size and working frequency range. However, not all of the governing factors are tightly fixed

as stated. For the ease of standardization in both theoretical and experimental study, some of the parameters are fixed to default values, which allow satisfactory result without altering the design in a large extent. Some of the design parametric values used in both Finite Element Analyses and experiments are listed in Table 5.

Type	Parameter	Value	
Input	Displacement	200 – 2000 μm	
Magnet	Material	Nd-Fe-B	
	Mass	192 – 219mg	
	Dimension	3mm x 3mm x 3mm	
	Young's modulus	207GPa	
	Density	8120kg/m^3	
	Magnetic coercive force	964kA/m	
	Residual induction	1.312T	
Spring	Material	Copper	Silicon
	Thickness	0.11mm	-
	Young's modulus	110GPa	112.4GPa
	Poisson's ratio	0.35	0.28
	Density	8960 kg/m^3	2329kg/m^3
Environment	Damping ratio	0.05	
Coil	Coiling technique	Printed Circuit Board (PCB)	Hand-wired coil
	Diameter	24mm	15mm
	Coil Length	2.7m	
	Number of turns	-	1500

Table 5. Design parametetric values.

2.2.2 Material Selection

2.2.2.1 Mechanical Resonating Structure

The selection of material used to fabricate the resonating structure is crucial in the optimisation of the micro generator. If the mass of the magnet is known (governed by the state-of-art technology for small volume and high field strength material) and assuming that all the mechanical power can be converted into electrical power, Equation (8) may be used to find the power output for the generator at a given vibration frequency.

Consider a l_s long single beam cantilever string (Figure 6) with a homogeneous rectangular cross-section (w_s x t_s). Given the thickness t_s of the spring (110μm) and the maximum allowable tensile stress σ_{max}, the maximum allowable bending load the spring can withstand, F, may be calculated by Equation (11) with the width w_s and the length l_s of the springs being the varying parameters. The maximum shear stress τ_{max}, on a cantilever is given in Equation (12). With $l_s >> t_s$ in most cases, the shear stress is usually much smaller than the tensile stress (Equation 13) and ignored. Hence, the total stress on the spring may be assumed to be contributed by the tensile stress only. Given the yield stress of the material (Cu: 300MPa, Si: 120MPa), the maximum allowable load on the spring, F, is calculated from Equation (11).

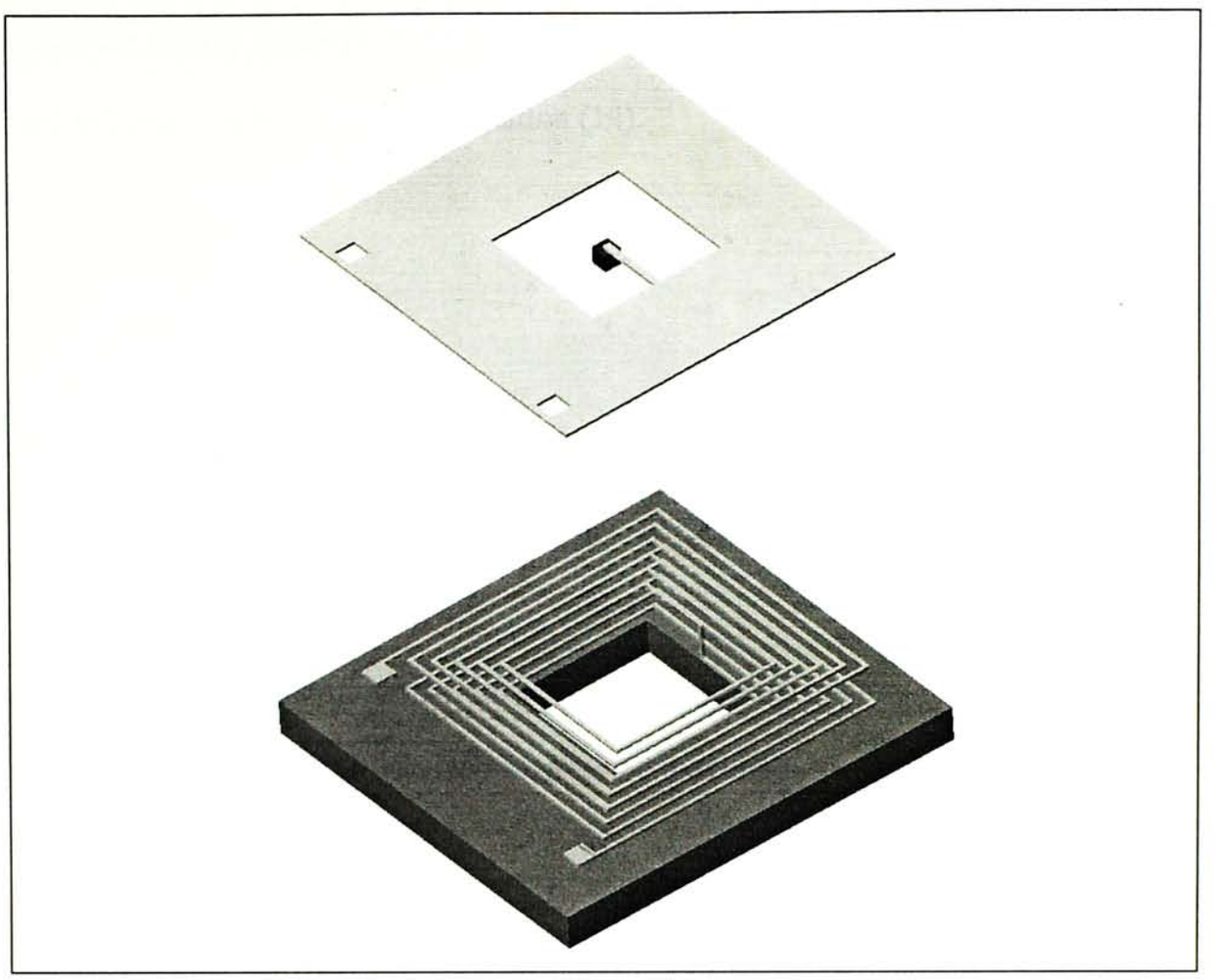

Figure 6. Proposed design of an integrated micro power generator.

Maximum tensile stress on a cantilever spring:

$$\sigma_{\max} = \frac{6Fl_s}{w_s t_s^2} \tag{11}$$

Maximum shear stress on a cantilever spring:

$$\tau_{\max} = \frac{3F}{2w_s t_s} \tag{12}$$

$$\frac{\sigma_{\max}}{\tau_{\max}} = \frac{4l_s}{t_s} \tag{13}$$

Now, the spring constant of the spring is determined by the spring geometry and material property governed by equitation (14).

$$k = \frac{3EI}{l_s^3} \tag{14}$$

where E and I are the Young's modulus and moment of inertia respectively by well-known cantilever deflection equation.

Hence, the maximum allowable deflection of the spring relative to the coil z_0 can be calculated by dividing the previous determined maximum load by the spring constant.

$$z_0 = \frac{F}{k} = \frac{\sigma_{\max} w_s t_s^2 l_s^2}{18EI} \tag{15}$$

The system power output in Equation (8) is reformed and restated in Equation (16). By assuming that all the mechanical energy is converted into electrical energy, the power output of a generator system with cantilever spring may be calculated by Equation (15) and (16), and is plotted in Figure 7.

$$P = \frac{m\zeta_e Y_0^2 \omega_n^3}{4\zeta^2} = m\zeta_e \omega_n^3 z_0^2 \tag{16}$$

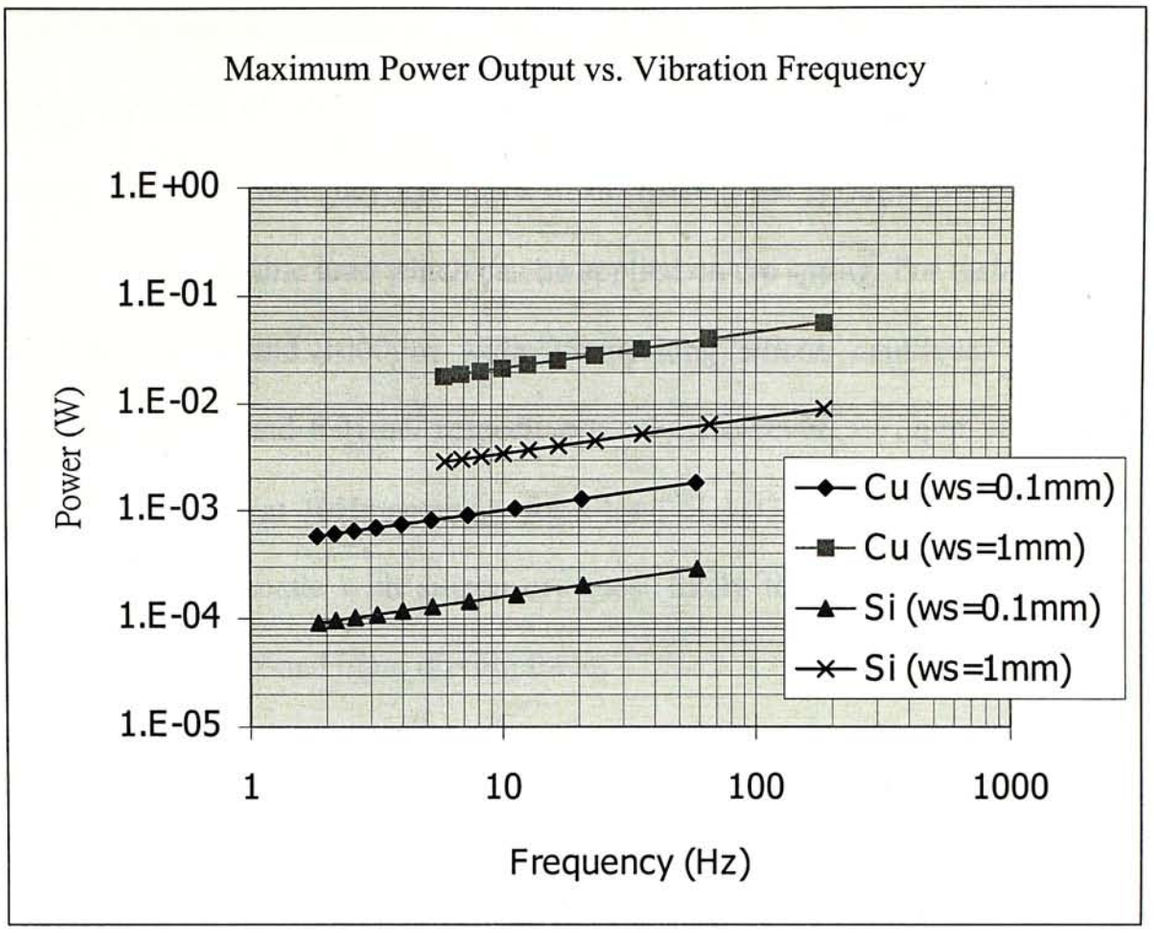

Figure 7. Maximum system power output vs. vibration frequency using generators with cantilever springs.

Figure 7 indicates the maximum power output of a generator with cantilever spring. Two sets of spring width are tested with the spring length being a varying parameter. By increasing the length of the spring, the resonant frequency may be lowered to the desired given environmental value. While 100μm being the conservative estimate for Si bulk-micromachining technology, shortening the spring length also minimizes the total system power output. In order to achieve the required 30μW power output at 10 Hz, it is necessary to build a 15mm and 35mm long cantilever spring if 100μm and 1000μm wide springs are employed respectively.

Figure 8 indicates the maximum allowable load the spring is able to withstand without crossing the limit of yield stress for copper and silicon springs. It is shown that lowering the input frequency by means of decreasing the spring constant minimizes the maximum allowable load which can be applied on the spring. For instance, 100μm wide 15mm long and 1000μm wide 35mm long silicon cantilever springs can withstand 1.61mN and 6.91mN respectively only. However, an input vibration with the amplitude 2mm at 10Hz accounts for a total of 1.73mN force (i.e. $F_0=mY_0\omega_n^2$). Therefore, springs made with silicon are most likely to suffer from damage from sudden shock or overload input driving force.

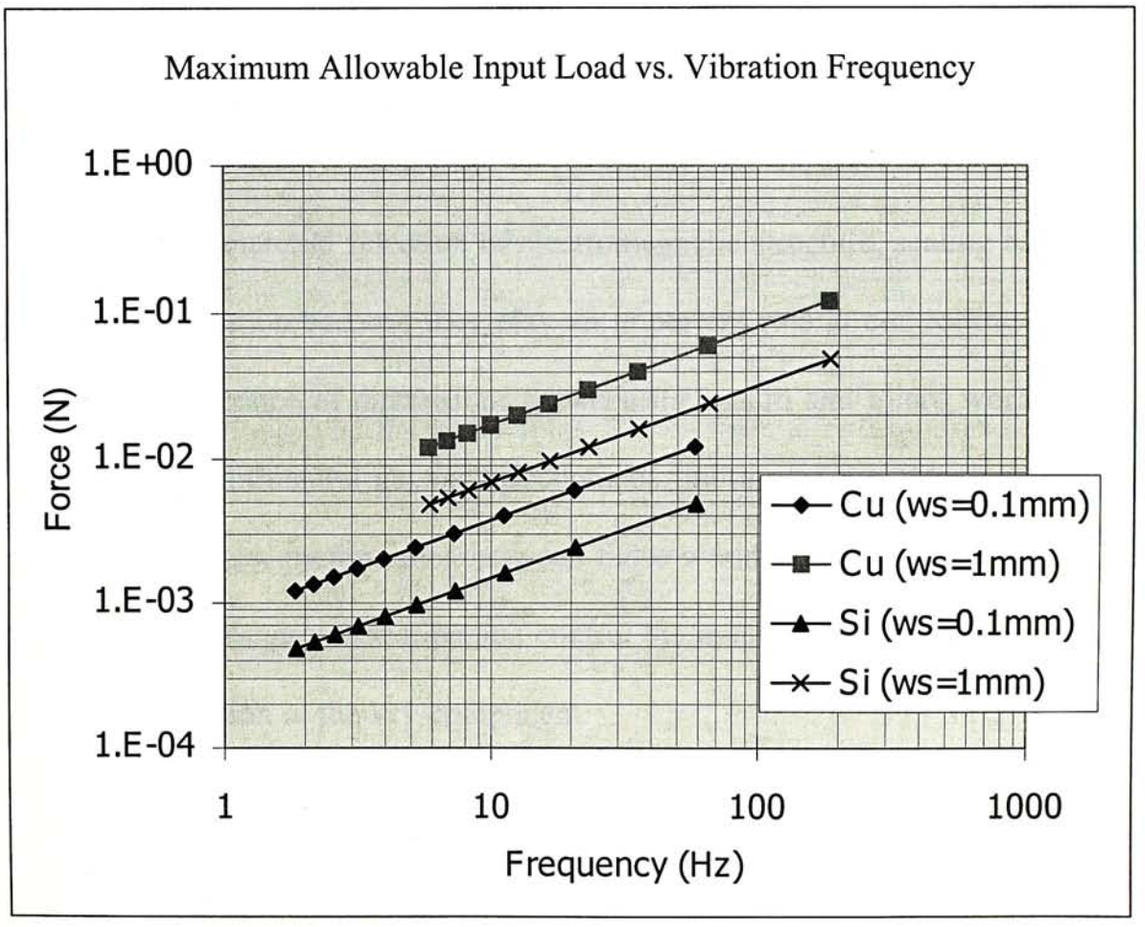

Figure 8. Maximum allowable input load vs. vibration frequency using generators with cantilever springs.

On the other hand, copper is relatively a suitable material for the application of micro springs. It is non-magnetic in natural and has a low spring constant. The yield stress of copper (300MPa) is twice as much as that of Silicon, meaning that copper spring is able to withstand higher stress level without being broken. The density of copper (8960 kg/m^3) is much higher than that of Silicon. By Equation (4), a lower frequency can be achieved. Moreover, the required thickness of copper may be as low as 10μm, which is readily available commercially. Previous experimental works have demonstrated that copper is, in general, a better material in making a micro generator than silicon. Hence, this paper will focus on the usage of copper mainly.

2.2.2.2 Electromagnetic Structure

In the design and material selection of electromagnetic structure, scaling effects must be under consideration because they play an important role in controlling devices in micro scale. Difference of dimensions between the macro and micro world causes a difference in the influential physical phenomena, motion of the objects and relative change of the system performance between those worlds. These differences are very important in the design, fabrication and control the micro mechanical system because of the miniaturization of the key component.

Taking a micro electromagnetic actuator as an example, the dimension of the electromagnetic force generated in a solenoid coil is shown in Equation (17).

$$\left[F_{magnetic}\right]=\left[\frac{S_m B}{2\mu_0}\right]=\frac{B}{2\mu_0}\left[L^2\right] \tag{17}$$

where S_m is the surface area of cross section of the solenoid, B is the magnetic field density and μ_0 is the permeability.

From Equation (17), it can be observed that the solenoid generates the electromagnetic force proportional to the square of the length. Hence, miniature of the structure decreases the electromagnetic force at the same time. The same situation of scaling effects occurs in the case of micro generator as well. While minimizing the structure for application objectives such as space conservation or integration, the output power generated by the micro generator decreases at the same time. For example, minimization of the micro generator restricts the available usable space for the magnet and the coil, which, in case, reduces the possible voltage output.

As a solution of tight resources in micro scaled design, a rare earth Nd-Fe-B magnet with high magnetic density is employed in the design. A 27mm^3 Nd-Fe-B magnet is measured to have 0.22T (2200G) surface field strength. A comparison of magnetic energy among different magnetic materials is given in Figure 9. From the figure, it is shown that Nd-Fe-B can, in general, produce larger magnetic field strength comparing with the other magnetic materials of the same class.

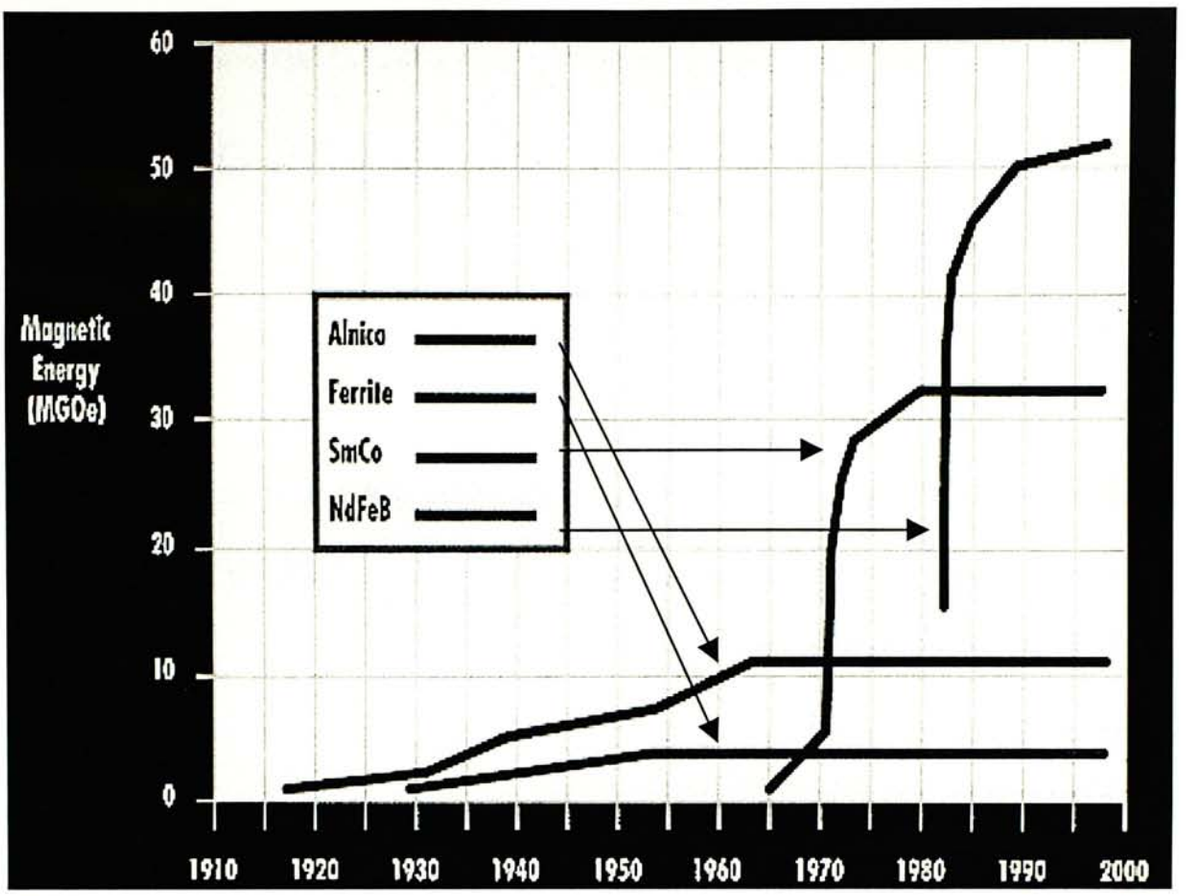

Figure 9. Comparison of magnetic energy among different kinds of magnets. (Reprinted from http://www.dextermag.com/pmp.htm)

2.3 LASER MICROMACHINING OF SPRING STRUCTURE

2.3.1 Si Bulk Micromachining

Both silicon bulk-micromachining and laser micromachining have been tested to fabricate the spring structures. A resonating spring structure fabricated by Si micromachining is shown in Figure 10 and 11. The structure is 5mm x 5mm in size with two supporting beams of 100μm thickness, 300μm width and 2mm length. Previous experiments on Si bulk-micromachined resonating structure have indicated that Si springs are very fragile to environmental vibrations and are easily damaged. Vibration generated in handing and sudden shock might also lead the Si springs to mechanical failure. Since long-term service is expected in the proposed applications, silicon may not be the optimal choice of material used in fabrication of our micro springs.

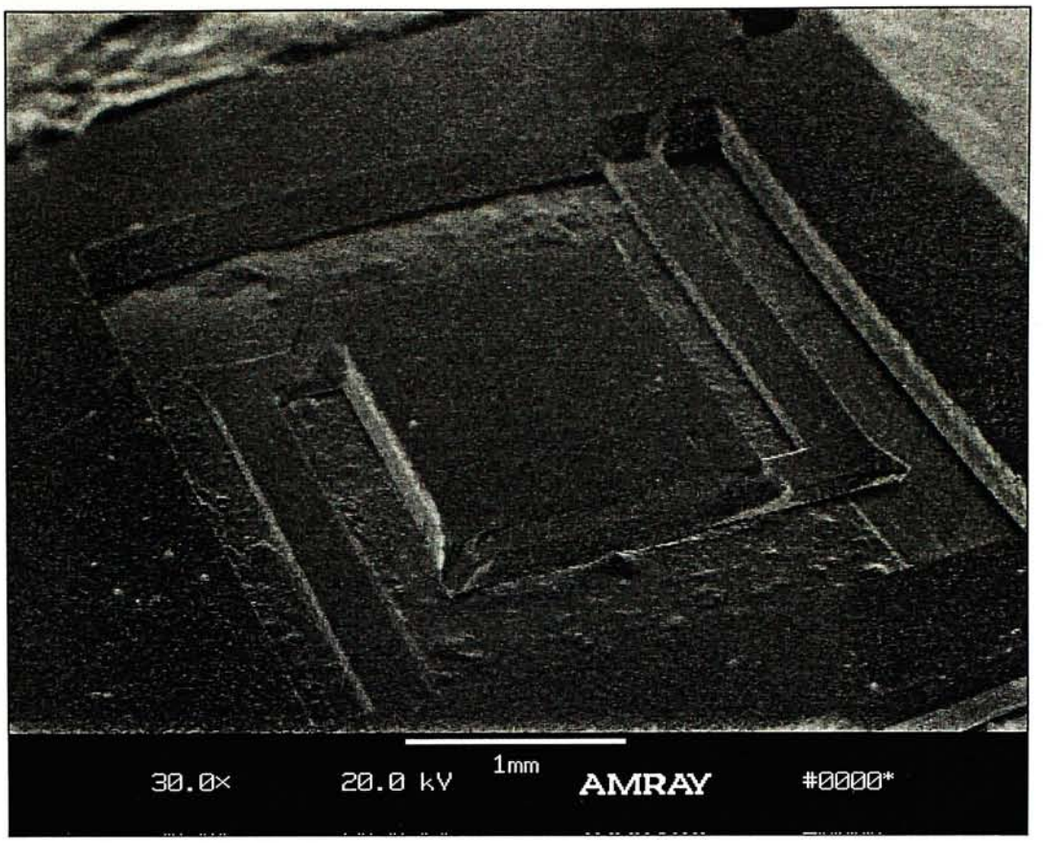

Figure 10. A bulk-micromachined Si spring structure.

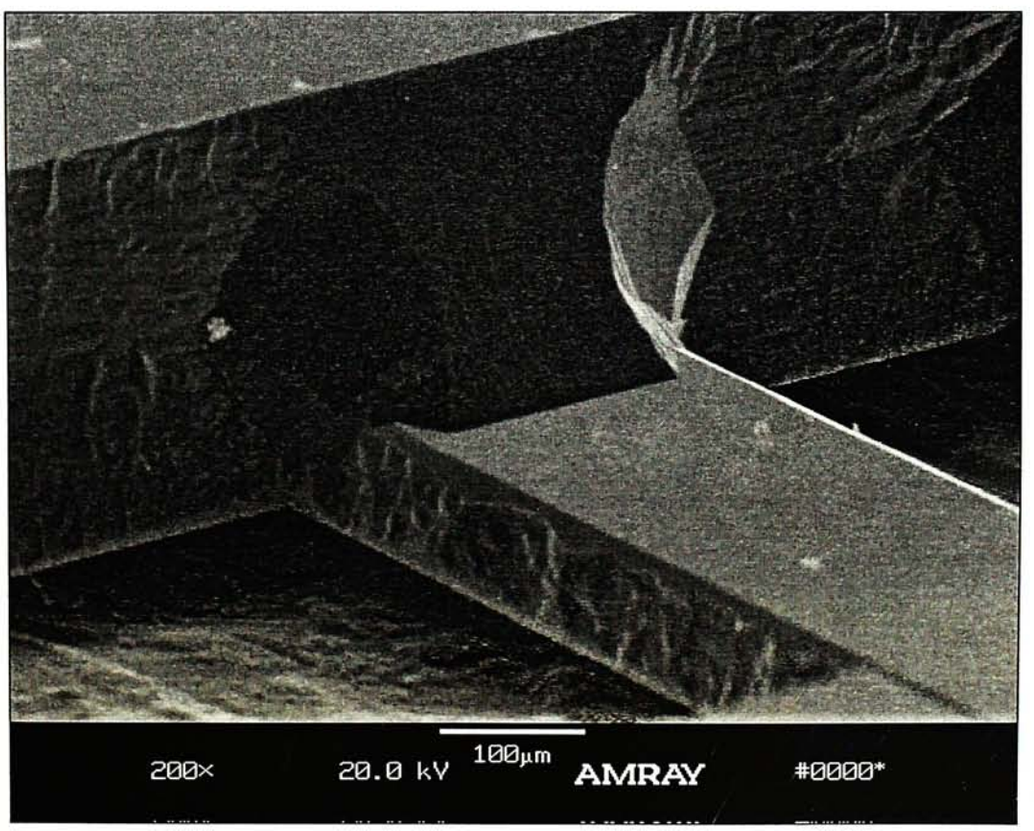

Figure 11. Micro spring of Si bulk-micromachined spring structure.

2.3.2 Laser Micromachining

As discussed in the earlier section, copper is a more suitable material for the fabrication of micro spring vibrating structure. A Nd: YAG (Electrox) laser machine has been used to micromachine the copper spring structures. A copper resonating structure with 5mm diameter is shown in Figure 12.

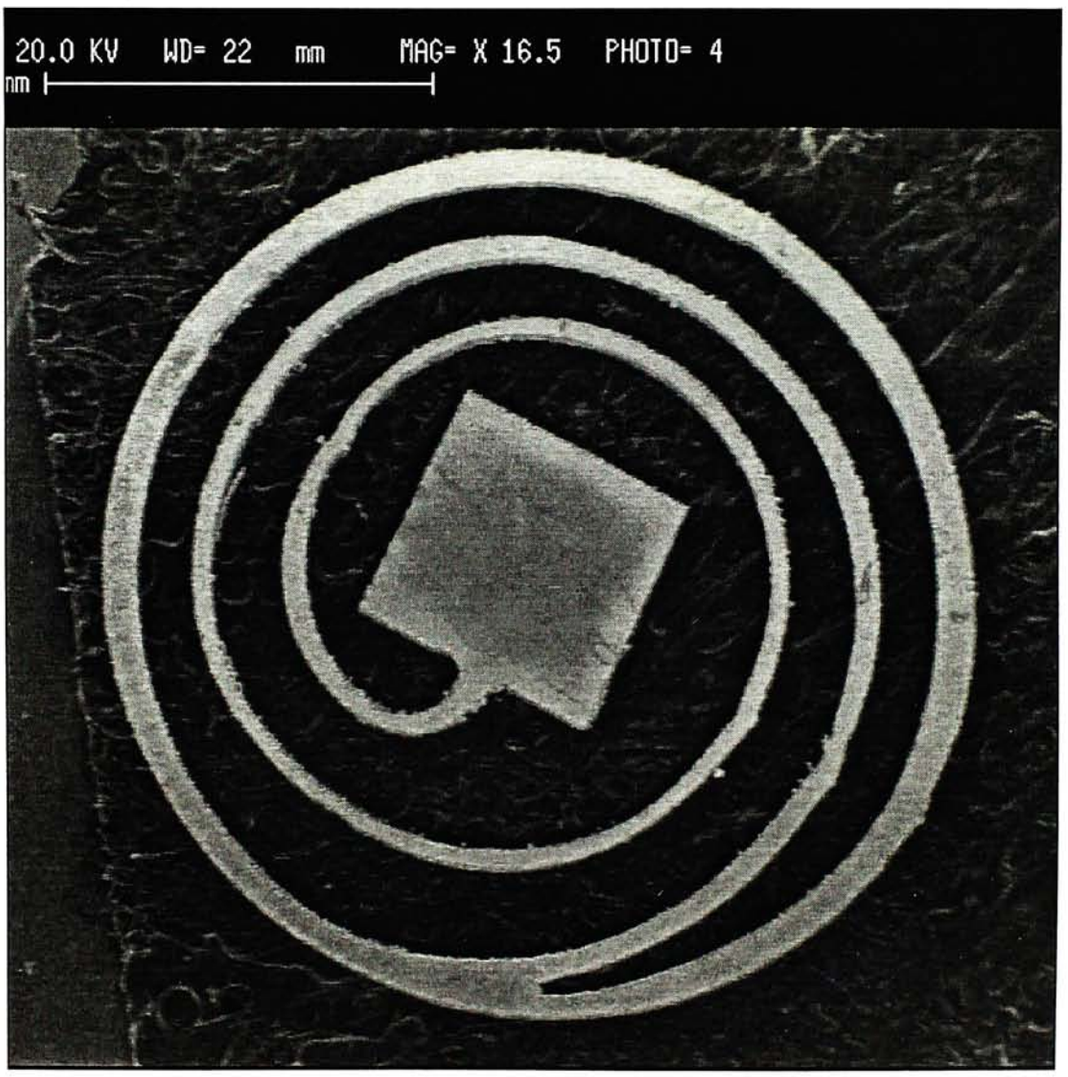

Figure 12. A laser micromachined Cu spring structure.

Unlike Si bulk micromachining, laser micromachining usually produces rough surfaces on copper springs. A SEM image of the surface of the Cu laser

micromachined springs is shown in Figure 13, in which the spring edges are rough and irregular while comparing with the smooth edges of Si springs in Figure 11. Such deviation of surface quality may lead to the difference of working frequency and allowable stress in structures even with the same configuration. Meanwhile, satisfactory quality of micromachined spring surfaces requires precise control of the laser power, input pulse rate and scan speed. With the use of an interferometer, the fabricated resonating structures are inspected. The width and pattern of the fabricated springs are measured such that the dimensions of the resonating structure are kept to be closed to the expected value with high accuracy (Figure 14 and 15).

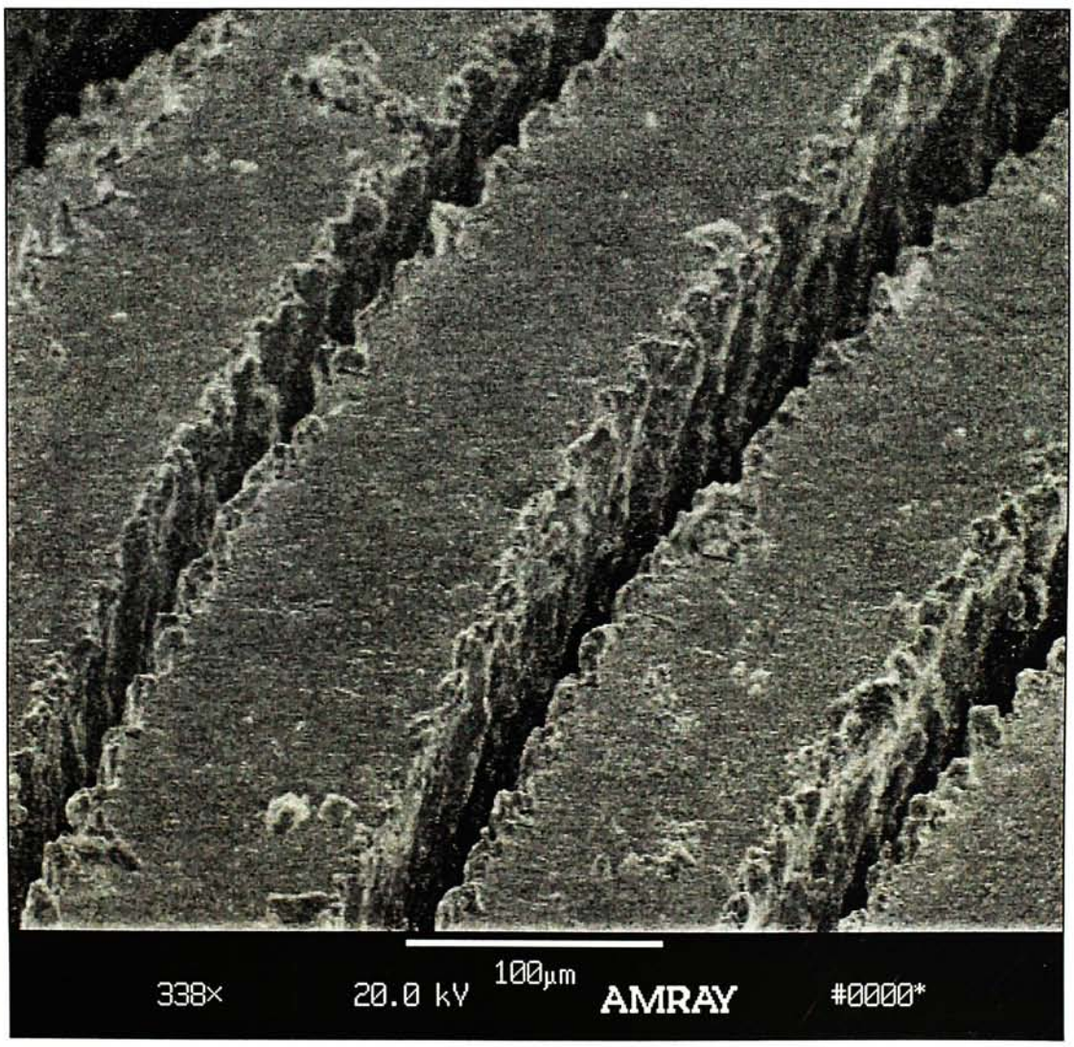

Figure 13. Laser micromachined Cu springs.

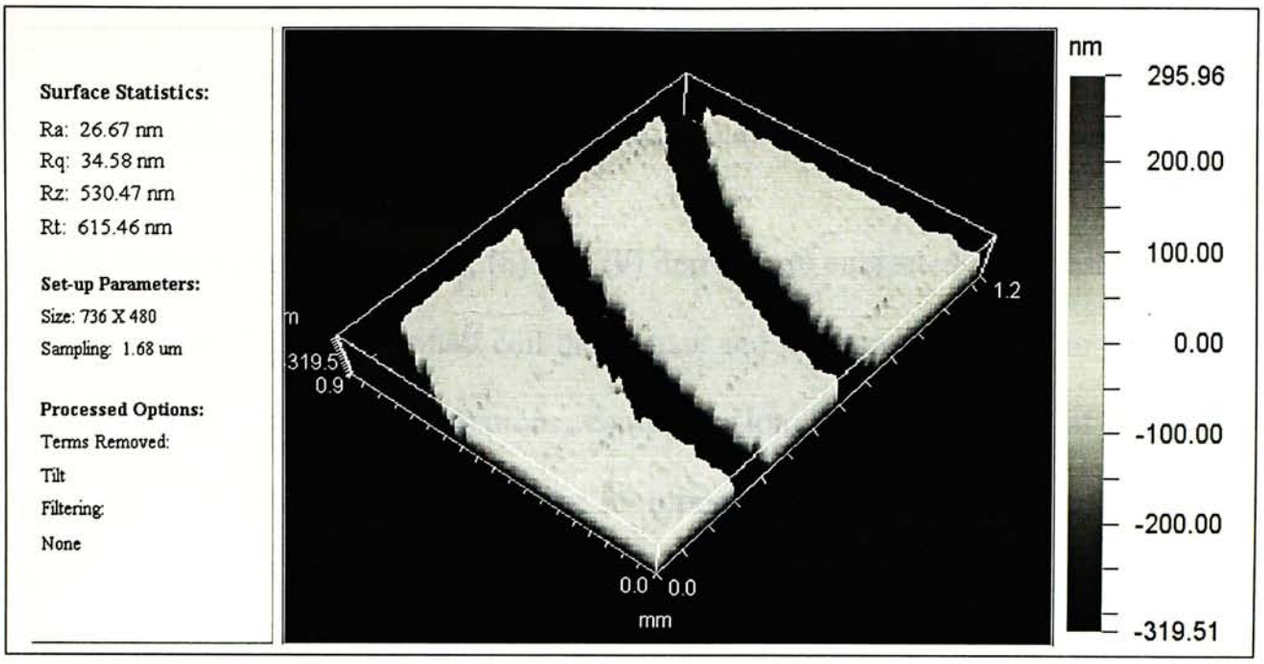

Figure 14. Interferometor is used to measured the dimensions of the fabricated resoanting structure.

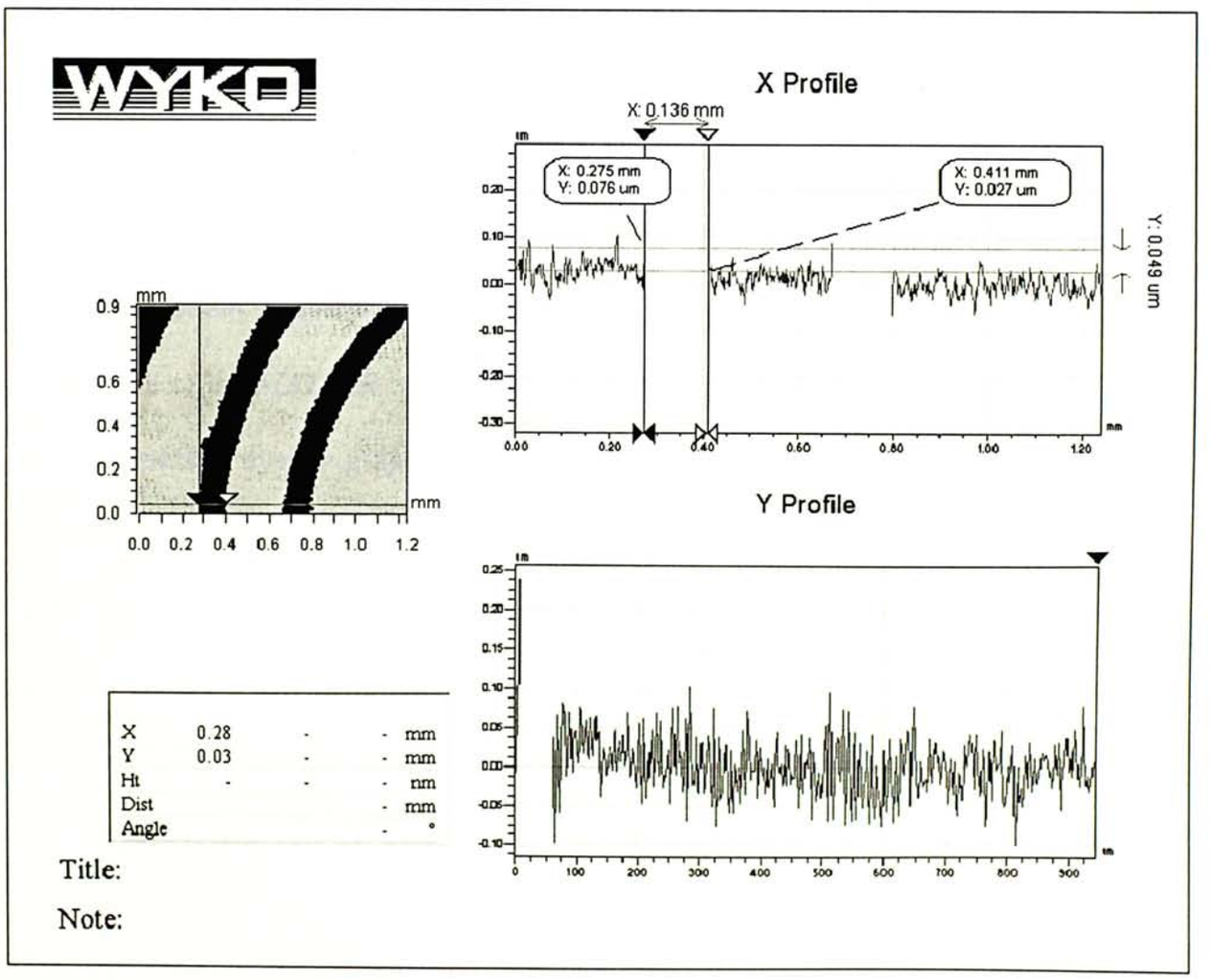

Figure 15. Interferometer diagram indicating a 136mm gap between two springs.

CHAPTER 3 COMPUTER SIMULATION

The generator output Equations (8) and (9) derived are subjected to the assumptions of fast electrical pole, and small coil inductance and resistance. In order to verify the significance of the derived equations, computer simulations by means of *MATLAB* and Finite Element Analysis (FEA) are preformed. Chapter 3 focuses on simulation process by *MATLAB* and simulation by Finite Element Analysis (FEA) will be discussed in Chapter 4.

3.1 TRANSIENT VOLTAGE AND POWER OUTPUT

To serve as a preliminary study of the transient response of the generator output, a simulation of the micro generator is performed with the use of *MATLAB* program. The program written is given as a supplement in Appendix B(I). The program written makes use of the *MATLAB* built-in functions to simulate the transient behaviour of the micro generator system graphically. It begins with the input of the numerical values of the interested system parameters, which govern the system response. The transfer function is then converted to the state variable form with generated voltage as the output. Noticed that the system power output is equal to the square of the instant voltage divided by the load resistance, the average power generated by the micro generator system can be determined. An example is given in Figure 16 with the system parameters given in Table 6.

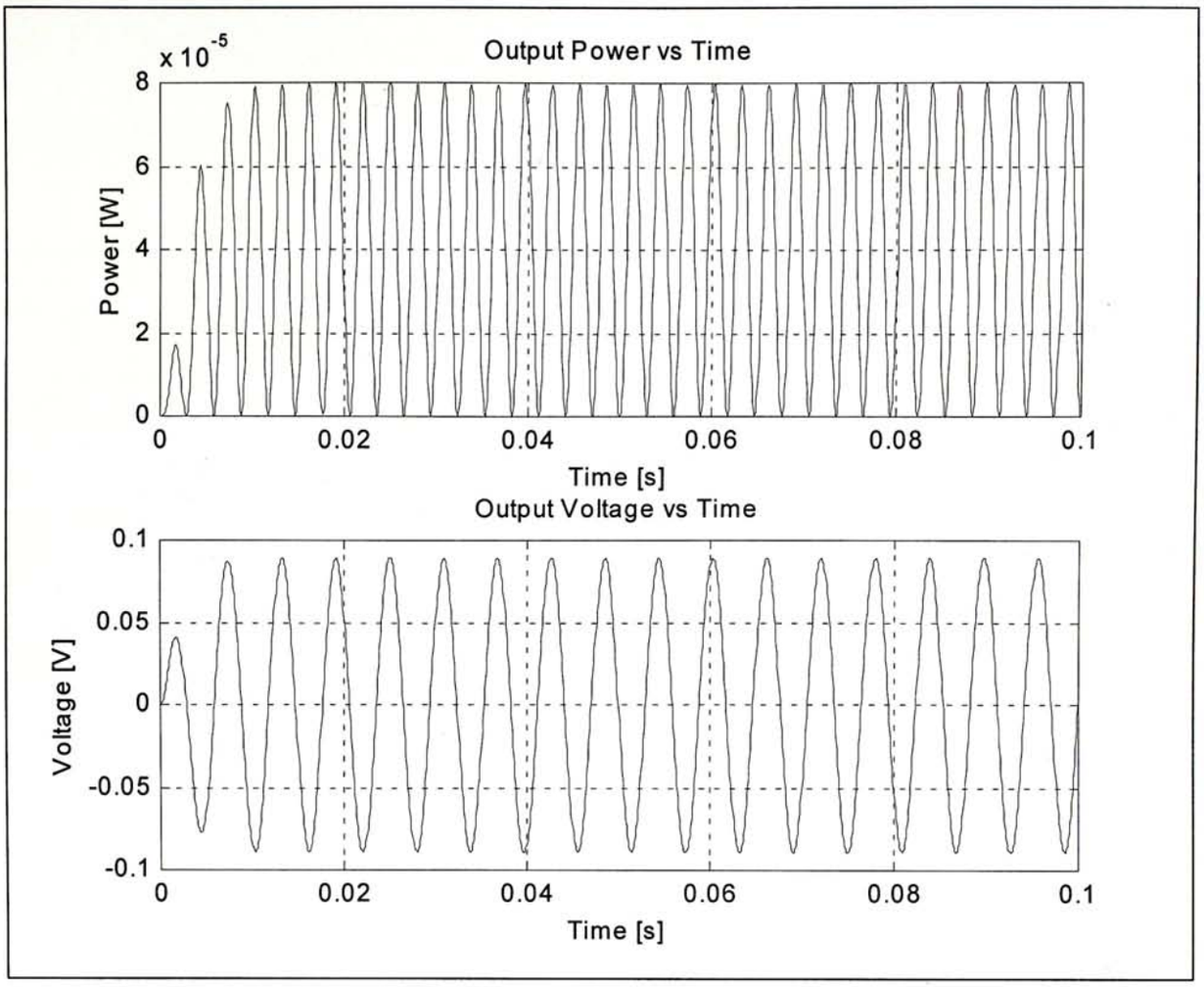

Figure 16. Prediction of transient voltage and system power output using *MATLAB* program. (System parameters are given in Table 6.)

Input Parameters			
m	219mg	R_c	10Ω
d	0.2kg/s	l	60mm
k	250N/m	B	1.312T
L	1mH	Y_0	1mm (F_0 = 0.25N)
R	100Ω	ω	ω_n = 1.0684k rad/s = 170Hz
P_{input}	133.5mW		
Output parameters			
ζ_m	0.4274	P	4.8383×10^{-5} W
ζ_e	1.3242×10^{-4}	V_0	98.4mV
ζ	0.4275		

Table 6. System parameters used in *MATLAB* program simulation in Figure 16.

Figure 16 is given as an example of a transient response of the generator system simulated by the *MATLAB* program written. From the resultant figure, it is shown that the system power output vibrates at twice the frequency of the output voltage. The numerical values of voltage and power output shown in Table 6 are the predictions by the derived Equation (8) and (9) whereas Figure 16 is the real-time response. By comparing the theoretical predictions with the transient response, it is shown that both them draw to the same numerical power and voltage results. Moreover, parametric value obtained from Equation (6) revealed that the electrical damping ratio ζ_e is, in general, much smaller than the mechanical damping ratio as shown in Table 6 because of the fast electrical pole. In other words, damping due to the electrical system may be ignored if the vibration frequency is low enough.

Equations derived in the previous chapter (e.g. Equation 8 and 9) incorporate an assumption of small coil inductance. Assuming the coil used in the micro generator

structure as a perfect copper solenoid, i.e. relative permeability $\mu_r = 1$, the inductance of the coil may be calculated by the following equation.

$$L = \frac{\mu_0 \mu_r N^2 A}{l} \tag{18}$$

where μ_0 is the free space permeability ($4\pi \times 10^{-7}$ H/m), N is the number of turns of conductor in the solenoid, A is the cross section area of solenoid and l is the length of solenoid over which conductor turns are arranged. With the use of Equation (18) and an experimental data of a 25mm diameter PCB coils ($N = 50$, $A = 1.96 \times 10^{-3}$ m^2, $l =$ 3m), the inductance of the PCB coil can be calculated to be 2.05×10^{-6}H.

3.2 SYSTEM RESPONSE WITH VARYING PARAMETERS

Even if the size of the generator is known as a priori, there are still many parameters which govern the optimisation of a generator (as stated in Table 3). Hence, the *MATLAB* program demonstrated in the previous section is modified. The revised program is able to indicate the system response by locating the peak output voltage with two pre-selected control parameters. The program source is given in Appendix B(II).

With the input parameters being the same as Table 5 in the previous chapter, the output voltage of the system with varying coil length at different frequency is shown in Figure 17. As indicated from the figure, given a constant driving input amplitude (1mm), the power output of the system may be maximized by increasing the vibration frequency. Moreover, precise control of the coil length is needed in optimising the voltage output, especially for vibration at high frequencies. A minimum of 2m long wire is required to maximize the system output voltage. By simple estimation of available area on a PCB board, a 25mm diameter single PCB coil with 10mm diameter micro generator (i.e. total area = 412mm^2) cannot be fabricated to provide a 50μm wide coil with the length more than 8.3m (i.e. 412 mm^2/50μm).

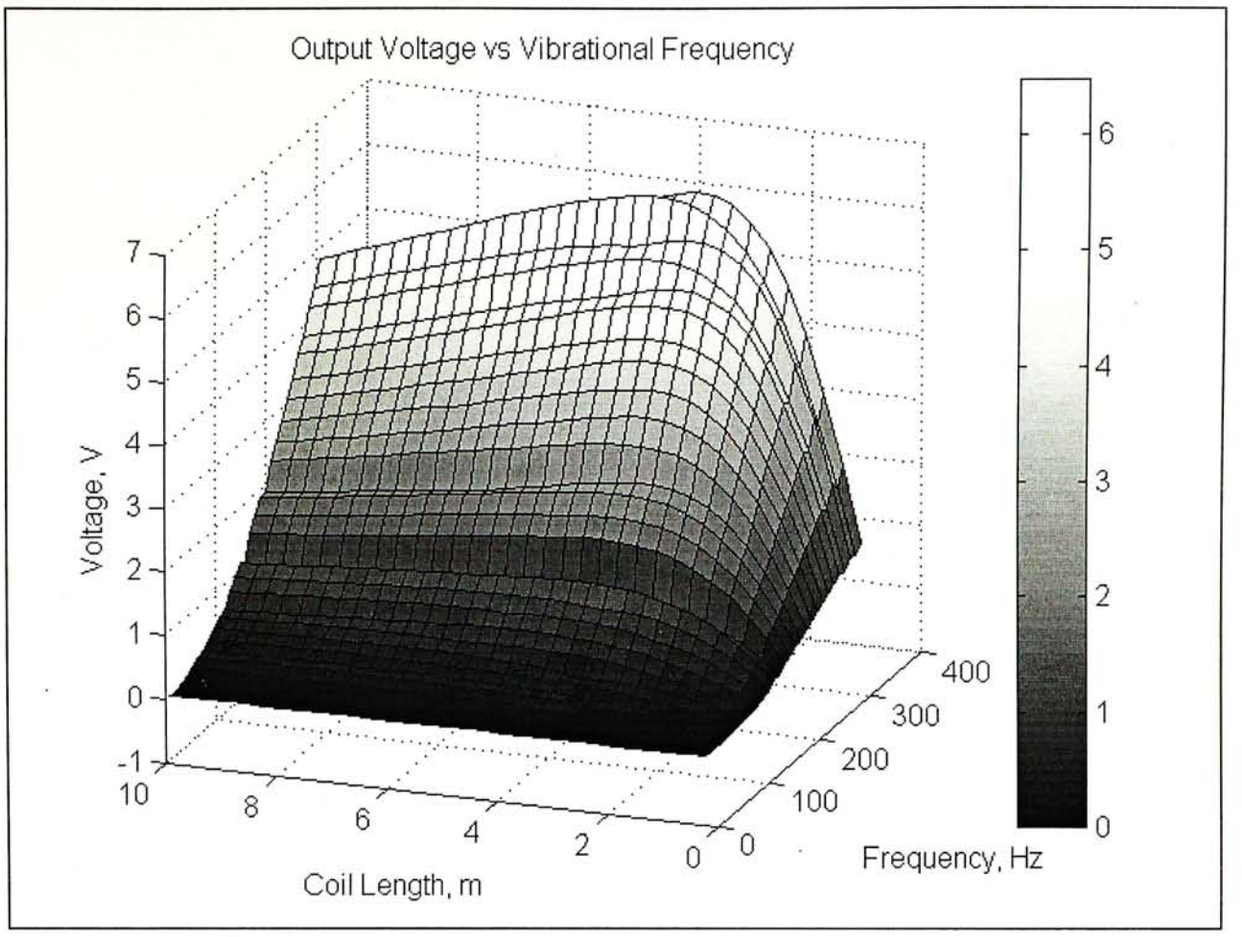

Figure 17. Output voltage vs. frequency vs. coil length simulated by *MATLAB* program.

Figure 18 demonstrates another voltage plot with the spring constant being the control parameter. Increasing or decreasing the value of the spring constant of the resonating structure in one way does not guarantee a maximum system power output. As stated in the previous chapter, the vibration resonant frequency of the system is mainly determined by the spring constant of the mechanical resonator structure and the mass of the magnet with the relationship being $\omega_n=(k/m)^{0.5}$ (Equation 4). By carefully adjusting the dimension, shape and design of the mechanical resonating structure, the vibration frequency of the system can be configured to match the environmental frequency of a specific application for resonant vibration and maximised power output.

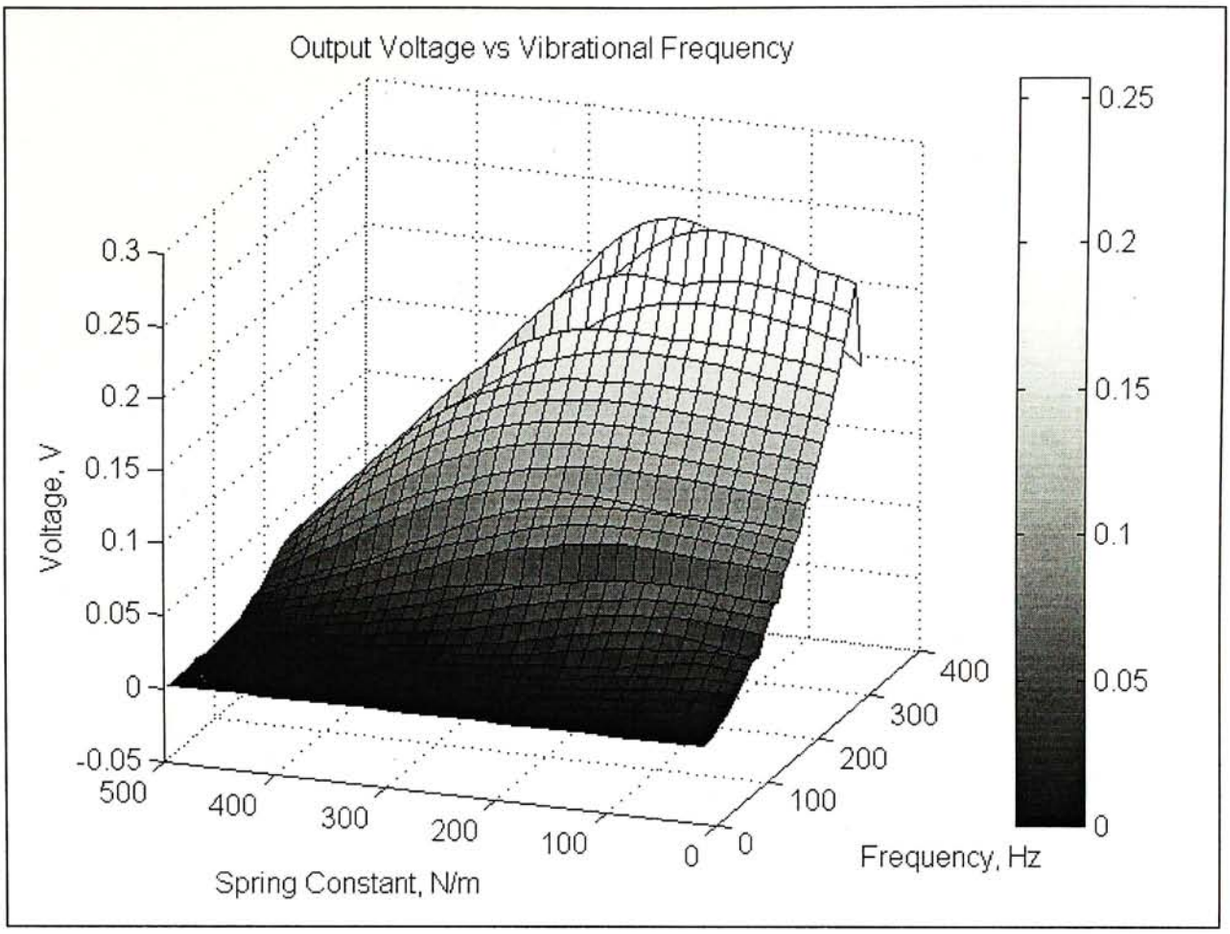

Figure 18. Output voltage vs. frequency vs. spring constant simulated by *MATLAB* program.

As stated before, there are many parameters which govern the optimisation of the system. An interesting observation is given in Figure 19, in which, the voltage output of the system is plotted as a function of the coil length and the magnetic field strength of the center magnet. From Figure 19, there exists a quadratic relationship between the coil length and the magnetic field strength for peak voltage. Further study reveals that peak voltage may be found at $(Bl)^2=Rd$. Since the magnetic field strength B is fixed for a specific magnet employed and d is usually environmental dependent, the circuit load resistance and the coil length must be carefully optimised in order to produce a maximized power output.

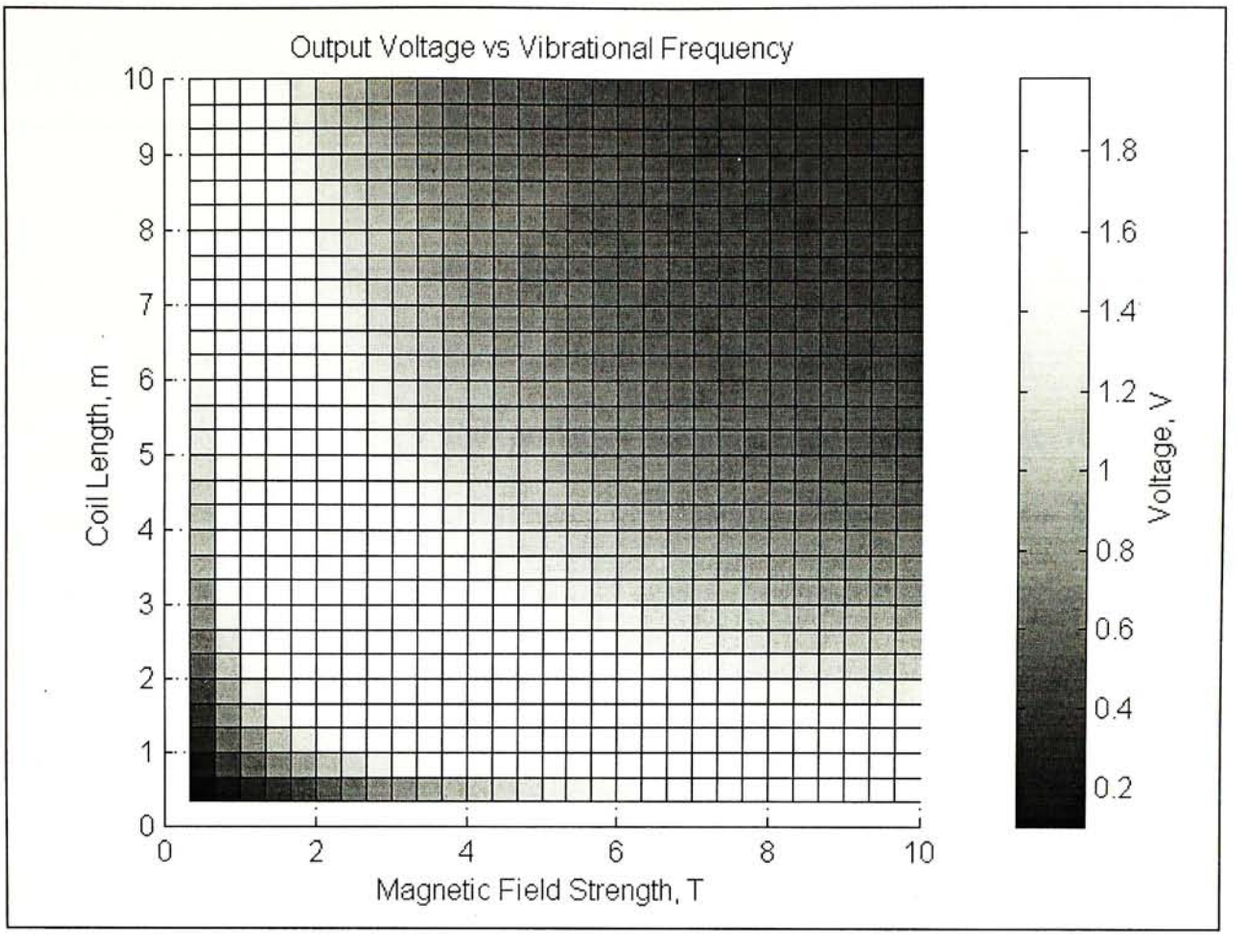

Figure 19. Output voltage vs. magnetic field strength vs. coil length simulated by *MATLAB* program.

CHAPTER 4 FINITE ELEMENT ANALYSIS

The maximization of the micro generator system performance involves complex optimisation of system parameters. Simplified governing equations and *MATLAB* simulations demonstrated in the previous chapters may not be able to provide sufficient information on the performance of a fabricated micro generator. In order to carry out a systematic study of specific design of generator for optimisation, a relatively reliable simulation method - Finite Element Analysis (FEA) is employed.

With the use of a commercially available software, *ANSYS*, the design features of the proposed micro generator are varied and studied. It is expected that FEA will help us in the areas of understanding the behaviour of individual designs as well as estimating the performance of the systems. The resultant information is important in the judgment of whether or not individual configuration, design and parametric value are able to achieve the specific goals such as obeying the frequency limitation or stress limit. Of all the analysis types available in *ANSYS*, some of them are listed in the following table.

Analysis Type	Information Provided
Structural Static Analysis	Static analysis is used to determine displacements, stresses, etc. under static loading conditions. Spring constant can be calculated from the results and is used in further simulations such as harmonic response analyses.
Modal Analysis	Modal analysis is used to calculate the natural frequencies and mode shapes of a structure. Understanding how the micro generator vibrates at which frequency range is important in the design of the resonating structure.
Harmonic Response Analysis	Harmonic analysis is used to determine the response of a structure to arbitrarily time-varying loads. Given a sinusoidal input force, the vibration and rotation amplitudes of the generator system are studied.

Table 7. List of analysis types in *ANSYS*.

4.1 STRUCTURAL STATIC ANALYSIS

A static analysis calculates the effects of steady loading conditions on a structure, while ignoring inertia and damping effects. With the use of static analyses, the spring constant and stress distribution of a particular structure can be calculated. The information collected is essential to the determination of actual reaction force acting on the resonating structure. By carefully altering the system parameters and design of the resonating structure, a maximization of the system output power is expected while the stress level on the springs being kept under limit. The actual dynamic response of the system can thus be simulated in the following-up harmonic analyses.

4.1.1 Building a Model

In order to carry out a Finite Element Analysis, a defined finite element model must be built. While adjustment of parametric values and change of design are regular in the design process, three-dimensional CAD models are usually built before Finite Element modeling as a means of geometric modeling. The resultant geometric model will be transferred to *ANSYS* and undergo further Finite Element modeling. In this paper, three types of resonating structure designs have been developed and tested. Two of them are designed at the early stage with the use of Si bulk-micromachining technique and the last one is designed for copper laser micromachine in general. Even thought not all of the structure designs are employed in the latter experiments due to unsatisfactory performance or high stress concentration, their geometric models are shown in the following figures.

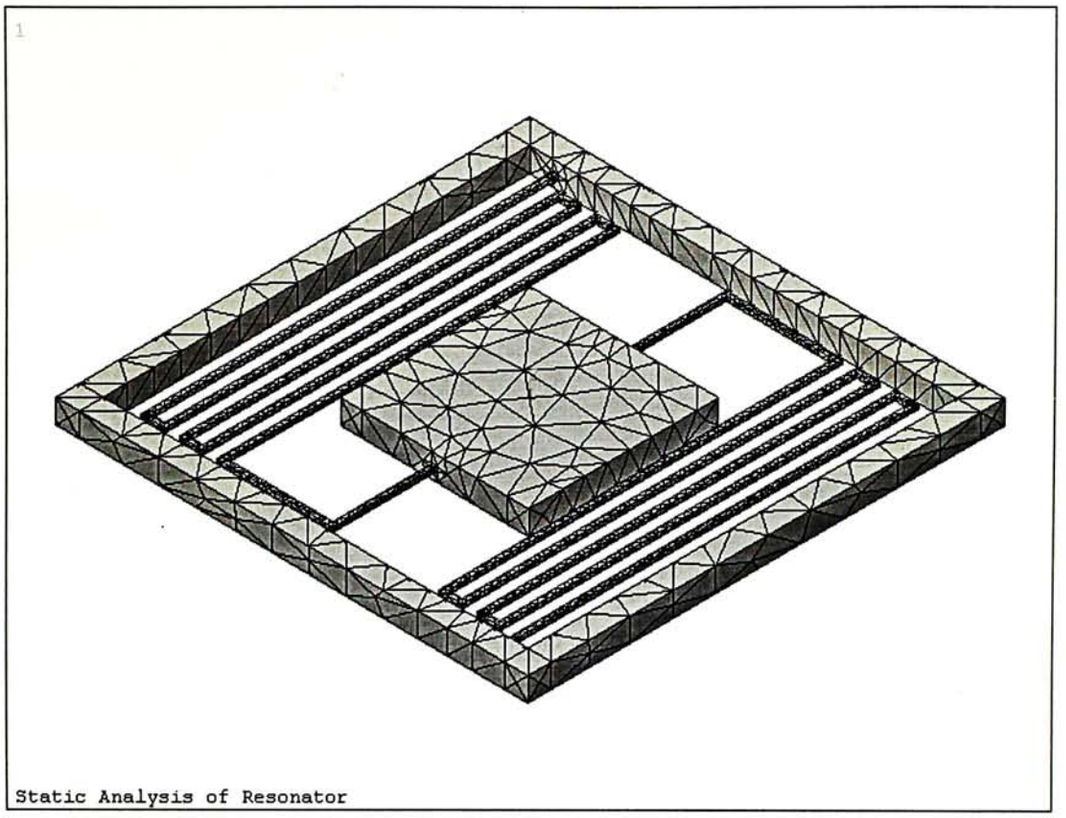

Figure 20. Finite element model of a micro generator with zigzag form of silicon springs.

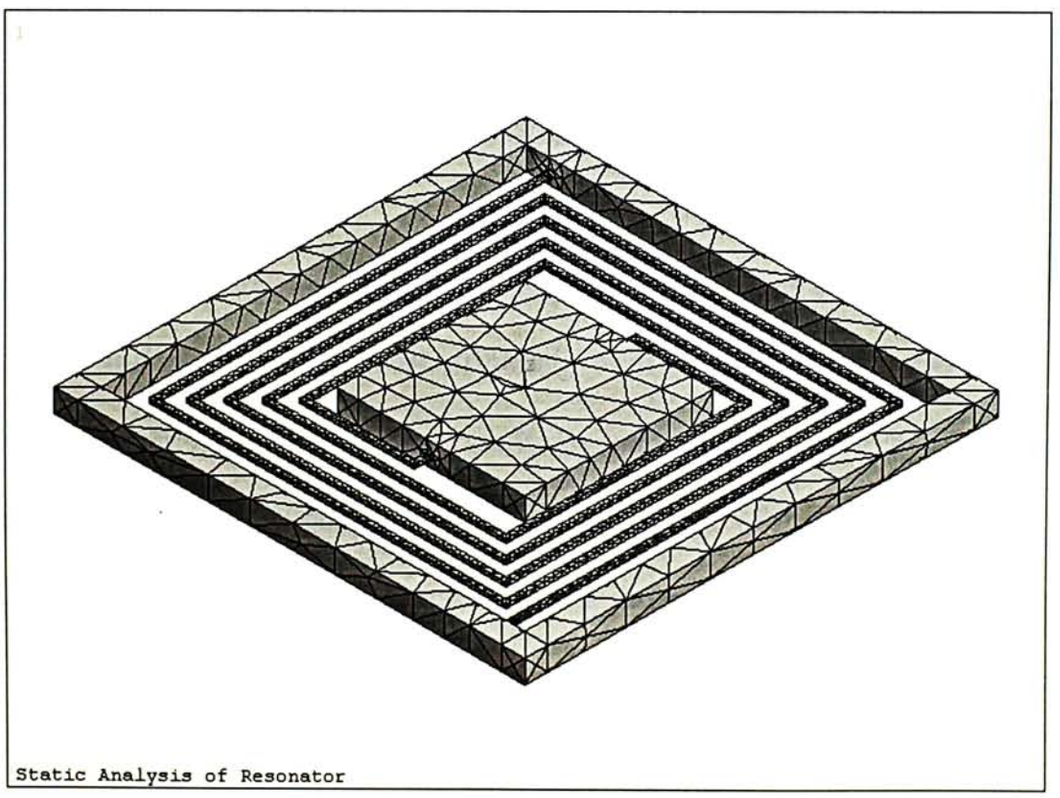

Figure 21. Finite element model of a micro generator with spiral form of silicon springs.

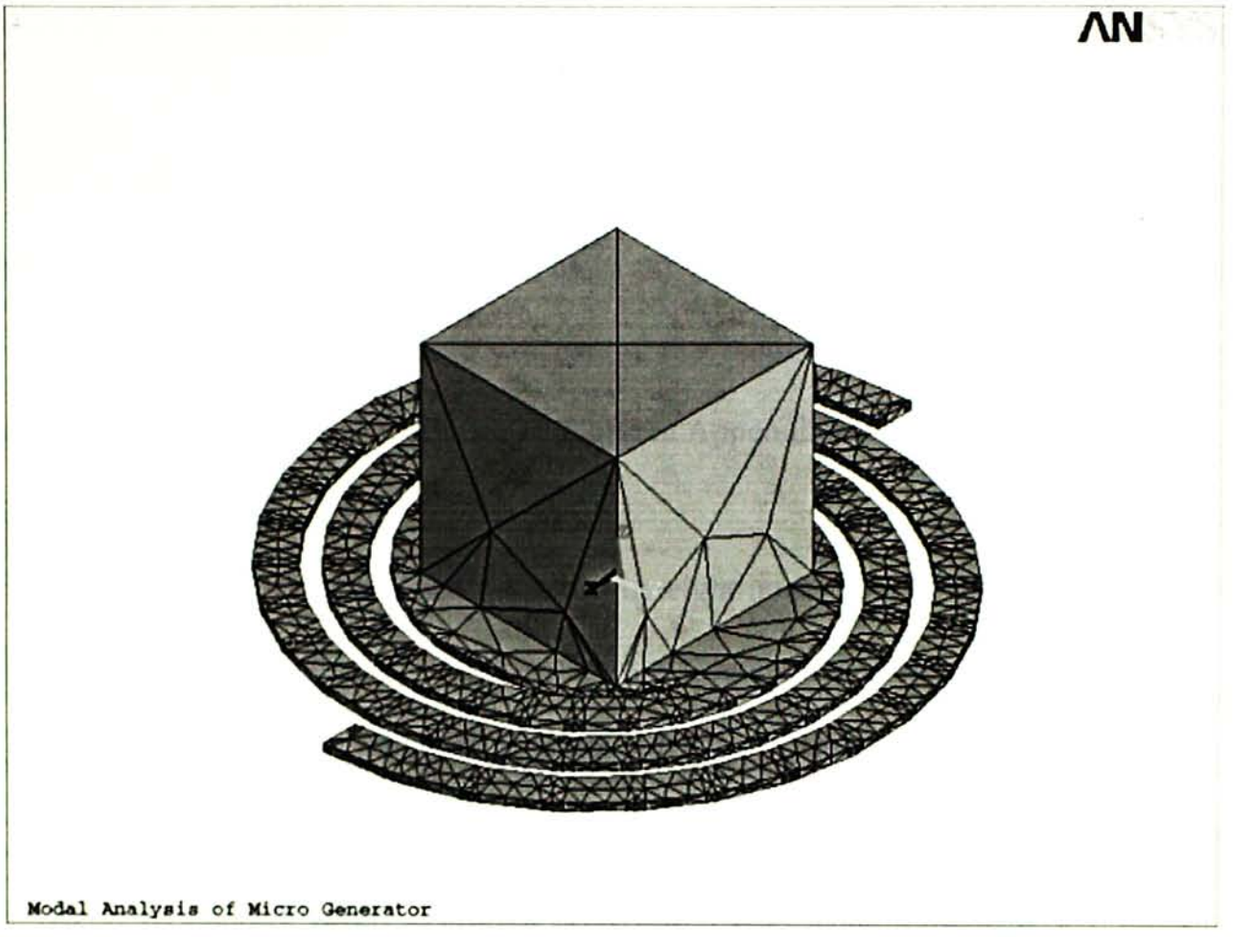

Figure 22. Finite element model of a micro generator with circular spiral copper springs.

Two rectangular vibrating structures with different patterns of springs are shown in Figure 20 and 21. The models are originally built for silicon bulk micromachining at the early stage. However, further study on stress distribution by Finite Element Analyses reveals high concentration at the turning edge of the springs in both designs. A round micro generator with circular spiral springs is shown in Figure 22. The model is designed for laser micromachining with copper and is currently undergo repeated experimental study and parametric readjustment.

Repeated simulations and frequent adjustment of design parametric values are essential in the process of development through Finite Element Analysis. In order eliminate the extra effort on building additional geometric models for each design with parametric change, automation through programming is performed. With respect to each of the described models in Figure 20, 21 and 22, an *AutoLISP* program is written to enhance the building process of the required model in *AutoCAD*. The complete program source codes can be found in Appendix C.

A three-dimensional solid element defined by eight nodes is used to model the micro generator structure (Figure 23). There are six Degrees Of Freedom (DOF) on each node (i.e. translations in the nodal x, y and z directions, and rotations about the nodal x, y and z axes) making up an element with a total of 48 DOF. In additional to the standard prism shaped elements, tetrahedral, wedge and pyramid shaped elements may also be formed as an option.

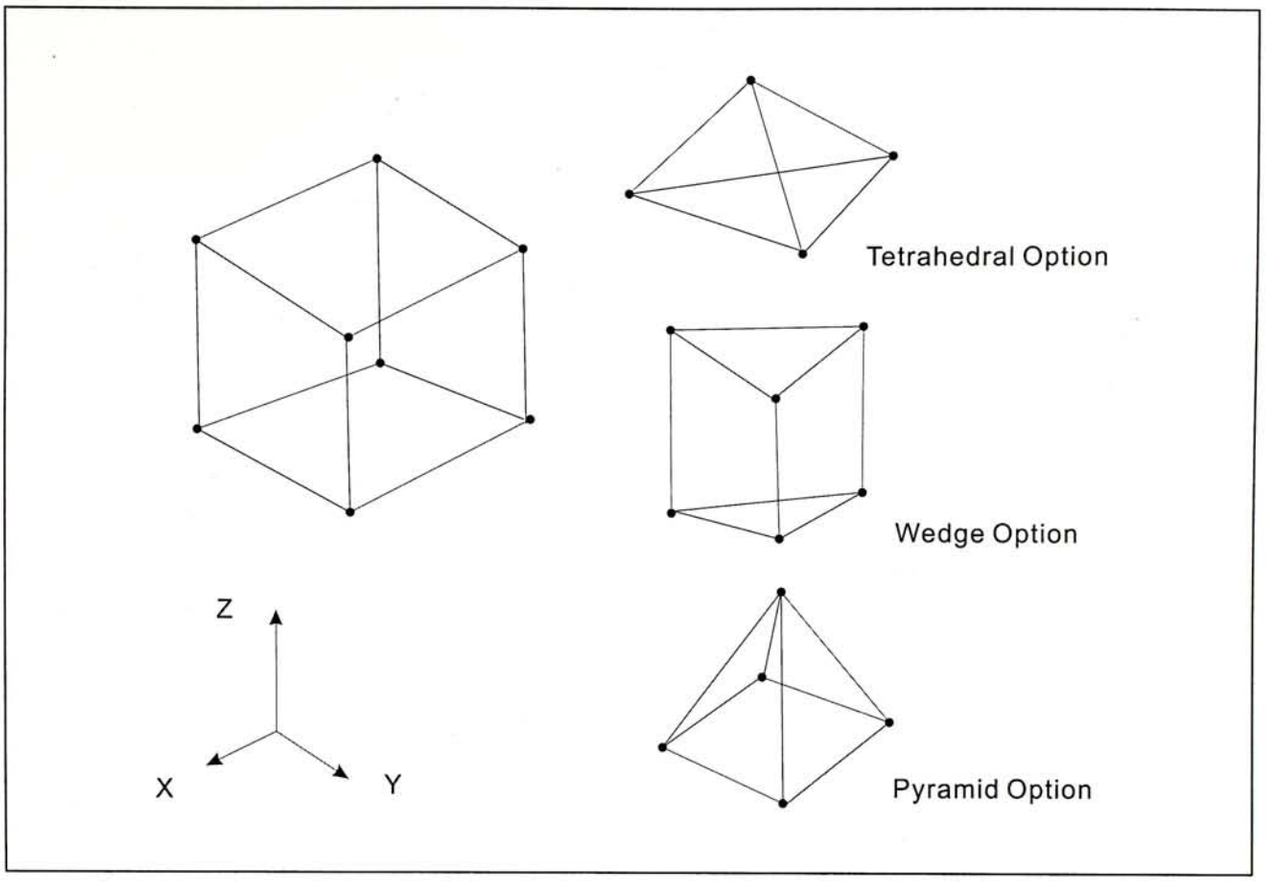

Figure 23. Three dimensional solid element with eight nodes.

4.1.2 Material, Loading And Boundary Condition

The main goal of Finite Element Analysis is to examine how a structure or component responds to certain loading conditions. Therefore, specifying the proper loading, material property and boundary conditions is a key step in the analyses. In the real situation, we would expect a sinusoidal driving force (no matter it is a translation or rotation force) acting on the frame of the resonating structure, vibrating the magnet at the center. However, Finite Element models with no fixed boundary node always lead to a unstable system and, thus, a divergent solution. Meanwhile, a single driving input load is assumed be applied at the center node of the magnet (Figure 24) instead of a vibrating frame driving the entire structure.

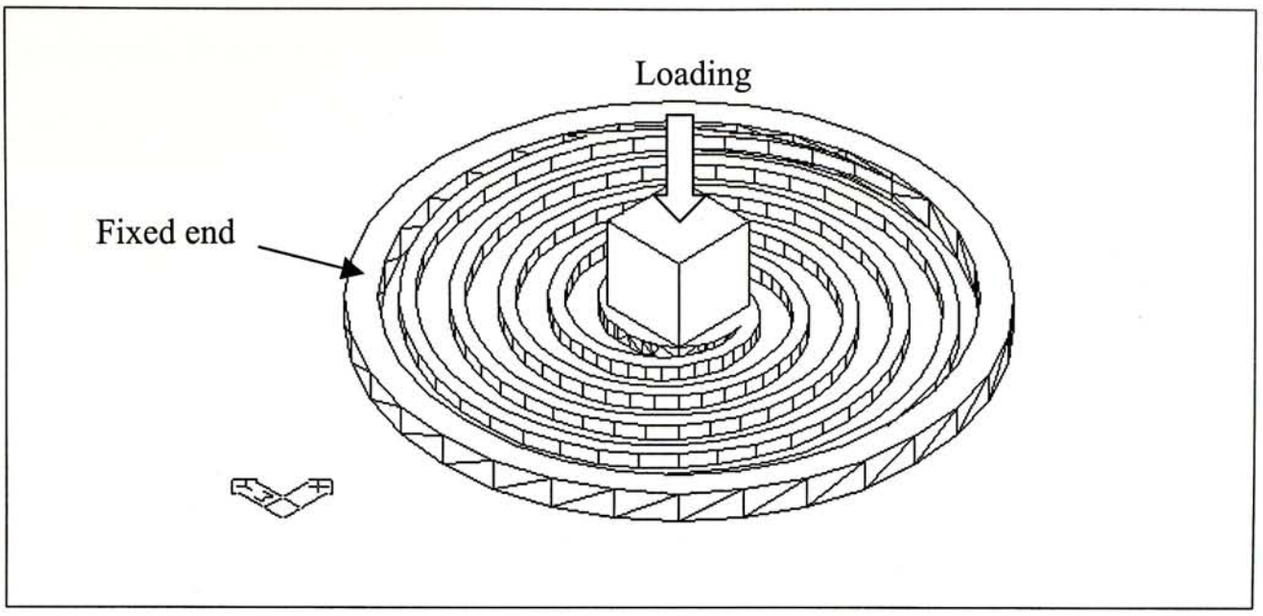

Figure 24. Loading at micro generator.

The material properties (Nd-Fe-B magnet and copper springs) are assumed to be linear isotropic with large deflection and stress stiffness accounted in the harmonic analyses. A single DOF boundary condition constraint is added to the mechanical resonating system of the micro generator representing the fixed still frame.

4.1.3 Comparison Between Generator Designs

In order to compare the performances of different generator designs and to verify the significance of Finite Element results through *ANSYS*, standard stress distribution analyses are performed. In this section, generators with zigzag and spiral patterned springs are under Finite Element Analysis study and a comparison of their performances is made. The aim of these analyses is to verify that the spiral springs are able to provide better performance than the zigzag ones, in term of space utilization, deflection capability as well as stress withstanding. Given the same configuration and parametric values including the structure size, spring dimensions and magnet

properties, Finite Element Analyses results will indicate that the spiral springs are able to provide more deflection and, thus, higher power output, with less stress level than the zigzag springs.

The Finite Element models of the two resonating under test are shown in Figure 25. The modeling techniques employed in modeling the zigzag springs are the same as those described in the pervious section. The overall structure is modelled by the 8-node 3D solid elements, each node having 6 DOF. On the other hand, the spiral patterned spring resonating structure is modelled in quite a different way than what we have described for minimizing the total computational resources required in the simulations. The magnet is modelled the same way as the zigzag case whereas the spiral springs and the round mass support are modelled by the 2-node 3D uniaxial beam elements (each node having 6 DOF) and the 4-node 3D shell elements respectively. The mass support in the spiral case is used as a connection between the center magnet and the spiral springs. Theoretically, the round mass support under the magnet does not make significant contribution to the performance of the overall structure as the springs are comparatively much flexible than it. Moreover, the extreme large aspect ratio (long springs with small cross section area) of the spring elements makes it a good approximation to model the springs with beam elements instead of solid elements. The usage of 2-node beam elements may reduce the unnecessary extra computational resources required. An *ANSYS* program of Finite Element Analyses with spiral generator is provided in Appendix D.

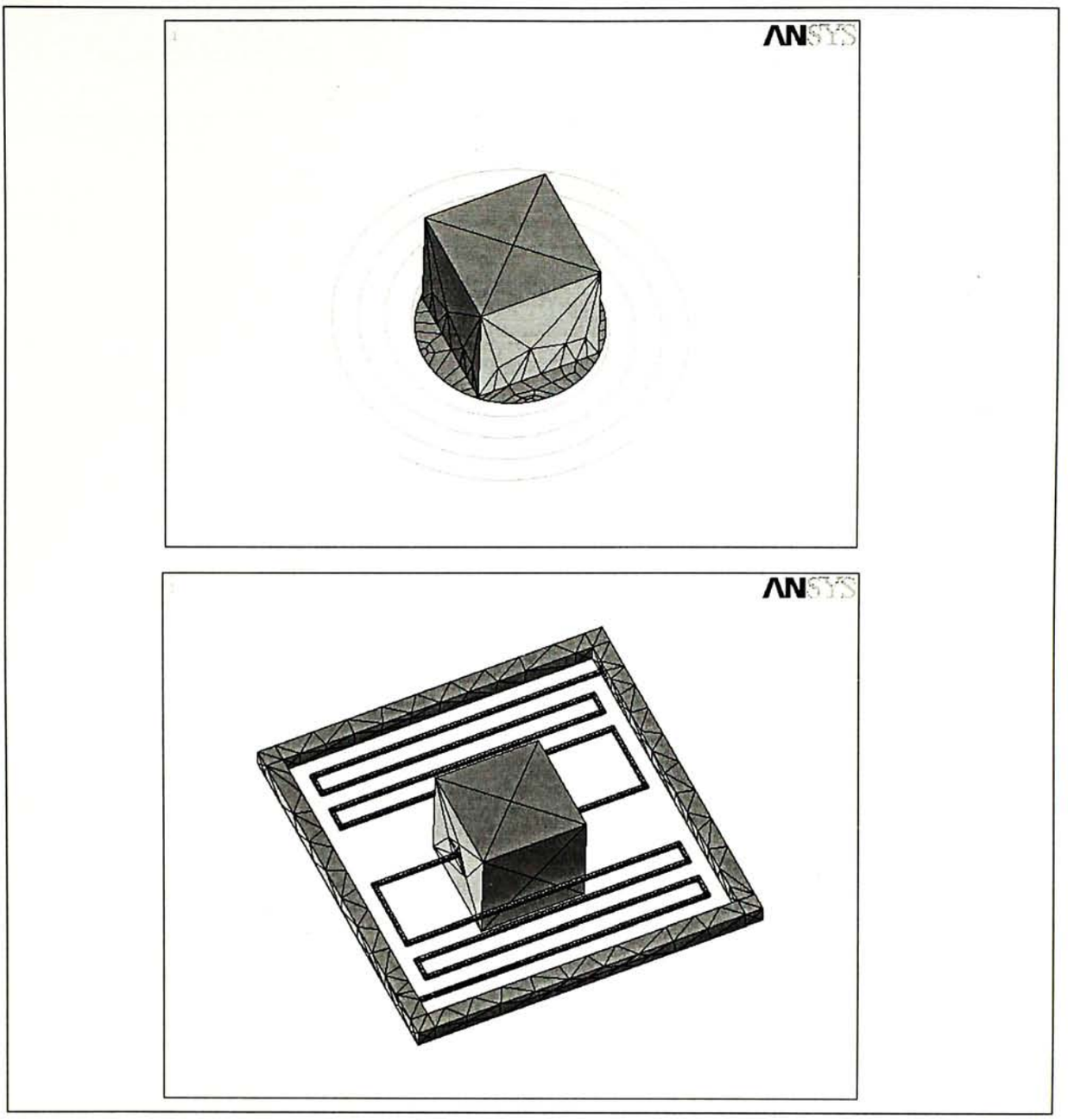

Figure 25. Finite element models of resonanting structures under *ANSYS* simulation.

Both the structures are assumed to be made with the same material – copper for consistent comparison. The parametric values used in the simulations are listed in Table 8. With a single load applied at the center of the magnet, the resultant deflection and maximum stress are shown in Table 9.

Component Type	Parameter	Spiral	Zigzag
	Generator size	10mm x 10mm	
Spring	Width	0.1mm	
	Thickness	0.11mm	
	Number	2	
	Gap distance	0.5mm	
	Total length	79.1mm	76.9mm
	Spring constant	3.47N/m	6.64N/m
	Young's modulus	110GPa	
	Poisson's ratio	0.35	
	Density	8960 kg/m^3	
Frame	Cross-section	0.5mm x 0.5mm	
Magnet	Dimension	27mm^3 cube	
	Density	8120kg/m^3	
	Mass	219mg	
	Young's modulus	207GPa	
	Poisson's ratio	0.28	

Table 8. Parametric values used in Finite Element simulations.

	Spiral	Zigzag
Spring constant	3.47N/m	6.64N/m
Stress / Input force	2.05GPa/N	13.4GPa/N

Table 9. Comparison between spiral and zigzag springs.

Table 9 indicates the spring constant and the resultant maximum stress of the two generator designs. The spring lengths of the two structures are kept to be closed (spiral: l=70.1mm, zigzag: l=76.9mm) with the same configuration as stated in Table 8. The springs pattern in the spiral form are able to provide twice as much deflection as those in zigzag form. Hence, a higher power output may be generated with the

spiral springs. Since stress concentrates most at the turning edges of the springs (Figure 26), spiral pattern is able to spread the stress distribution and reduce unwanted high stress concentration. Meanwhile, a spiral spring may withstand higher amplitude of vibration and sudden shock.

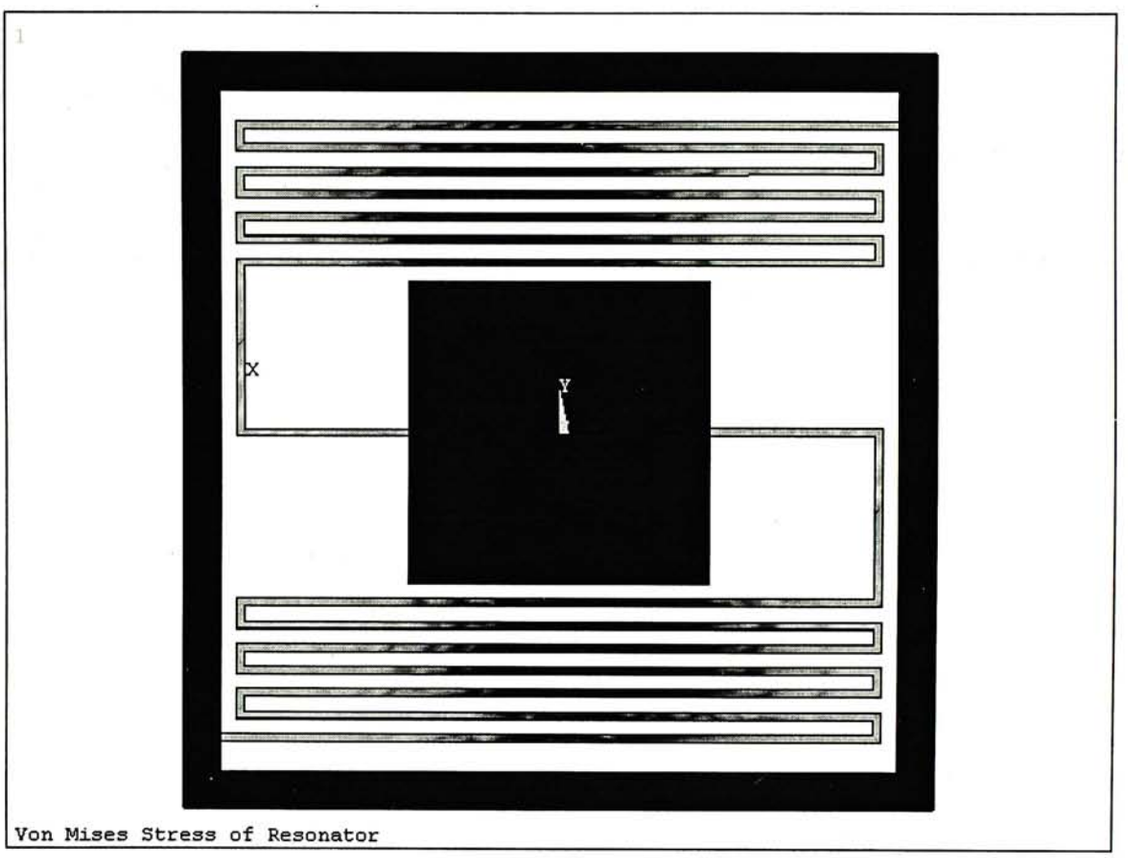

Figure 26. Stress distribution of a micro generator with zigzag patterned springs. (Higher stress level is indicated in light colour.)

4.2 MODAL ANALYSIS AND HARMONIC RESPONSE ANALYSIS

Modal analyses and harmonic response analyses are the follow-up analyses of the static analyses used to study the dynamic response of the generator structures. A brief introduction of the two analyses are given in this section and their corresponding results will be discussed in Chapter 5, with the comparison with the experimental results.

Modal analysis is used to determine the dynamic vibration characteristics such as natural frequencies and mode shapes of a structure. In the case of the study of micro generator performance, modal analyses are used as a starting point for another, more detailed, dynamic harmonic response analysis. The natural frequency and mode shapes determined are important parameters in the design of the resonating structure for dynamic loading conditions. By monitoring the design features of the resonating structure, the vibrating frequency may be kept to the desired frequency range.

Harmonic response analysis is a technique used to determine the steady-state response of a linear structure to loads that vary sinusoidally with time. Any sustained cycle load will produce a sustained cyclic response in a structural system. Harmonic response analysis is used to predict the sustained dynamic behaviour of a structure, thus enabling one to verify whether or not a design is able to successfully overcome resonance, fatigue, and other harmful effects of forced vibrations.

4.3 NONLINEARITY

Nonlinear structural behaviour arises from a number of causes, which can be grouped into two principal categories – geometric nonlinearities and material nonlinearities. In this section, a brief discussion on how nonlinearity affects the results of Finite Element Analysis is presented and the corresponding assumptions are provided.

If a structure experiences large deformations, its changing geometric configuration can cause the structure to respond nonlinearly. An example would be the spring deformation under heavy load. Under light lateral loads, the spring is extremely flexible with low lateral stiffness. As lateral load increases, the spring deflects so much that the moment arm decreases appreciably. Hence, large deformation is unfavourable in Finite Element Analyses.

Besides the shortening of moment arm of spring, large deflection can also cause the spring to undergo increasing stiffness at higher loads. The overall stiffness of a structure depends on the orientation and individual stiffness of its elements. As the nodes of an element undergo displacement, the contribution of that element to overall structural stiffness can change in two ways. First, if the shape of an element changes, the element stiffness will change. Second, if the orientation of an element changes, the transformation of the local stiffness into global components will also change.

Small deflection employed in Finite Element Analysis assumes that displacements are small enough that the resulting stiffness changes are insignificant. Experimental results indicate a maximum transverse deflection of 7mm for a 55mm long copper

spring. Meanwhile, small deflection is assumed in FEA simulations.

4.4 PROBLEM ENCOUNTERED

While Finite Element Analysis is only an analytical simulation of the real system, approximations and assumptions must be made to overcome problems encountered during simulations. The occurrence of nonlinearity was discussed in the previous section. It leads to the increase of computational complexity and, sometimes, unconvergent solution. In order to simply the computational process, linear physical and material properties were employed.

Generator system response is affected by noises such as fabrication deviation, resistance, driving force variation and magnetic induction. Some of these parameters, such as the damping ratio (caused by resistance), may be estimated from the experiments and some may not. In the determination of system response with FEA, experimental values were often used in place of parametrically designed values. For example, a constant 16mN input driving force is employed in the harmonic analyses even if the generator structure is not designed for a specific constant loading.

FEA requires an unavoidable procedure of dividing the whole structure into many tiny elements. Since the formation of pattern of element mesh is arbitrary, singularity may occur, leading to unconvergent solution or even misleading result. During the development of micro generator in this project, experiments are often performed as a verification of the FEA results. By comparing the experimental results with the theoretical simulations, mismatch of performance may be located and, hopefully, corrected.

CHAPTER 5 COMPARISON OF MODELING AND EXPERIMENTAL RESULTS

The development of our micro generator involves parallel studies on computer simulations and experiments (Figure 1). Based on the simulation results from repeated trials of Finite Element Analyses, prototypes of micro generators were fabricated and tested. This chapter focuses mainly on the experiments carried out to study the performance of the fabricated structures. The equipment setup and measuring techniques are discussed in the first section. Finally, a comprehensive comparison between the Finite Element Modeling simulations and experimental results are presented.

5.1 EXPERIMENT SETUP

5.1.1 Generator System

The fabricated generator prototype is composed of three parts: the micromachined springs, the magnet and the coil structure. As stated in the previous chapter, we have used a Nd:YAG laser machine to micromachine the copper spring resonating structure (Figure 27). Due to the extraordinary small size (~1cm^2) and thickness (~110μm) of the fabricated resonating structure, a housing structure is designed for the attachment of the springs.

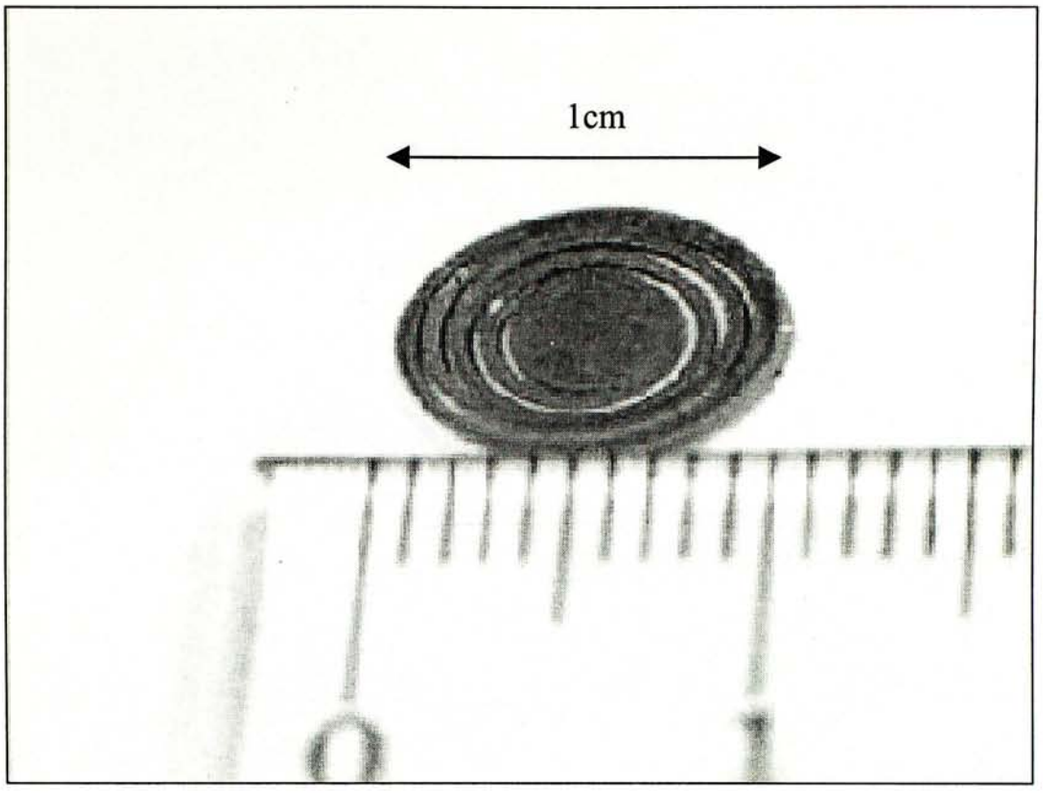

Figure 27. A micromachined copper spring with 1cm diameter.

Two types of fabrication techniques have been tested to fabricate the coil structure: hand-wired coil and Printed Circuit Board (PCB). The hand-wired coil structure is composed of the coil, the outer housing for the coil and the inner housing of the spring. The housing is fabricated by a rapid prototyping machine (*StrataSys* FDM 1600 RP Machine) using ABS plastic. A coil structure is shown in Figure 28. The entire housing has a diameter of 15mm, a height of 7mm, and allows 1500 turns of insulated 50μm diameter coils. A $27mm^3$ magnet cube is attached on the copper laser-micromachined springs and the springs are fixed in the middle of the coil structure. The ends of the coil are connected to a CRO for voltage reading. The micro generator is then mounted on the vibrator for further experiment (Figure 29 and 30).

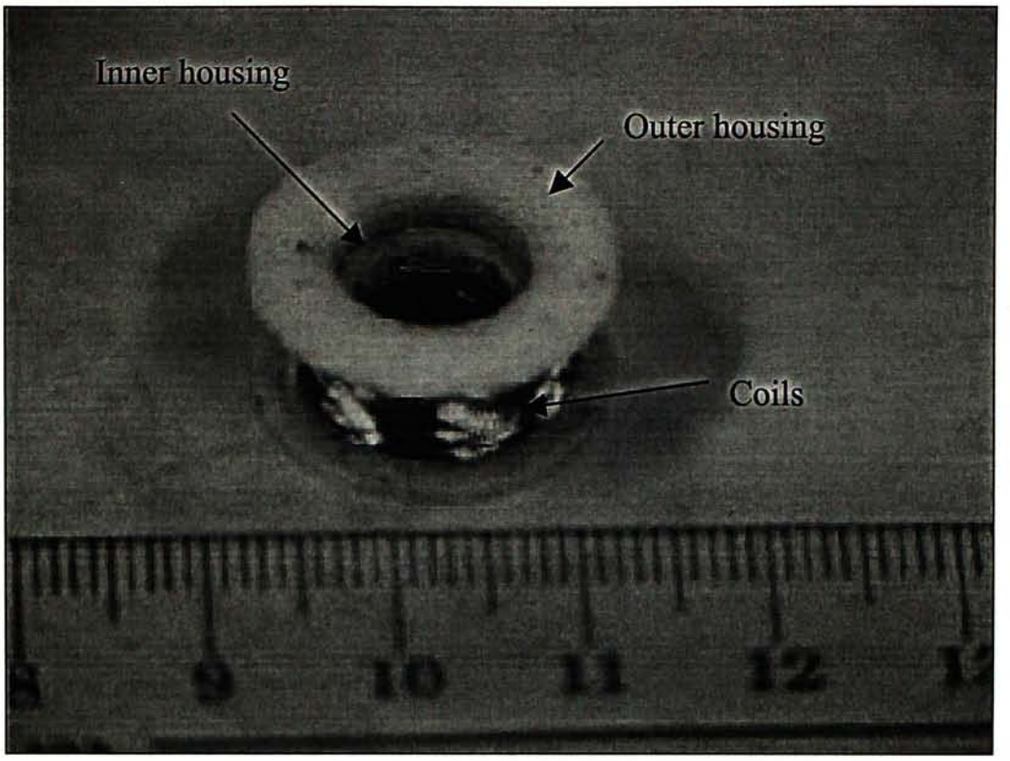

Figure 28. A 15mm diameter coil structure with ABS plastic housing.

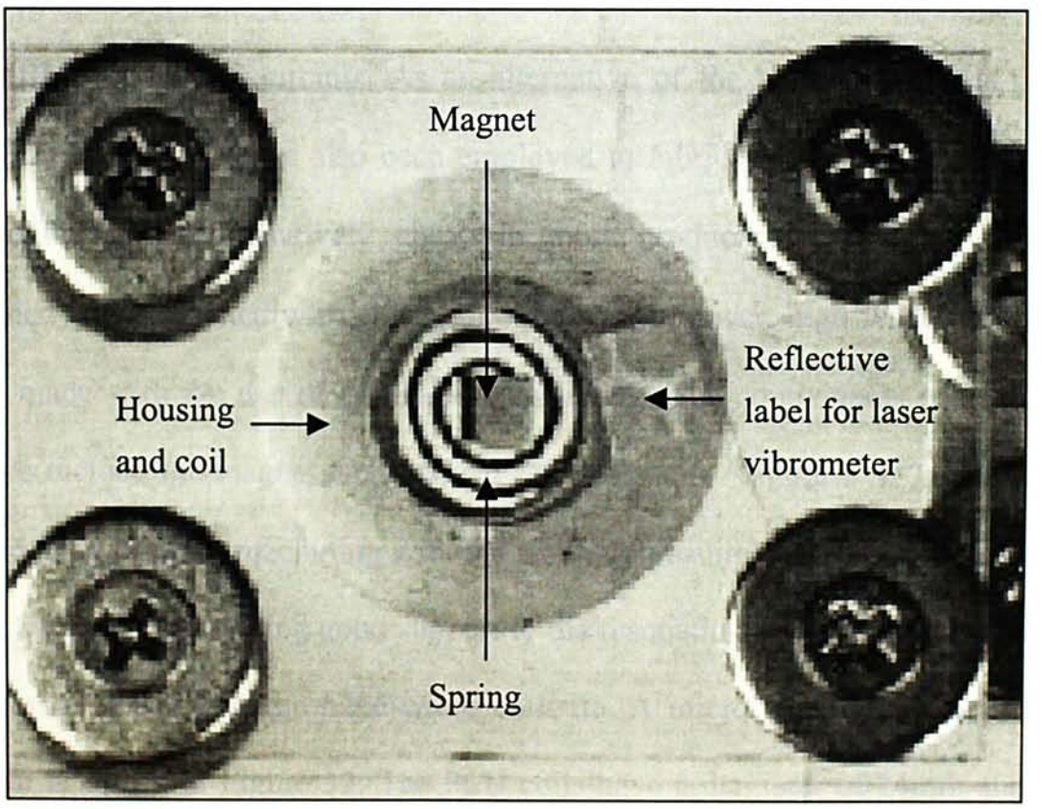

Figure 29. Micro generator structure with hand-wired coils. (Top view)

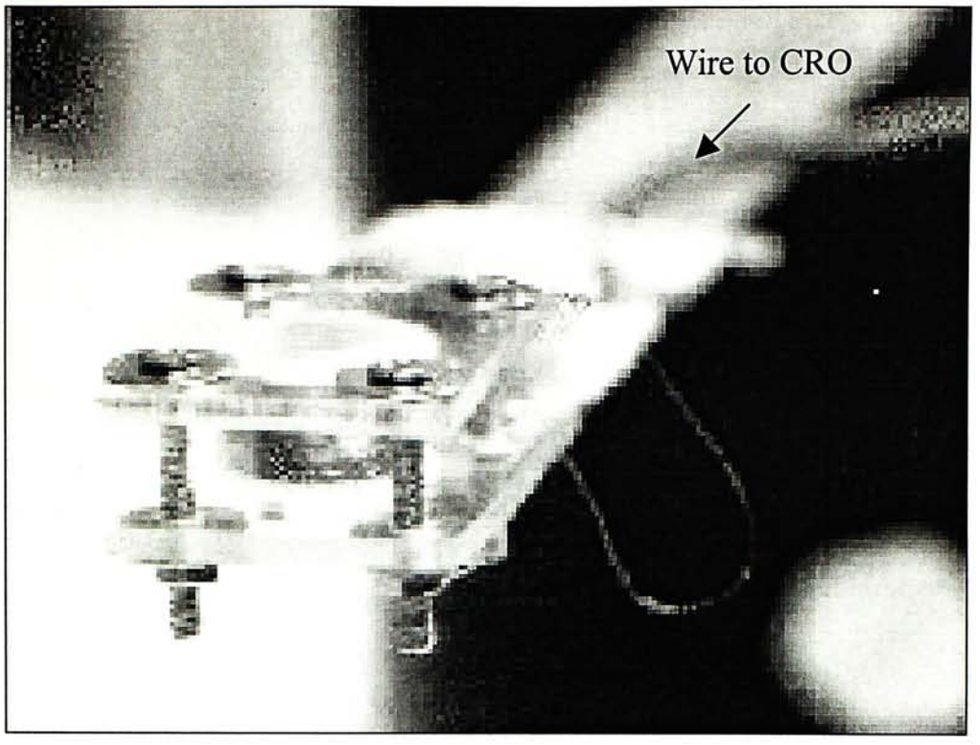

Figure 30. Micro generator structure with hand-wired coils.

The hand-wired coils are, in general, macro in size and suffer from incompatibility with MEMS or CMOS circuits. As an alternative of the hand-wired coils, Printed Circuit Boards (PCB) have also been employed to fabricate the coil structure. Coils made with PCB are relatively cheap in mass production. They can be easily assembled and integrated with electronic circuits. Moreover, high resolution of coils can be made with the use of laser micromachining. The components of a PCB coil structure include the magnet, springs and the PCB coils (Figure 31). The PCB coils are fabricated by laser machining with the resolution as high as 80μm per turn. Since PCB is capable of providing good support to the resonating structure, there is no need for a plastic housing as the hand-wired coils do. A micro generator with PCB coil structure is shown in Figure 32. The PCB coils have a diameter of 24mm and allow 48 turns of coils, making a total of 2.7m long wire.

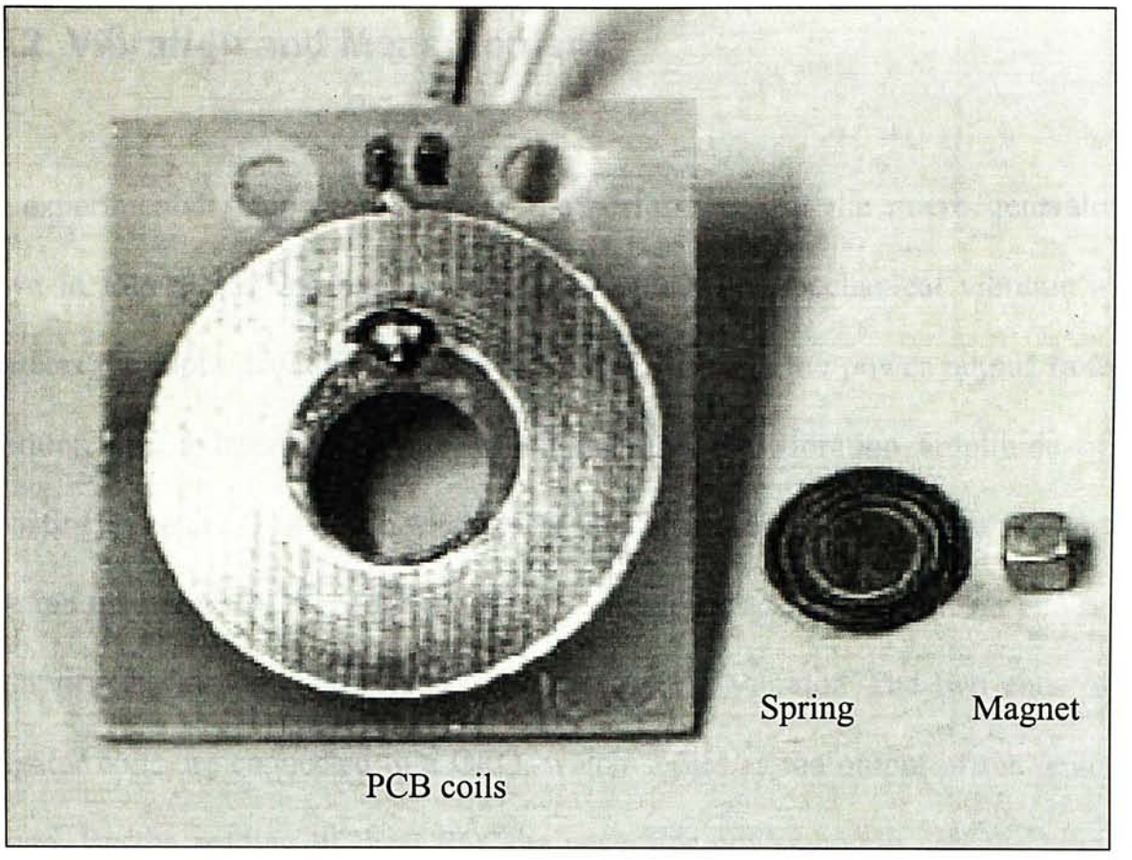

Figure 31. Components of PCB coil sturcture.

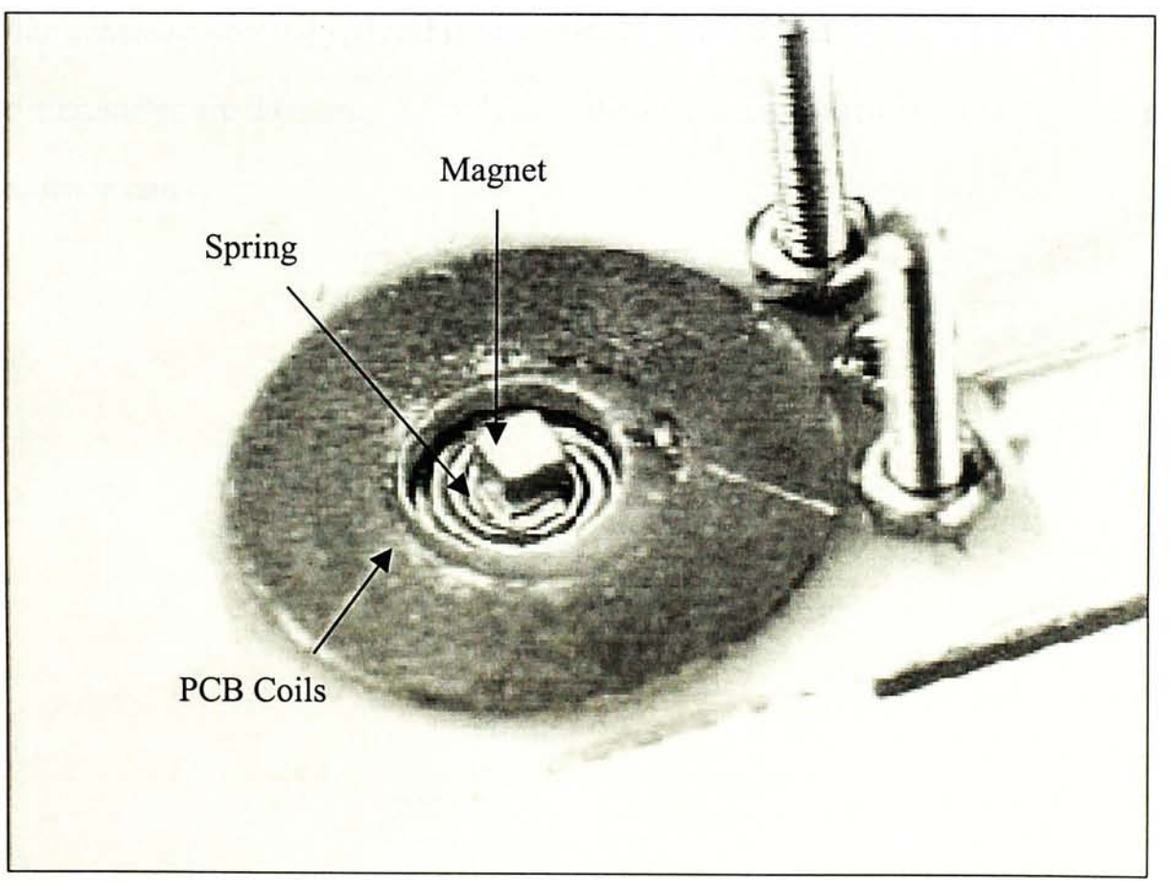

Figure 32. Micro generator structure with PCB coils.

5.1.2 Vibration and Measurement

The experimental setup used to study the performance of the micro generators is shown in Figure 33. The required equipment include a mechanical vibrator which generates the input driving force, a CRO which displays the power output from the generator, and a laser vibrometer which measure the vibration amplitude of the resonating structure. The micro generator is attached to an aluminium bar fixed on the vibration membrane of the vibrator. The aluminium bar acts as a cantilever and is able to amplify the vibration amplitude generated by the vibrator. The two ends of the generator coils are connected to a CRO, which serves as the output of the generator voltage. By the reading of the CRO, the generator power output and the vibration frequency may be recorded. A laser vibrometer is used to measure the vibration frequency of the device. With the use of the laser vibrometer, the vibration amplitudes of the generator housing $y(t)$ and the magnet $z(t)$ may be measured. The readings from the vibrometer are then used to study how the resonating structure vibrates at certain frequency range.

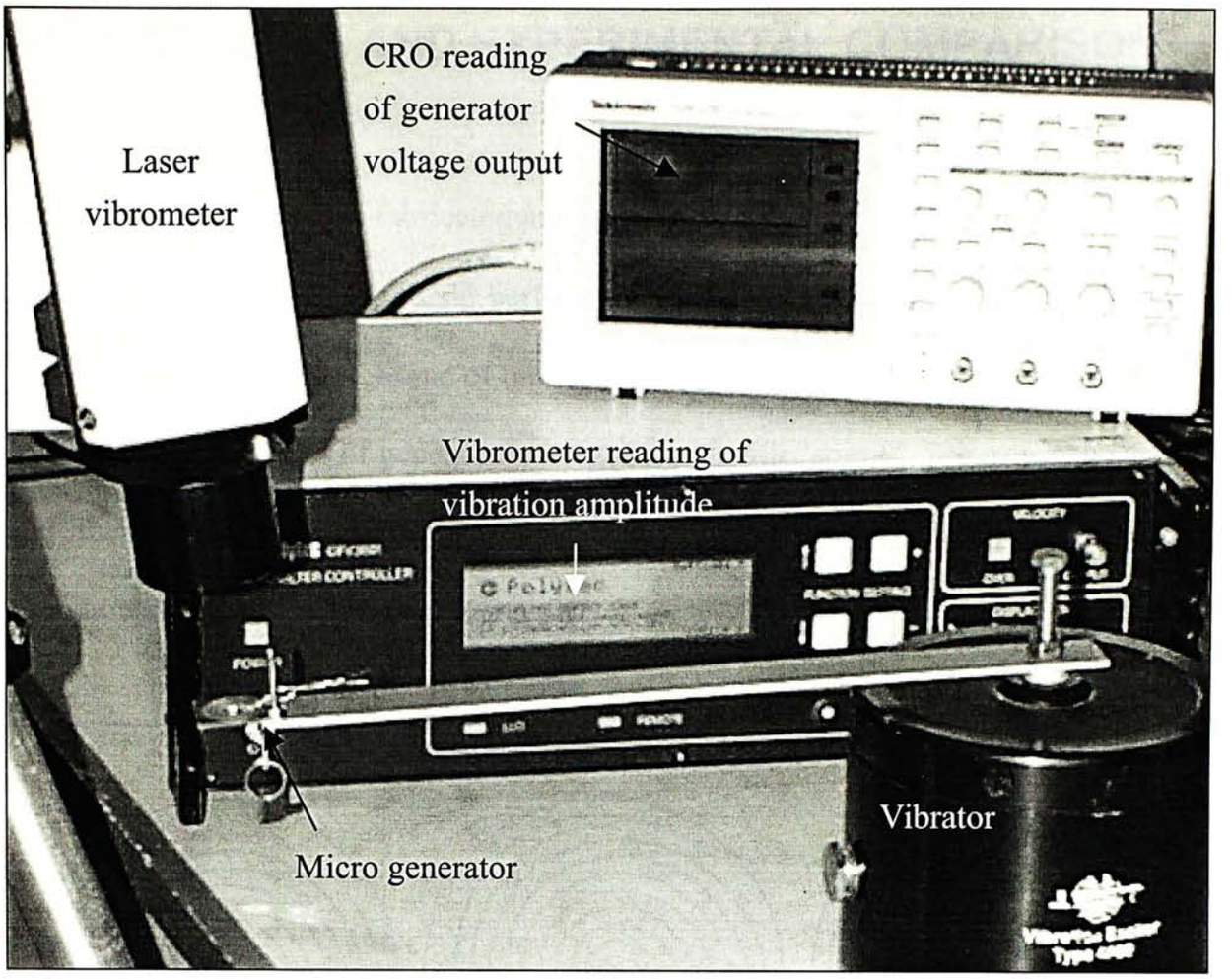

Figure 33. Experimental setup.

5.2 MODELING AND EXPERIMENTAL COMPARISON

Among all the prototypes fabricated and tested, the so called "spiral" spring design is found to provide the most stable performance while being capable of providing the greatest amount of power. Some of the "spiral" spring designs are shown in Figure 34. In this section, two sets of generator configurations with "spiral" springs are presented and their corresponding experimental results are compared with the theoretical simulations using Finite Element Analysis.

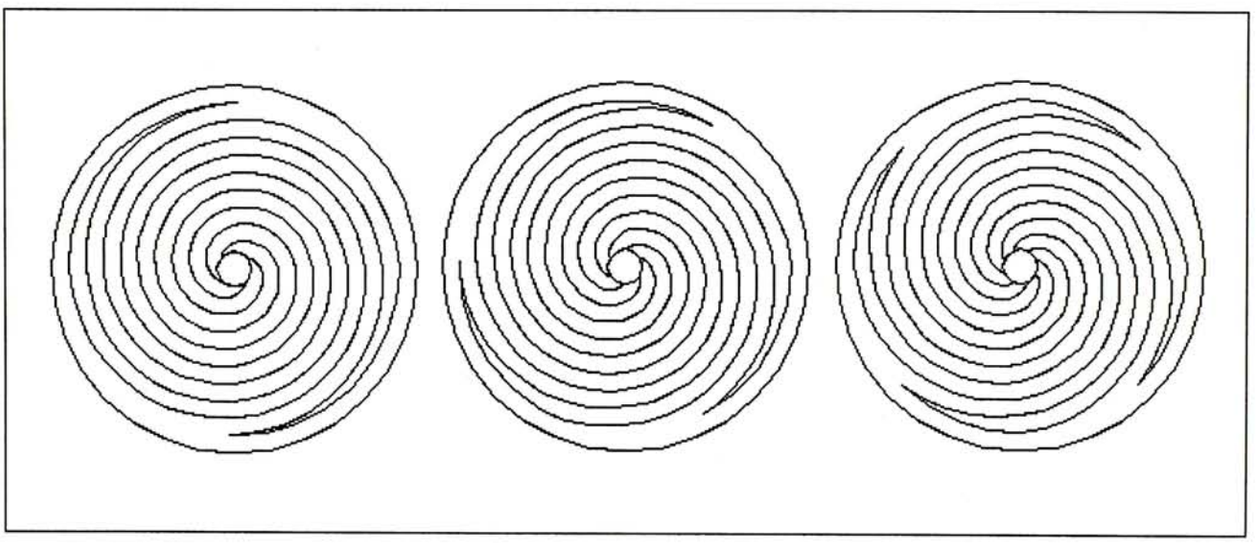

Figure 34. Spiral springs.

The experimental parameters used in testing the two micro generators are listed in Table 10. The first set of experiments makes use of the PCB coiling technique while the second uses the hand-wired coils as presented in the previous section. Both of the prototypes are ~1cm^3 in size with two laser micromachined copper springs patterned in the form of spiral lines. The dimensions of the springs, i.e. width and thickness, are carefully adjusted such that the two resonating structures have more or less the same length of effective springs.

	PCB coils	Hand-wired coils
Design	10mm x 10mm spiral with 2 copper springs	10mm x 10mm spiral with 2 copper springs
Magnet	3mm cube	3mm cube
Total spring length	55.3mm	49.15 mm
Gap between springs	0.2mm	0.25mm
Spring dimension	0.5mm x 0.11mm	0.5mm x 0.11mm
Coil	25mm diameter PCB	1500 turn hand wired coil

Table 10. Experimental configurations of micro generator using PCB coils and hand-wired coils.

The experiments were conducted using the setup shown in Figure 33. Besides the generator voltage output, two more readings are measured by the vibrometer – the magnet and the housing vibration amplitudes. Since an aluminum cantilever was used to amplify the input vibration from the vibrator, the total power input generated from the vibrator to the resonating structure may vary, depending on the resonant frequency of the aluminum beam. It was recorded that a lower input vibration frequency will result in a higher input amplitude. As shown in Figure 35, the input vibration amplitude varies from as high as 2.5mm at about 20Hz to as low as 200μm at about 100Hz. In order to measure the exact vibration amplitude of the magnet $z(t)$, the contribution of the varying driving vibration $y(t)$ must be taken into account by subtracting the vibrometer reading, $y(t)+z(t)$, by the input amplitude $y(t)$. The information gathered is important in helping us understanding how the mode behavior of the resonating structure is affected by changing frequency range.

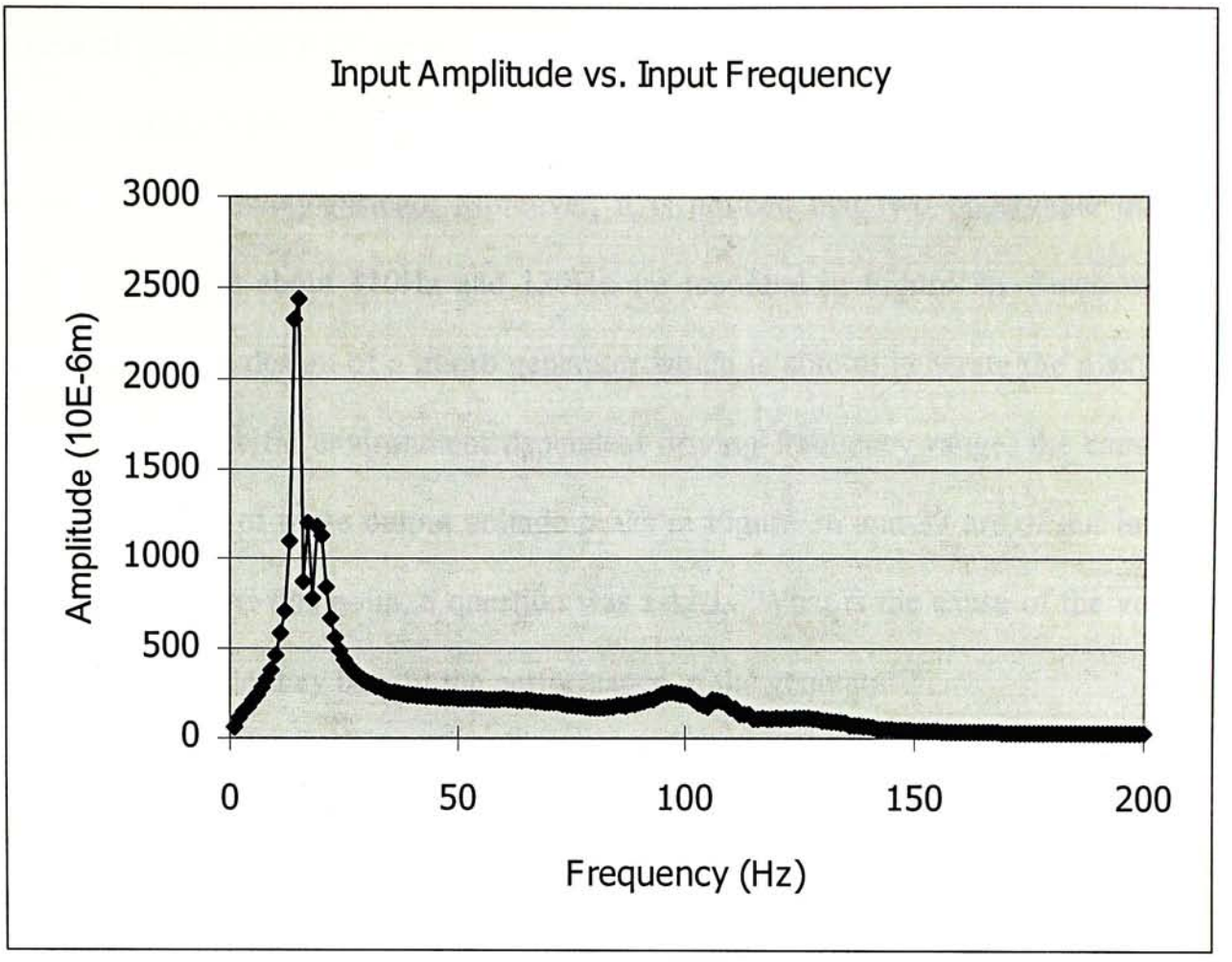

Figure 35. Input vibration frequency vs. beam vibration amplitude.

5.2.1 Voltage and Power Comparison

Given input vibration as described in Figure 35, the voltage generated by the micro generators and the vertical vibration amplitudes of the magnet are measured with the use of CRO and laser vibrometer. The experimental results generated by the specified generator configurations are shown in Figure 36 and 37. By comparing the two figures with each other, it is shown that there exists an unique trend of peak voltage output occurrences at 70~80Hz and 90~130Hz in both configurations. The exact frequency values may differ from each other between the two configurations because of the slight difference of the original parameters employed, e.g. coiling technique and spring length but a distinct trend is observable. At about 70~80Hz, output voltage

peaks of 18mV and 1.1V are recorded in the experiments using PCB and hand-wired coiling respectively. At 90~130Hz, output voltage peaks of 20mV and 3.1V are recorded respectively instead. Moreover, it is noticed that two observable distinct voltage peaks at about 110Hz and 120Hz are recorded in Figure 36. Since we are interested in the design of a micro generator which is able to generate the maximum voltage at a specific environment dependent driving frequency range, the causes of the occurrences of those output voltage peaks in Figure 36 and 37 are of our interest in this project. At this point, a question was asked, "What is the cause of the voltage peaks and how do they benefit the performance of the generator?"

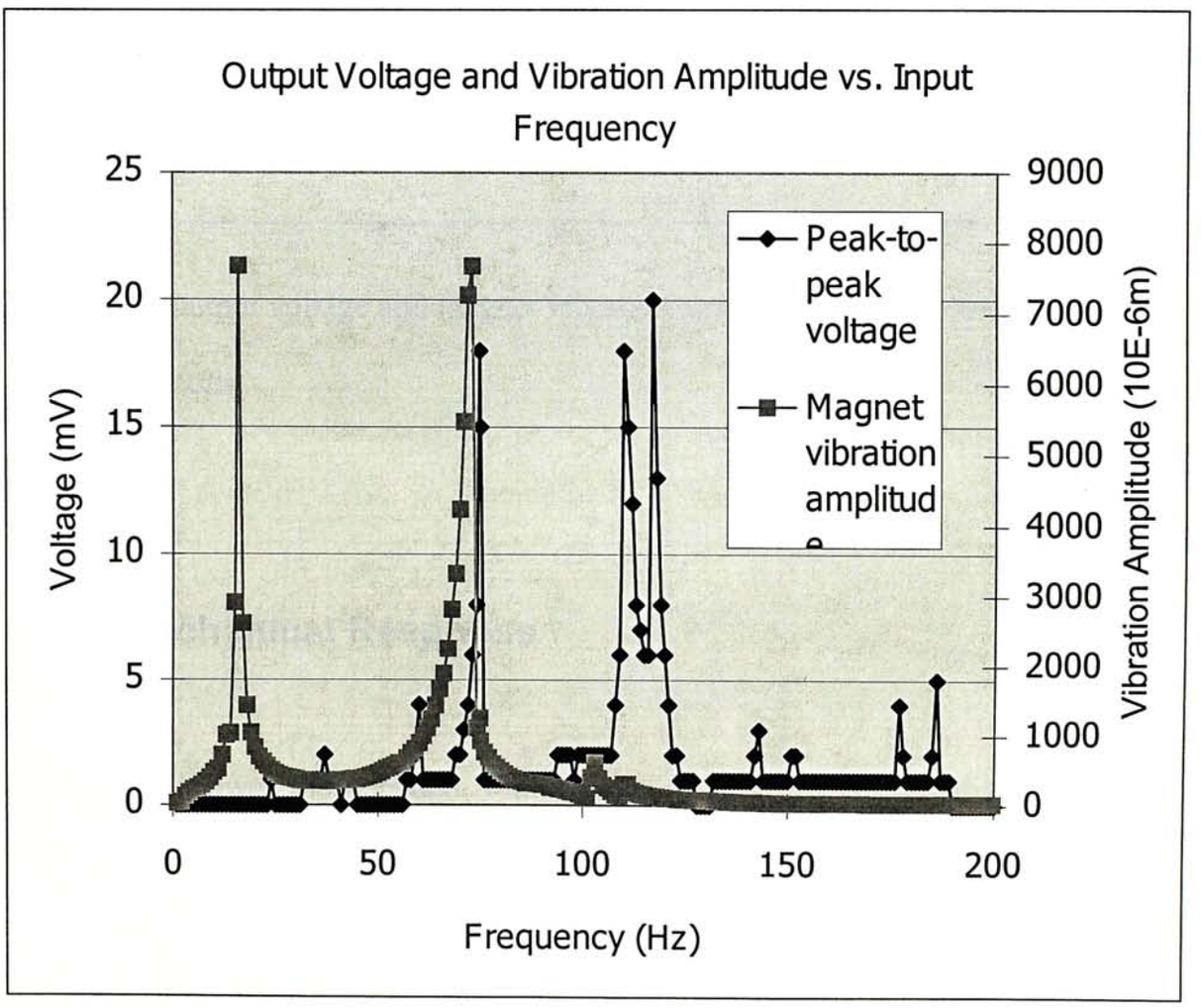

Figure 36. Output voltage and magnet vibration amplitude vs. input frequency using PCB coils.

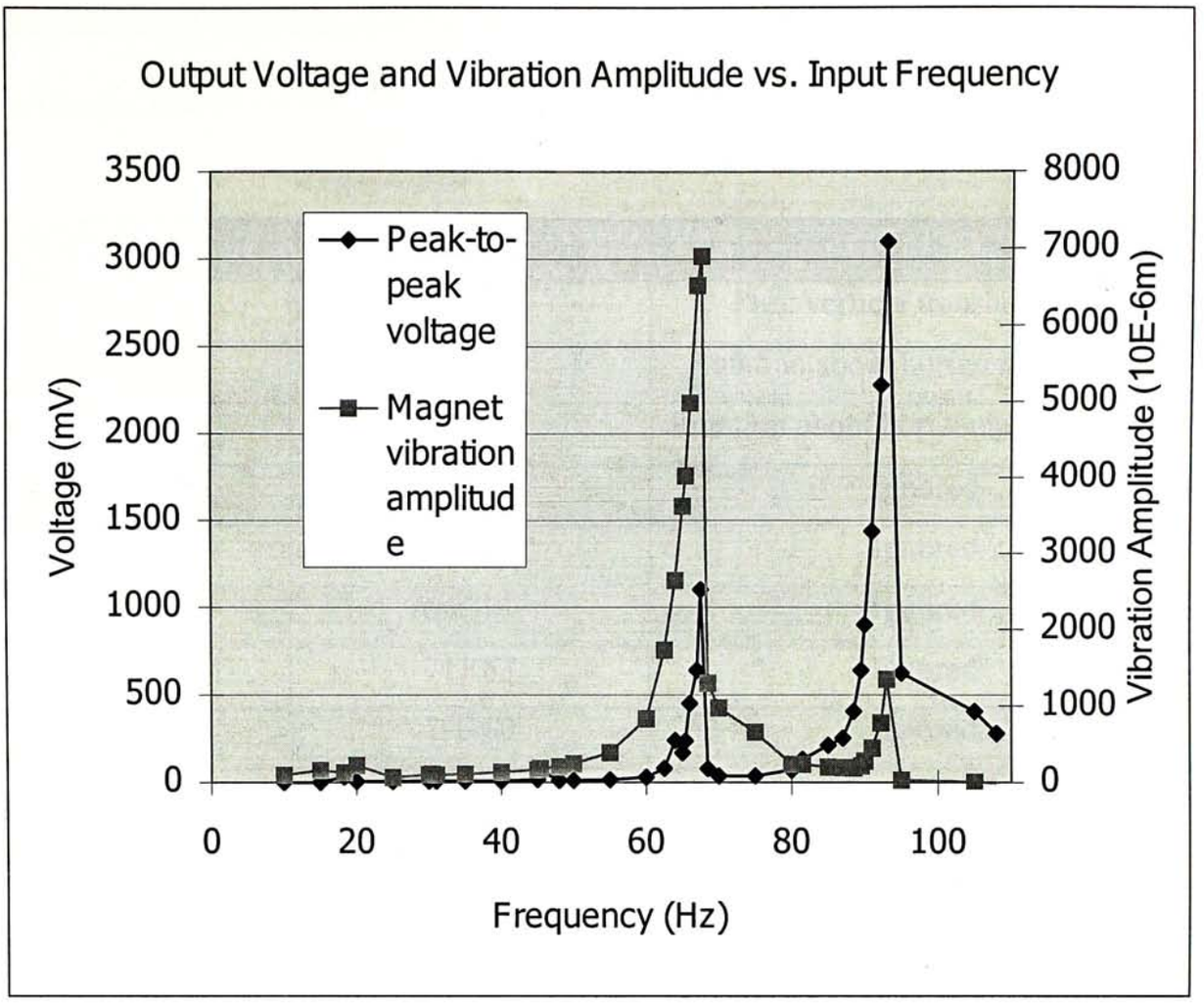

Figure 37. Output voltage and magnet vibration amplitude vs. input frequency using hand-wired coils.

5.2.2 Mechanical Response

In order to answer the question, Finite Element Analysis was used to simulate the micro generator response with parameters given in Table 10. The configuration of the hand-wired coils is employed in Finite Element modelling and the exact Finite Element model is shown in Figure 22 in the previous chapter. By performing series of modal analyses as described in Chapter 4, the mode frequencies of the resonating structure (frequencies at which the resonating structure vibrates at the resonant mode)

are calculated. The complete table of the mode frequencies of the micro generator under test is given in the following table.

Mode number	Frequency (Hz)	Mode shape
1	81.528	Pure vertical translation (z).
2	131.50	Rotation about horizontal axis (x).
3	135.59	Rotation about horizontal axes (x, y).
4	581.37	Ignored
5	613.48	Ignored
6	645.71	Ignored
7	711.83	Ignored
8	790.60	Ignored

Table 11. Resultant mode frequencies from Finite Element Analysis modal analysis.

From Table 11, it is shown that modal analyses reveal the occurrence of the first three mode frequencies at 82Hz, 132Hz and 136Hz. Since vibration at low frequencies is of our interest, higher frequency values and mode shapes are ignored in the study. According to the modal analysis results, the first mode occurs at 82Hz, which corresponds to the output voltage peak at 70~80Hz in Figure 36 and Figure 37 from the experimental results. The power output is mainly contributed by the resonant vertical movement of the magnet (Figure 38). By comparing the mode shape in Figure 38 with the large vertical magnet vibration amplitude at about 80Hz in Figure 36 and 37, it may be concluded that both the Finite Element simulation results and the experimental results are comparable. A series of slow motion pictures of the actual resonator movement occurred at the first mode frequency are shown in Figure 39. From the figures, it may be observed that the spiral springs can allow a large extent of vertical deflection while maintaining the overall structure stable.

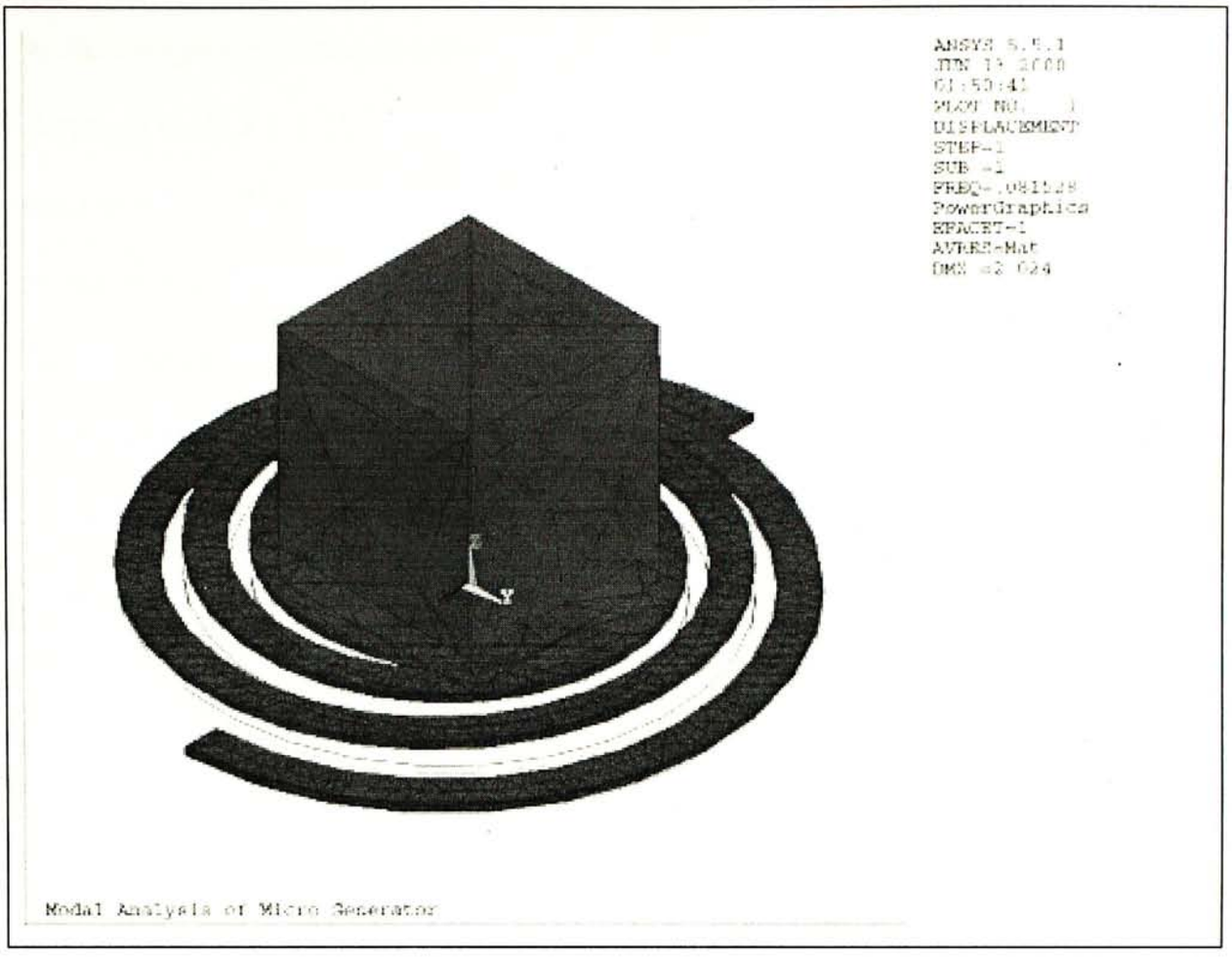

Figure 38. Finite element simulation of the first mode shape indicating a resonant vertical vibration at 81.528Hz.

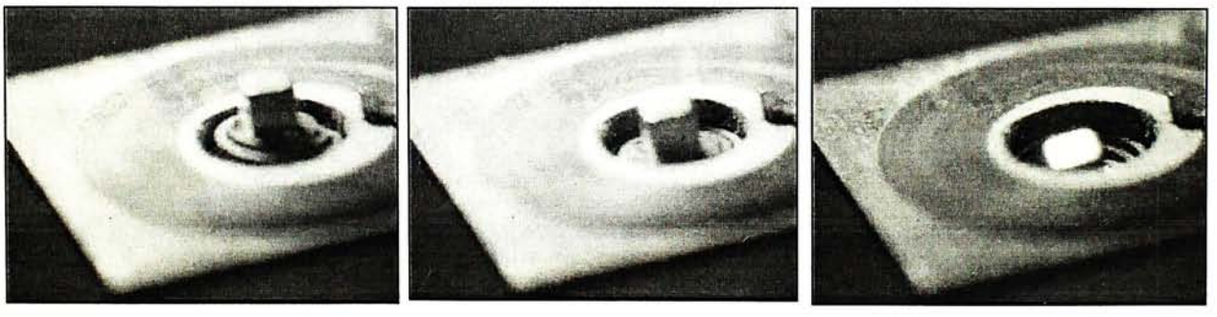

Figure 39. Photos captured in experiments indicating a resonant vertical vibration at the first mode frequency.

The second mode occurs at somewhere between 90Hz and 130Hz according to the experiments carried out. A relatively clear observation can be found at 113Hz in Figure 36. Unlike the first mode where large vertical deflections are measured, the

vertical magnet vibration amplitude is small (~300μm) at the second mode frequency. Hence, it is clear that the voltage peak occurring at the second mode frequency is not contributed by the vertical spring vibration as designed. Modal analyses reveal the occurrence of the second mode frequency at 132Hz (Figure 40). As shown in Figure 41, the voltage peak at 132Hz is mainly contributed by resonant magnet rotation about the horizontal x-axis. The rotation of the magnet is much larger than the vertical deflection at this driving frequency range such that a large power is generated even with a small input amplitude (~200μm).

Figure 40. Finite element simulation of the second mode shape indicating a resonant rotational vibration at 131.504Hz.

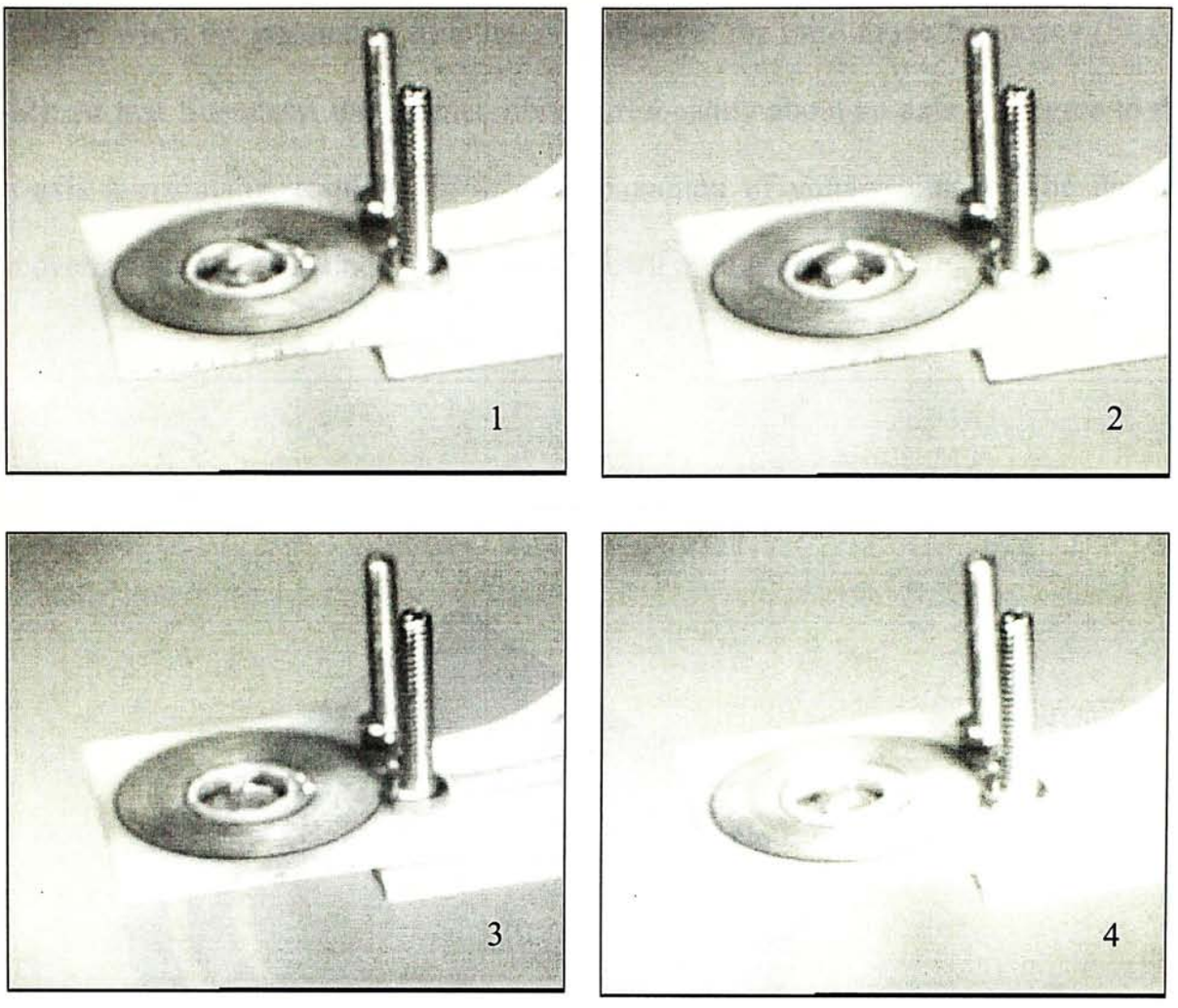

Figure 41. Photos captured in experiments indicating a resonant rotational vibration at the second mode frequency.

By experimental observations, the third mode can be treated as an extension of the second mode. The third mode frequency is closed to the second mode frequency that it is sometimes undetectable during the experiments as in Figure 37. Modal analyses reveal the third mode frequency at 136Hz and the closest matched experimental result can be observed at 120Hz in Figure 36. At the second mode frequency, the magnet rotates resonantly about the x-axis purely as described (Figure 40). When the input driving frequency is increased, the "axis of rotation" begins to shift towards the y-axis about the z-axis, resulting in a decrease of voltage output. The power generated by the micro generator continues to drop and then rise until reaching a vibration frequency of

136Hz, when the resonating structure is vibrated at the third mode frequency (Figure 42). At that frequency, the magnet vibrates resonantly about an axis 45 degree to the x-axis horizontally, resulting in a local maximum of voltage output. The magnet movement at the third mode frequency is shown in Figure 43.

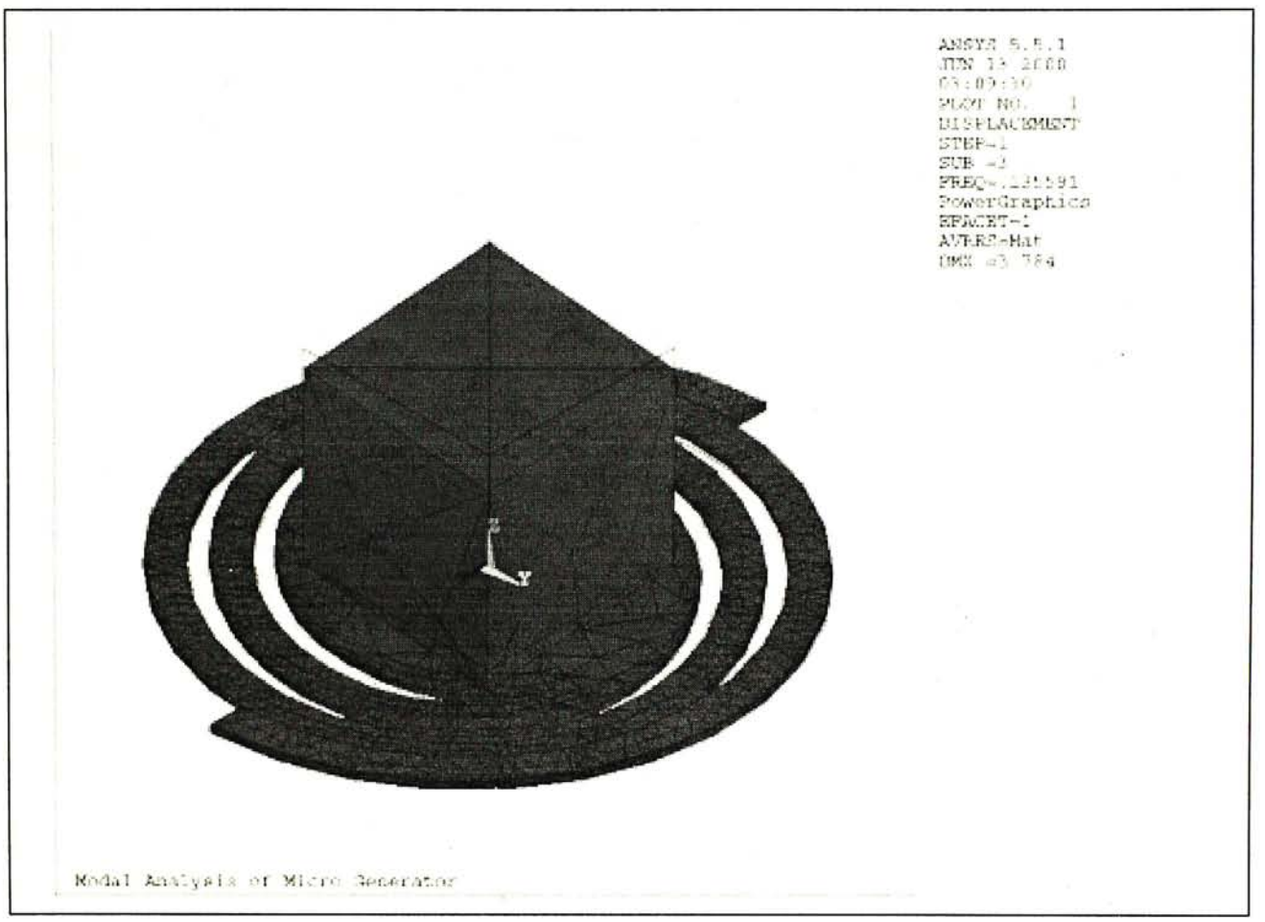

Figure 42. Finite element simulation of the third mode shape indicating a resonant rotational vibration at 135.591Hz.

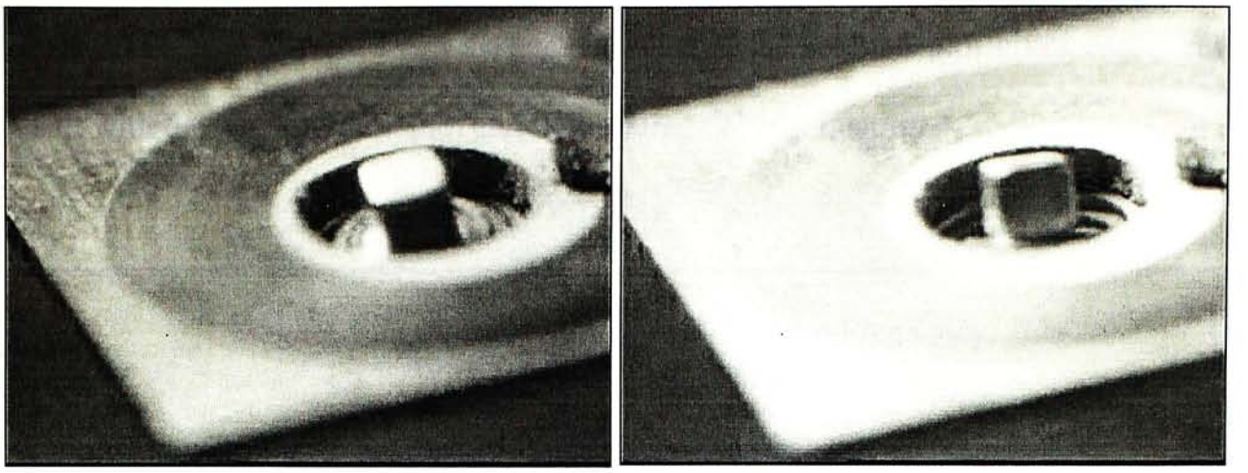

Figure 43. Photos captured in experiments indicating a resonant rotational vibration at third mode frequency.

5.2.3 Mechanical Properties

Experimental results and finite element simulations described in the previous section demonstrated that geometry is the determining factor of the occurrence of resonating vibration. By compromising physical properties with the geometric values of the resonating structure, maximized voltage output may be achieved. This section serves as a supplementary study of how physical properties affect the system response by comparing the system output with different mass values and damping ratios.

The mass vertical vibration amplitudes of three generator systems are shown in Figure 44. All three systems have the same configuration as that stated in the previous experiment section. The value of the magnet mass is set to be the control variable to study its contribution to the system response. As shown in Figure 44, for a vertically driven resonating system with fixed spring constant, heavy mass always results in low vibration frequency (Equation 4). Figure 45 indicates the magnet rotation about the

vertical axis for different mass system. In general, the rotation plot gives consistent result with the displacement plot and both of them obey Equation 4.

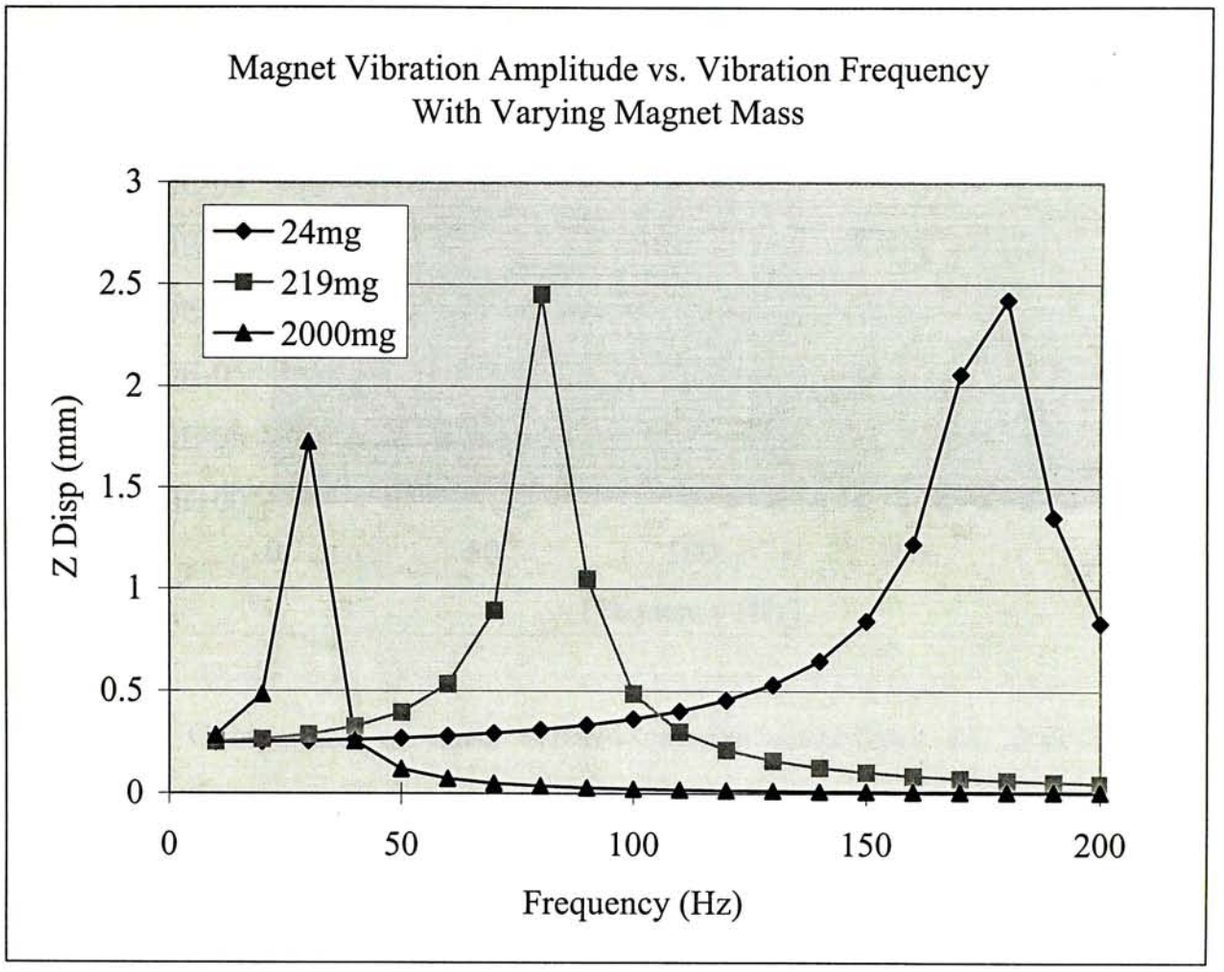

Figure 44. Comparison of mass vertical vibration amplitudes (Z Disp) with different mass value.

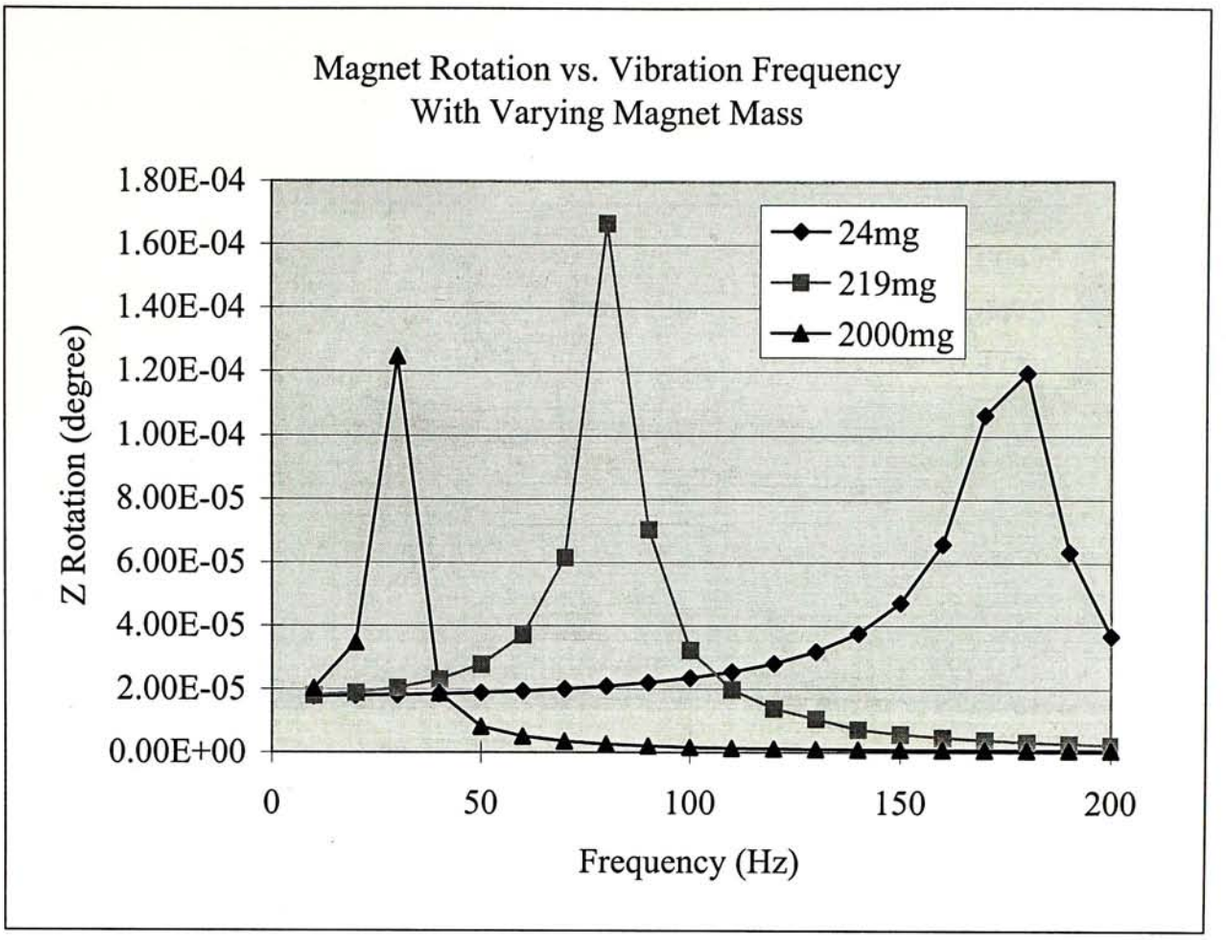

Figure 45. Comparison of mass vertical rotation amplitudes (Z Rotation) with different mass value.

The mechanical responses of systems with different damping ratios are shown in Figure 46 and 47. Environmental dependent damping ratio contributes no visible effect on the vibration frequency but the vibration amplitudes – both linear and angular. Given a 16mN vertical driving force, the experimental setup demonstrated in the early section exhibits a damping ratio of 0.04.

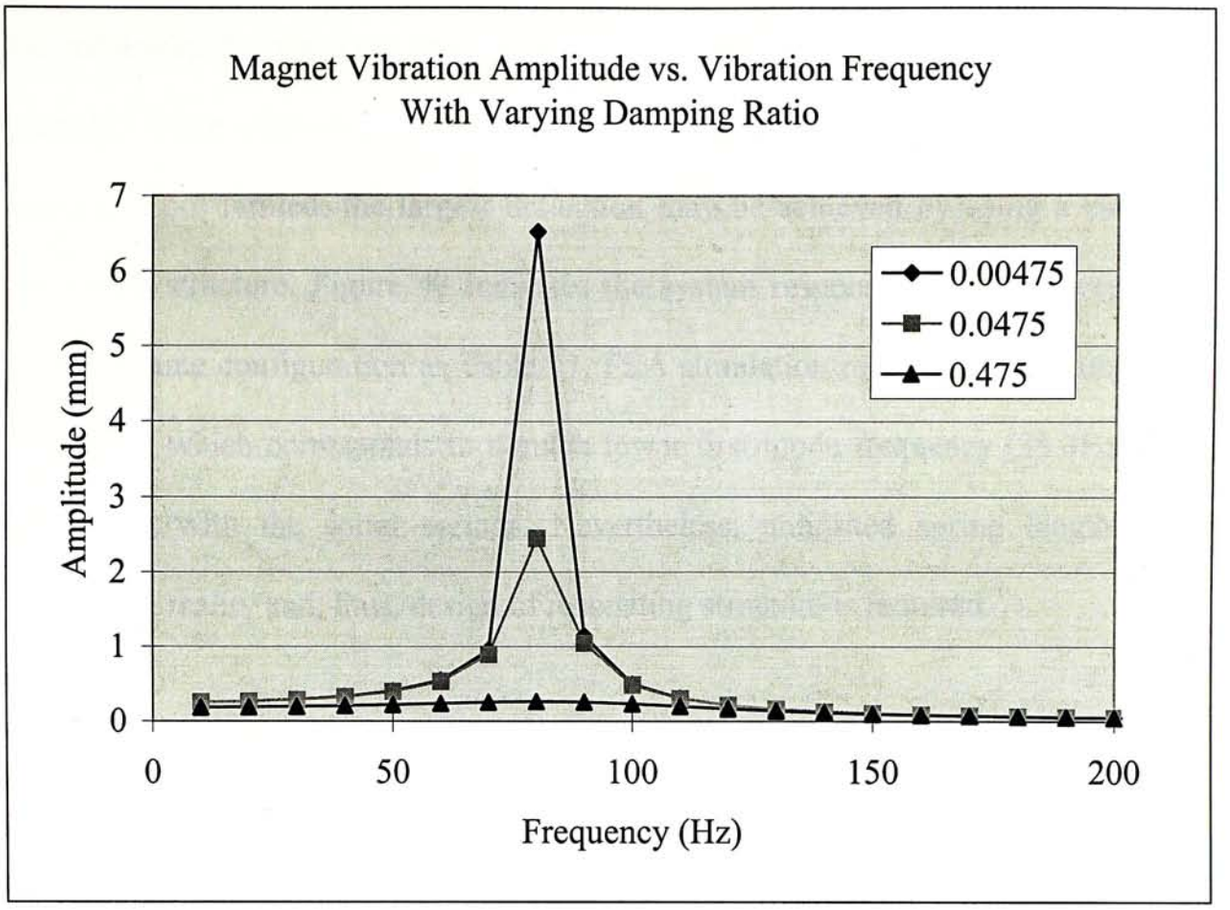

Figure 46. Comparison of mass vertical vibration amplitudes (Z Disp) with different damping ratio.

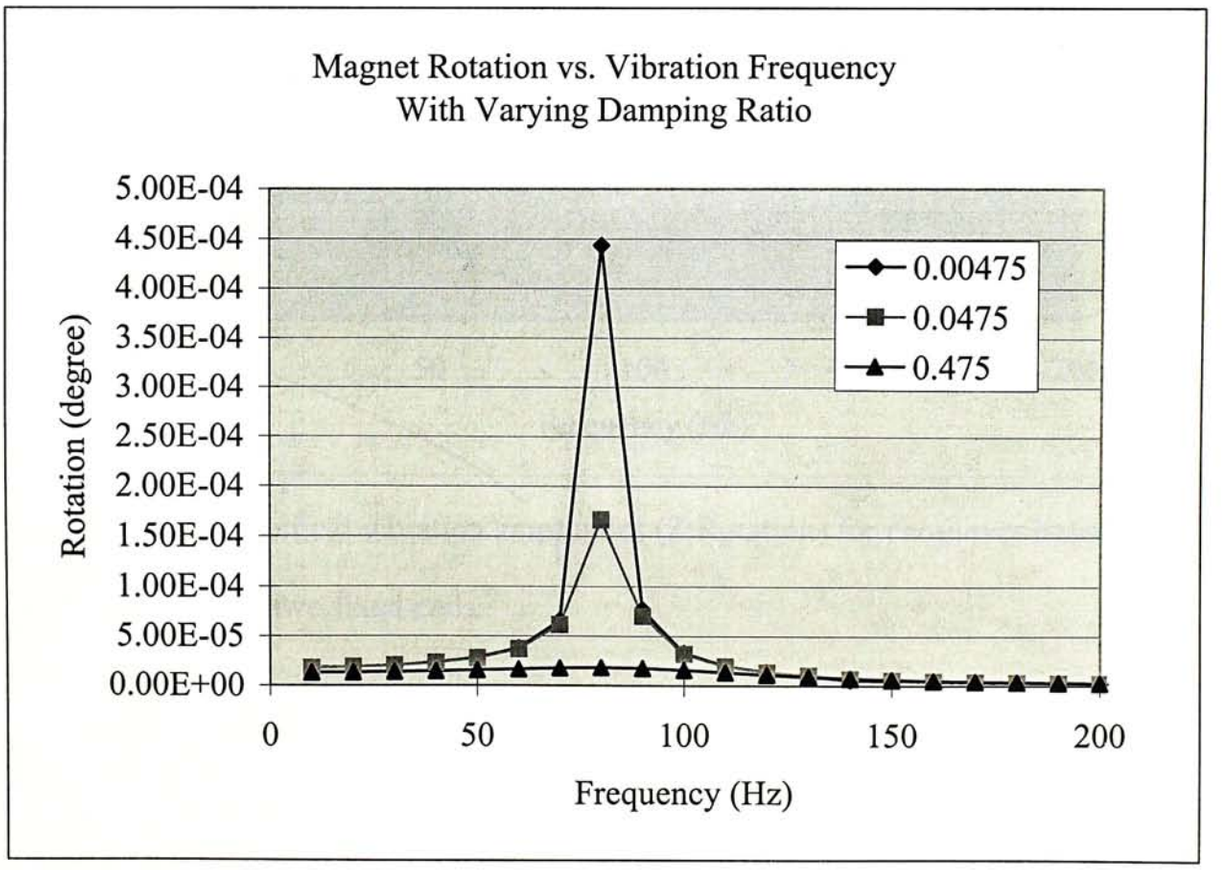

Figure 47. Comparison of mass vertical rotation amplitudes (Z Rotation) with different damping ratio.

Demonstrated development process of micro generator aims to increase mechanical vibration while minimizing the stress level and vibration frequency. Supposed that spacing is not limited, the largest deflection may be achieved by using a cantilever resonating structure. Figure 48 indicates the system response of a cantilever spring with the same configuration as Table 11. FEA simulation revels a spring constant of 10.79N/m, which corresponds to a much lower first mode frequency (35.3Hz) while comparing with the spiral springs. Nevertheless, unlimited spring length is not possible in reality and, thus, design of resonating structure is required.

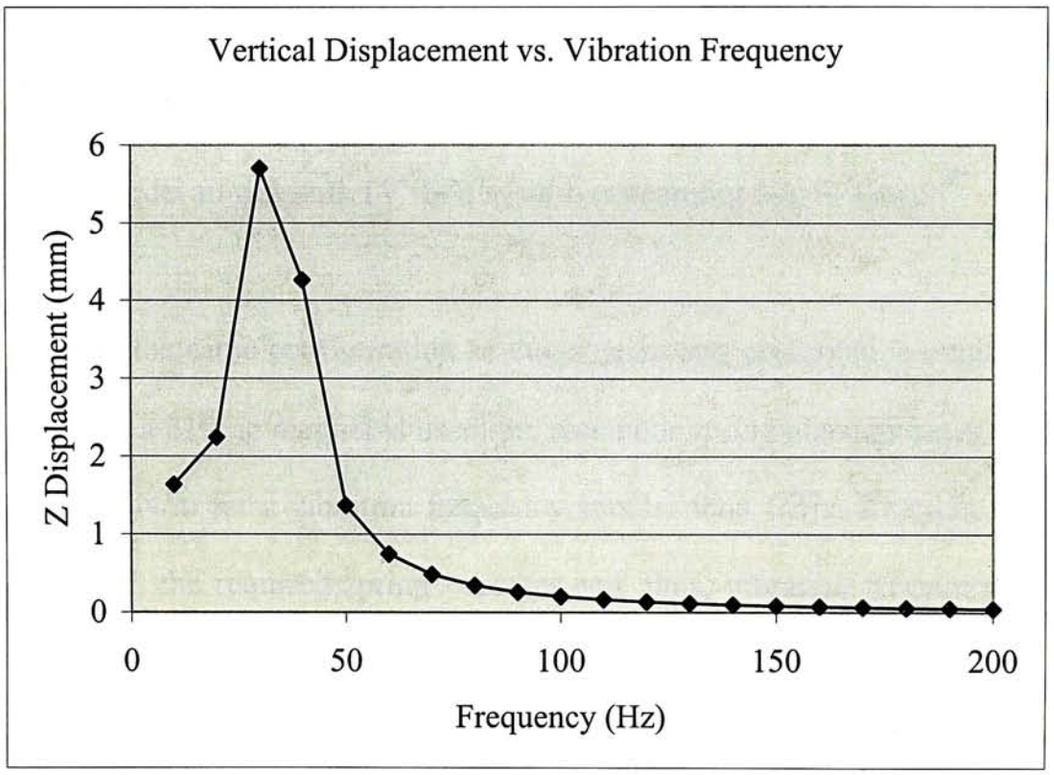

Figure 48. Mass vertical vibration amplitudes (Z Rotation) for cantilever beam with center loading and two fixed ends.

CHAPTER 6 SUGGESTIONS FOR POWER GENERATOR WITH RESONATING FREQUENCY BELOW 10HZ

The ultimate goad of this project is to develop a micro sized electric power generator which is capable of producing enough voltage to drive a low-power IC circuit systems or micro sensors for robotics and automation applications in low frequency range. With a driving frequency of ~10Hz, it is justified to ask what the smallest generator possible is in order to generate 1V for a system consuming 30μW power.

Supposed that the same configuration as the experiments presented is employed (e.g. t_s=110μm) and a 219mg magnet is used, the resonator spring constant must be at least less than 0.865N/m for a vibration frequency smaller than 10Hz. Keeping the spring thickness fixed, the required spring constant and, thus, vibration frequency, may be maintain by decreasing the spring width and the total spring length at the same time. The dimension configuration required for a single copper spring to resonate at 10Hz is shown in Figure 49. As indicated from the figure, the total spring length required is minimized with decreasing spring width. A 16mm long copper spring is needed for a spring width equal to 100μm (A conservative estimation of the highest resolution a laser machine is able to fabricate). However, when the dimensions of the structure are minimized, the amount of the vibration force the resonating structure can withstand decreases as well. The vibration amplitudes at which the copper spring reaches its yield point are labeled in the figure. Numerical data reveal that a resonating structure

with a 16mm x 100μm x 110μm copper spring is incapable of withstanding vibration amplitude higher than 4.33mm. However, having taking a safety factor of ten into account, the micro generator will most likely to suffer from mechanical failure higher than 400μm vibration amplitude.

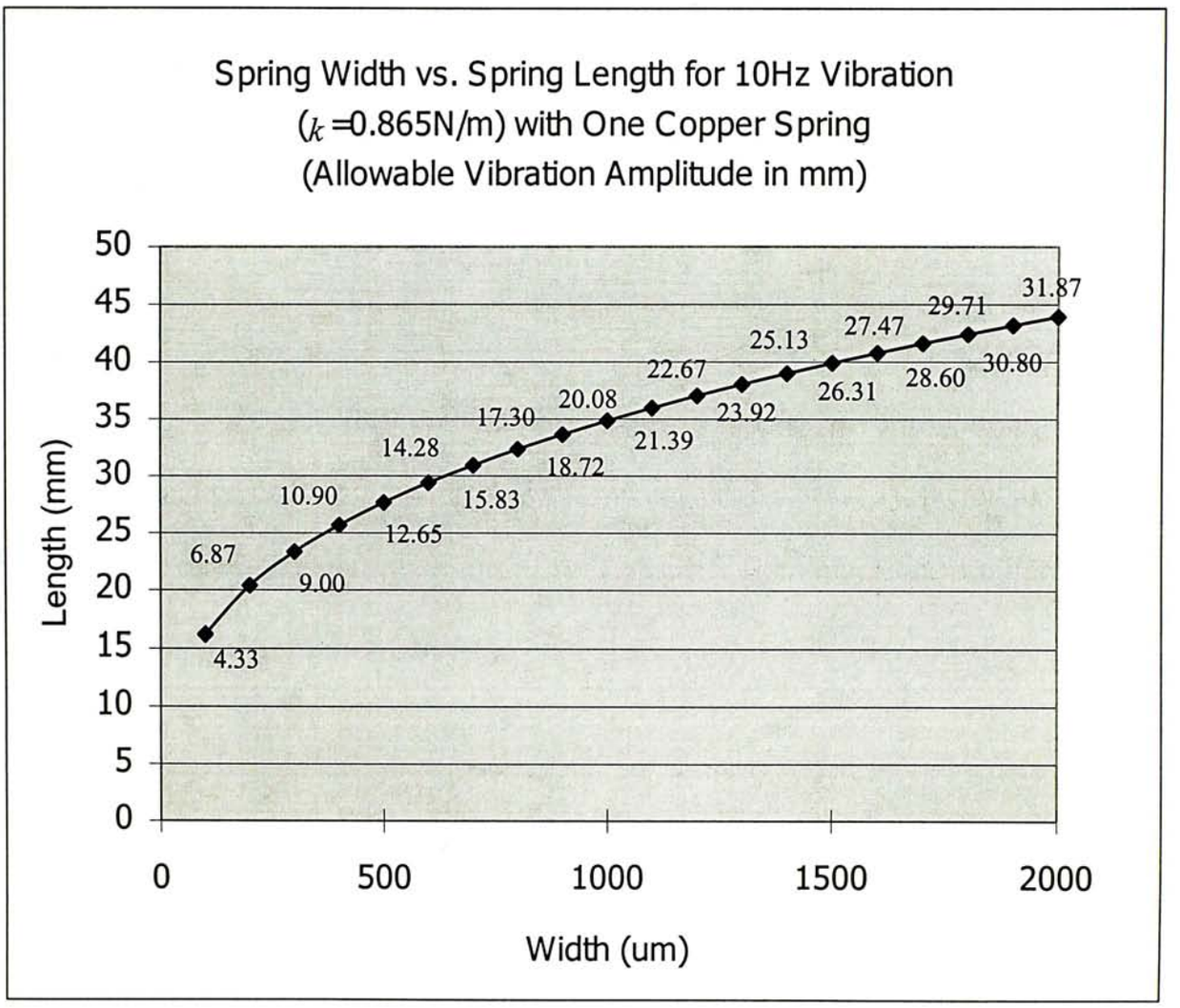

Figure 49. Spring dimensions required for one copper spring vibration at 10Hz. (Allowable vibration amplitudes are inidcated in figures.)

Even if single spring resonating structures require less space and shorter springs for the same output as the two-spring structures, they may not be the optimal choice in term of performance and stability. The dimension configuration required for a two-spring copper resonating structure to resonate at 10Hz is shown in Figure 50. In

general, half the spring width is required for a two-spring structure to perform the same as the single spring case. A total spring length of 70mm (each spring being 35mm long) is needed for two 500μm wide copper springs to meet the required frequency.

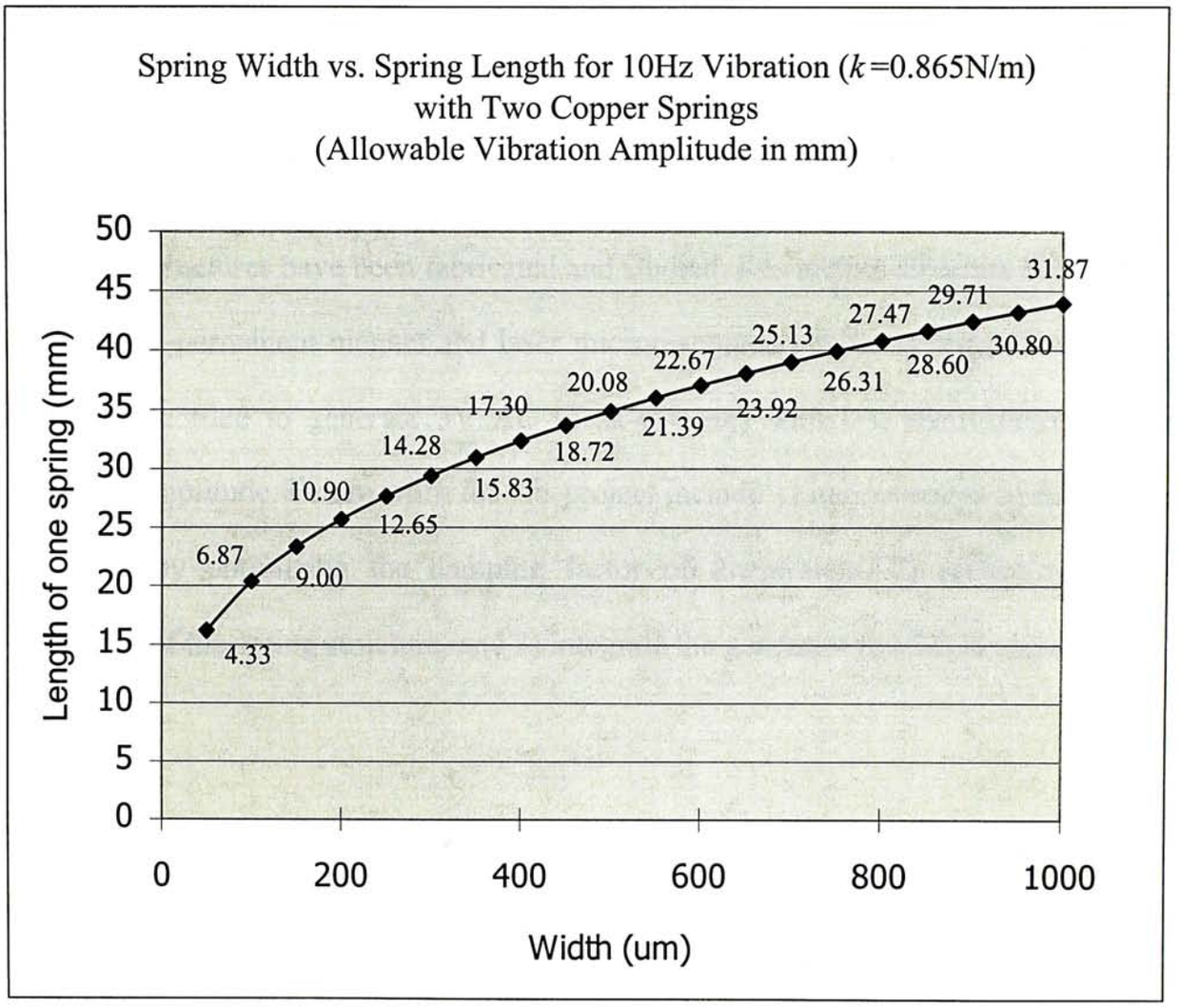

Figure 50. Spring dimensions required for two copper spring vibration at 10Hz. (Allowable vibration amplitudes are inidcated in figures.)

CHAPTER 7 CONCLUSION

This paper presented the design, analysis and experimental results of a micro-scale vibration-induced power generator with laser micromachined spring structure that converts mechanical vibration into electrical power. With the use of three-dimensional Finite Element Analysis (FEA), design of the mechanical resonating structures is developed and optimized for higher system power output. Prototypes of the proposed generator structures have been fabricated and studied. Resonating structure formed by a rare earth permanent magnet and laser micromachined copper springs vibrating at 90Hz is recorded to generate 3V AC (peak-to-peak) with less than 200μm input vibration amplitude. Future work for this project include 1) improvement of the micro generator by optimizing the damping factor of the system, 2) reduce resonant frequency of the spring structure, and 3) integrate the generator to CMOS chips.

APPENDIX A: Proof of System Formulae

Parameter	Description
F	Generator input force
y	Generator input displacement
z	Mass displacement relative to coil
V	Voltage output at load resistor
f_e	Feedback electromechanical force
m	Mass of magnet
d	Mechanical damping coefficient
k	Spring constant of springs
B	Magnetic field strength of magnet
l	Length of wire coil
R	Load resistance
L	Coil inductance
R_c	Coil resistance

Table 12. System parameter summary of micro generator studied. (Reprinted from Table 3)

The differential equation which describes the movement of the mass with respect to the wire coil is derived from the dynamic forces on the mass [20].

$$m\ddot{z}(t) + d\dot{z}(t) + kz(t) = F(t) \tag{A1}$$

The transfer function from the input force to the mass displacement relative to the wire coil is:

$$\frac{z(s)}{F(s)} = \frac{1}{ms^2 + ds + k} \tag{A2}$$

The behaviour of the electrical system is described by the following differential equation, in which *I(t)* is the current passing through the wire coil.

$$L\dot{I}(t) + (R + R_c)I(t) = Bl\dot{z}(t) \tag{A3}$$

The transfer function from the relative displacement of the mass to coil, to the output voltage at the load resistor is:

$$\frac{V(s)}{z(s)} = \frac{BlRs}{Ls + R + R_c} \tag{A4}$$

The feedback electromechanical force generated by the induced current in the wire coil is derived [19].

$$f_e = BlI = \left(\frac{Bl}{R}\right)V \tag{A5}$$

Recalled from Equations (A2), (A4) and (A5), the overall transfer function from the input force to the output load voltage can be derived. The block diagram of the micro generator system is reprinted in Figure 51.

$$\frac{V(s)}{F(s)} = \frac{BlRs}{(Ls + R + R_c)(ms^2 + ds + k) + (Bl)^2 s} \tag{1}$$

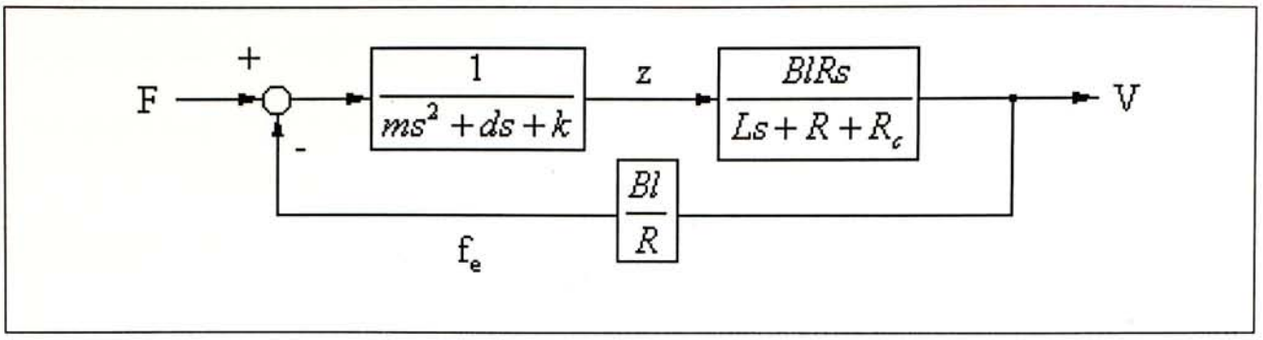

Figure 51. Block diagram of micro generator [4]. (Reprinted from Figure 5)

By assuming that both L and R_c are zero as stated, the system transfer function may be rewritten as the expression:

$$\frac{V(s)}{F(s)} = \frac{Bls}{(ms^2 + ds + k) + \frac{(Bl)^2}{R}s} \tag{2}$$

Let the resonant frequency and the damping ratios of the generator system be the following expressions.

$$\omega_n = \sqrt{\frac{k}{m}} \tag{4}$$

$$\zeta_m = \frac{d}{2\sqrt{mk}} \tag{5}$$

$$\zeta_e = \frac{(Bl)^2}{2R\sqrt{mk}} \tag{6}$$

$$\zeta = \zeta_m + \zeta_e \tag{7}$$

The system transfer system is then expressed as:

$$\frac{V(s)}{F(s)} = \frac{\frac{Bl}{m}s}{s^2 + 2\zeta\omega_n s + \omega_n^2} \tag{A6}$$

Supposed that the micro generator is driven by a sinusoidal excitation $y(t)=Y_0\sin(\omega t)$, the equivalent input force is:

$$\begin{aligned} F(t) &= -m\ddot{y}(t) \\ &= mY_0\omega^2\sin(\omega t) \end{aligned} \tag{A7}$$

$$F(s) = \frac{mY_0\omega^3}{s^2+\omega^2} \tag{A8}$$

By Equations (A6) and (A8), the output voltage at the load resistor can be derived as:

$$\begin{aligned} V(s) &= \frac{BlY_0\omega^3 s}{(s^2+\omega^2)(s^2+2\zeta\omega_n s+\omega_n^2)} \\ &= \frac{BlY_0\omega^3(\omega_n^2-\omega^2)}{(\omega_n^2-\omega^2)^2+4\zeta^2\omega_n^2\omega^2}\left(\frac{s+\dfrac{2\zeta\omega_n\omega^2}{\omega_n^2-\omega^2}}{s^2+\omega^2}-\frac{s+\dfrac{2\zeta\omega_n^3}{\omega_n^2-\omega^2}}{s^2+2\zeta\omega_n s+\omega_n^2}\right) \end{aligned} \tag{A9}$$

$$V(t) = \frac{BlY_0\omega^3(\omega_n^2-\omega^2)}{(\omega_n^2-\omega^2)^2+4\zeta^2\omega_n^2\omega^2}\left[\cos(\omega t)+\frac{2\zeta\omega_n\omega}{\omega_n^2-\omega^2}\sin(\omega t)-\ldots\right] \tag{A10}$$

$$\begin{aligned} V^2(t) &= \left[\frac{BlY_0\omega^3(\omega_n^2-\omega^2)}{(\omega_n^2-\omega^2)^2+4\zeta^2\omega_n^2\omega^2}\right]^2\left\{\cos^2(\omega t)+\left[\frac{2\zeta\omega_n\omega}{\omega_n^2-\omega^2}\right]^2\sin^2(\omega t)+\ldots\right\} \\ &= \left[\frac{BlY_0\omega^3(\omega_n^2-\omega^2)}{(\omega_n^2-\omega^2)^2+4\zeta^2\omega_n^2\omega^2}\right]^2 \\ &\quad \left\{\frac{1}{2}\left[1+\cos(2\omega t)\right]+2\left[\frac{\zeta\omega_n\omega}{\omega_n^2-\omega^2}\right]^2\left[1-\cos(2\omega t)\right]+\ldots\right\} \end{aligned} \tag{A11}$$

Only the first few terms in the expressions of $V(t)$ and $V^2(t)$ are considered in the above calculation because all the other terms involve multiples of either an exponentially decreasing function or a sinusoidal function, which will vanish in the steady state of the generator system. The instant output power of the generator system is given by the expression:

$$P(t) = \frac{V^2(t)}{R} \tag{A12}$$

By substituting Equation (A11) into (A12) and taking the limit of time to infinity, the average power output of the generator system is derived.

$$P = \frac{m\zeta_e Y_0^2 \left(\frac{\omega}{\omega_n}\right)^3 \omega^3}{\left[1-\left(\frac{\omega}{\omega_n}\right)^2\right]^2 + \left(2\zeta\frac{\omega}{\omega_n}\right)^2} \tag{3}$$

At resonance, the average power output of the generator system is maximised and is given by the expression [1]:

$$P = \frac{m\zeta_e Y_0^2 \omega_n^3}{4\zeta^2} \tag{8}$$

Hence, the peak voltage output of the generator system at resonance can be expressed as [1]:

$$\begin{aligned} V_0 &= \sqrt{2PR} \\ &= \frac{BlY_0\omega_n}{2\zeta} \end{aligned} \tag{9}$$

APPENDIX B(I): *MATLAB* Program – V(t) and P(t)

```
% A MATLAB program to calculate output voltage and power
% with input displacement given.
% Gordon Chan

clear

% System property
m = 219*10^-6;                  % Mass (kg)
d = 0.2;                        % Damping constant (kg/s)
k = 250;                        % Spring constant (N/m)
L = 0.001;                      % Inductance (H = Vs/A)
R = 100;                        % Load resistance (Ohm)
Rc = 10;                        % Coil resistance (Ohm)
l = 60*10^-3;                   % Coil length (m)
B = 1.312;                      % Magnetic field strength (T = N/(Am))

% Input parameter
Y0 = 10^-3;                     % Input Displacement (m)
w = (k/m)^0.5;                  % Input frequency (rad/s)

% ---- Program Start ----

Zeta_m = d/(2*(m*k)^0.5)
Zeta_e = ((B*l)^2)/(2*R*(m*k)^0.5)
Zeta = Zeta_m+Zeta_e
wn = (k/m)^0.5                  % Natural freuqency (rad/s)
Nat_Freq = wn/(2*pi)            % Natural frequency (Hz)
F0 = m*Y0*(w^2)                 % Input force (N)
F0_at_resonance = m*Y0*(wn^2)   % Input force at resonance (N)
P_average_at_resonance = Zeta_e*F0_at_resonance^2/(4*m*wn*Zeta^2)
V_peak_at_resonance = B*l*F0_at_resonance/(2*m*Zeta*wn)

num = [B*l*R 0];
den = [m*L d*L+m*(R+Rc) k*L+d*(R+Rc)+(B*l)^2 k*(R+Rc)];
[A1,A2,A3,A4] = tf2ss(num,den);
t = 0:0.0001:0.1;
F = F0*sin(w*t);
[V,o] = lsim(A1,A2,A3,A4,F,t);
P = (V.^2)./R;

subplot(2,1,1);
plot(t,P);
xlabel('Time [s]');
ylabel('Power [W]');
title('Output Power vs Time');
grid on;

subplot(2,1,2);
```

```
plot(t,V);
xlabel('Time [s]');
ylabel('Voltage [V]');
title('Output Voltage vs Time');
grid on;
```

APPENDIX B(II): *MATLAB* Program – V(t) with Varying Parameters

```
% A MATLAB program to calculate output voltage with varying parameters.
% Gordon Chan 2000

clear

% System property
m = 219*10^-6;                          % Mass (kg)
d = 0.2;                                % Damping constant (kg/s)
k = 250;                                % Spring constant (N/m)
L = 0.001;                              % Inductance (H = Vs/A)
R = 100;                                % Load resistance (Ohm)
Rc = 10;                                % Coil resistance (Ohm)
l = 60*10^-3;                           % Coil length (m)
B = 1.312;                              % Magnetic field strength (T = N/(Am))

% Input parameter
Y0 = 10^-3;                             % Input Displacement (m)
w = (k/m)^0.5;                          % Input frequency (rad/s)

% Display property
Max1 = 500;                             % Property 1 upper bound
Max2 = 2000;                            % Property 2 upper bound
Range1 = 30;                            % Number of rows
Range2 = 30;
Time1 = 20;                             % Initial sampling time (s)
Time2 = 30;                             % Final sampling time (s)

% ---- Program Start ----

Period1 = Max1/Range1;
Period2 = Max2/Range2;

for i = 1:Range1;
for j = 1:Range2;

k = Period1*i;                          % --- User input ---
w = Period2*j;

F0 = m*Y0*(w^2);                        % Input force (N)
num = [B*l*R 0];
den = [m*L d*L+m*(R+Rc) k*L+d*(R+Rc)+(B*l)^2 k*(R+Rc)];
[A1,A2,A3,A4] = tf2ss(num,den);
t = 0:0.0021:Time2;                     % Sample rate
F = F0*sin(w*t);
```

```
[V,o] = lsim(A1,A2,A3,A4,F,t);
V0 = max(V(Time1:Time2));                    % Locate peak voltage
ResultV(i,j) = V0;

end
end

x = Period1:Period1:Max1;
y = Period2:Period2:Max2;
y = y/(2*pi);                                % Change unit from rad/s to Hz


surf(y,x,ResultV);
title('Output Voltage vs Vibrational Frequency');
ylabel('Spring Constant, N/m');
xlabel('Frequency, Hz');
zlabel('Voltage, V');
view(-70,20);
colorbar;
%colormap(gray);
```

APPENDIX C(I): *AutoLISP* Program – Zigzag Spring

```
; Autolisp program to draw a rectangular 3D zigzag micro generator CAD model
; by Gordon Chan, 1999

(defun zigzag2()

 (setq SqW 10)                          ; Resonator width
 (setq W 0.1)                           ; Spring width
 (setq H 0.1)                           ; Spring height
 (setq G 0.3)                           ; Gap distance
 (setq Wb 0.5)                          ; Border width
 (setq Hb 0.5)                          ; Border height
 (setq Wm 4)                            ; Mass width
 (setq Hm 0.5)                          ; Mass height

 (command "polygon" "4" "0,0" "c" (rtos (* SqW 0.5)))
 (command "extrude" (entlast) "" (rtos Hb) "0")
 (setq solid1 (entlast))
 (command "polygon" "4" "0,0" "c" (rtos (- (* SqW 0.5) Wb)))
 (command "extrude" (entlast) "" (rtos Hb) "0")
 (command "subtract" solid1 "" (entlast) "")
 (command "move" (entlast) "" (strcat "0,0," (rtos (* -0.5 Hb))) "")
 (setq solid1 (entlast))

 (setq beamno (+ (fix (/ (- (- SqW Wm) (* 2 (+ Wb G))) (+ W G))) 1))

 (if (= (* 0.5 beamno) (fix (* 0.5 beamno)))
  (setq beamno (- beamno 1))
 )

 (setq margin (* 0.5 (- (- (- SqW Wm) (* 2 (+ Wb G))) (* (- beamno 1) (+ W G)))))
 (setq Xcoor (list (+ (* -0.5 SqW) Wb)))
 (setq Xcoor2 (list (+ (* -0.5 SqW) Wb)))
 (repeat (/ (- beamno 1) 2)
  (repeat 2
   (setq Xcoor (append Xcoor (list (- (- (* 0.5 SqW) Wb) G))))
   (setq Xcoor2 (append (list (- (- (- (* 0.5 SqW) Wb) G) W)) Xcoor2))
  )
  (repeat 2
   (setq Xcoor (append Xcoor (list (+ (* -0.5 SqW) Wb G W))))
   (setq Xcoor2 (append (list (+ (* -0.5 SqW) Wb G)) Xcoor2))
  )
 )
 (setq Xcoor (append Xcoor (list (- (* 0.5 SqW) Wb))))
 (setq Xcoor2 (append (list (- (* 0.5 SqW) Wb)) Xcoor2))
 (setq Xcoor (append Xcoor Xcoor2))

 (setq Ycoor nil)
 (setq Ycoor2 nil)
 (setq i 1)
```

```
 (repeat beamno
  (cond ((= i (* 0.5 (+ beamno 1))) (setq offset (* 0.5 (- Wm W))))
        ((> i (* 0.5 (+ beamno 1))) (setq offset (- Wm W)))
        (t (setq offset 0))
  )
  (repeat 2
   (setq Ycoor (append Ycoor (list (+ (* -0.5 SqW) Wb margin (* i G) (* 2 (* (fix (* 0.5 i)) W))
offset))))
   (setq Ycoor2 (append (list (+ (* -0.5 SqW) Wb margin (* i G) (* (+ 1 (* 2 (fix (* 0.5 (- i 1))))))
W) offset)) Ycoor2))
  )
  (setq i (+ i 1))
 )
 (setq Ycoor (append Ycoor Ycoor2))

 (command "pline")
 (setq i 0)
 (repeat (* 4 beamno)
  (command (strcat (rtos (nth i Xcoor)) "," (rtos (nth i Ycoor))))
  (setq i (+ i 1))
 )
 (command "c")

 (command "extrude" (entlast) "" (rtos H) "0")
 (command "move" (entlast) "" (strcat "0,0," (rtos (* -0.5 H))) "")
 (setq solid2 (entlast))

 (command "box" "c" "0,0,0" "l" (rtos Wm) (rtos Wm) (rtos Hm))
 (command "union" solid1 solid2 (entlast) "")

 (setq i 0)
 (setq TLength 0)
 (repeat (- (* 4 beamno) 1)
  (setq x (- (nth (+ i 1) Xcoor) (nth i Xcoor)))
  (setq y (- (nth (+ i 1) Ycoor) (nth i Ycoor)))
  (setq TLength (+ TLength (sqrt (+ (* x x) (* y y)))))
  (setq i (+ i 1))
 )
 (print "Total length of 2 springs:")
 (setq TLength (- (* 0.5 (- TLength W)) Wm))

)
```

APPENDIX C(II): *AutoLISP* Program – Rectangular Spiral Spring

```
; Autolisp program to draw a rectangular 3D spiral micro generator CAD model
; by Gordon Chan, 1999

(defun spiralsq()

 (setq SqW 10)                          ; Resonator width
 (setq W 0.1)                           ; Spring width
 (setq H 0.1)                           ; Spring height
 (setq G 0.2)                           ; Gap distance
 (setq Wb 0.5)                          ; Border width
 (setq Hb 0.5)                          ; Border height
 (setq Wm 4)                            ; Mass width
 (setq Hm 0.5)                          ; Mass height
 (setq springno 2)                      ; Number of spring: 2 or 4

 (command "polygon" "4" "0,0" "c" (rtos (* SqW 0.5)))
 (command "extrude" (entlast) "" (rtos Hb) "0")
 (setq solid1 (entlast))
 (command "polygon" "4" "0,0" "c" (rtos (- (* SqW 0.5) Wb)))
 (command "extrude" (entlast) "" (rtos Hb) "0")
 (command "subtract" solid1 "" (entlast) "")
 (command "move" (entlast) "" (strcat "0,0," (rtos (* -0.5 Hb))) "")
 (setq solid1 (entlast))

 (setq loopno (fix (/ (- (* 0.5 (- SqW Wm)) (+ G Wb)) (+ W G))))
 (setq margin (- (* 0.5 (- SqW Wm)) (+ G Wb (* loopno (+ W G)))))

 (setq Xcoor (list (+ (* -0.5 SqW) Wb)))
 (setq Ycoor (list (+ (* -0.5 SqW) (+ Wb G margin))))
 (setq Xcoor2 (list (+ (* -0.5 SqW) Wb)))
 (setq Ycoor2 (list (+ (* -0.5 SqW) (+ Wb G margin W))))
 (setq i 2)
 (setq exit 0)
 (while (= exit 0)

  (cond ((= (* 0.5 (fix (* 0.5 i))) (fix (* 0.5 (fix (* 0.5 i))))) (setq signx -1))
        (t (setq signx 1))
  )
  (cond ((= (* 0.5 (fix (* 0.5 (+ i 1)))) (fix (* 0.5 (fix (* 0.5 (+ i 1)))))) (setq signy 1))
        (t (setq signy -1))
  )

  (setq ScaleX (* (fix (* 0.5 i)) (* 0.5 springno)))
  (setq ScaleY (- (* springno (* 0.5 (fix (* 0.5 (+ i 1))))) (fix (* springno 0.25))))
  (setq x (* signx (- (* 0.5 SqW) (+ Wb margin (* ScaleX G) (* (- ScaleX 1) W)))))
  (setq y (* signy (- (* 0.5 SqW) (+ Wb margin (* ScaleY G) (* (- ScaleY 1) W)))))
  (setq x2 (* signx (- (* 0.5 SqW) (+ Wb margin (* ScaleX G) (* ScaleX W)))))
  (setq y2 (* signy (- (* 0.5 SqW) (+ Wb margin (* ScaleY G) (* ScaleY W)))))
```

```
(cond ((< (abs x2) (+ (* 0.5 Wm) G))
        (progn (setq x (* signy (* -0.5 W)))
               (setq x2 (* signy (* 0.5 W)))
               (setq Xcoor (append Xcoor (list x)))
               (setq Ycoor (append Ycoor (list y)))
               (setq Xcoor2 (append (list x2) Xcoor2))
               (setq Ycoor2 (append (list y2) Ycoor2))
               (setq y 0)
               (setq y2 0)
               (setq exit 1)
        )
       )
       ((< (abs y2) (+ (* 0.5 Wm) G))
        (progn (setq y (* signx (* 0.5 W)))
               (setq y2 (* signx (* -0.5 W)))
               (setq Xcoor (append Xcoor (list x)))
               (setq Ycoor (append Ycoor (list y)))
               (setq Xcoor2 (append (list x2) Xcoor2))
               (setq Ycoor2 (append (list y2) Ycoor2))
               (setq x 0)
               (setq x2 0)
               (setq exit 1)
        )
       )
)

  (setq Xcoor (append Xcoor (list x)))
  (setq Ycoor (append Ycoor (list y)))
  (setq Xcoor2 (append (list x2) Xcoor2))
  (setq Ycoor2 (append (list y2) Ycoor2))

 (setq i (+ i 1))
)
(setq ptno (* 2 i))

(setq Xcoor (append Xcoor Xcoor2))
(setq Ycoor (append Ycoor Ycoor2))

(command "pline")
(setq i 0)
(repeat ptno
 (command (strcat (rtos (nth i Xcoor)) "," (rtos (nth i Ycoor))))
 (setq i (+ i 1))
)
(command "c")

(command "extrude" (entlast) "" (rtos H) "0")
(command "move" (entlast) "" (strcat "0,0," (rtos (* -0.5 H))) "")
(setq solid2 (list (entlast)))

(repeat (- springno 1)
 (command "copy" (entlast) "" "0,0" "")
 (command "rotate" (entlast) "" "0,0" (rtos (/ 360 springno)))
 (setq solid2 (append solid2 (list (entlast))))
)

(command "box" "c" "0,0,0" "I" (rtos Wm) (rtos Wm) (rtos Hm))
(command "union" solid1 (entlast))
```

```
(setq i 0)
(repeat springno
  (command (nth i solid2))
  (setq i (+ i 1))
)
(command "")

(setq i 0)
(setq TLength 0)
(repeat (- ptno 1)
  (setq x (- (nth (+ i 1) Xcoor) (nth i Xcoor)))
  (setq y (- (nth (+ i 1) Ycoor) (nth i Ycoor)))
  (setq TLength (+ TLength (sqrt (+ (* x x) (* y y)))))
  (setq i (+ i 1))
)
(print "Total length of all springs:")
(setq TLength (* 0.5 springno (- (- TLength W) Wm)))

)
```

APPENDIX C(III): *AutoLISP* Program – Circular Spiral Spring

```
; Autolisp program to draw a circular 3D spiral micro generator CAD model
; by Gordon Chan, 1999

(defun spiral()

; ---------------------- Input parameters ----------------------

 (setq SpgNum 2)                          ; Number of springs
 (setq Frame_OutRad 10)                   ; Outer radius of frame (mm)
 (setq Frame_Wid 0.5)                     ; Frame width (mm)
 (setq Frame_Thk 0.5)                     ; Frame thickness (mm)
 (setq Mag_Wid 3)                         ; Center mass width (mm)
 (setq Mag_Thk 3)                         ; Center mass thickness (mm)
 (setq Mag_Rad (* 0.707106781 Mag_Wid)); Center mass support radius (mm)
 (setq Spg_Wid 0.5)                       ; Spring width (mm)
 (setq Spg_Thk 0.5)                       ; Spring thickness (mm)
 (setq Gap 1)                             ; Gap between springs (mm)
 (setq AngVel (/ (* 2 pi) 120))           ; Angular velocity (rad/time) - Small value gives
fine model

; ------------------------ Porgram start ------------------------

; Create solid frame - solid1
 (command "circle" "0,0" (rtos Frame_OutRad))
 (command "extrude" (entlast) "" (rtos Frame_Thk) "0")
 (setq solid1 (entlast))
 (command "circle" "0,0" (rtos (- Frame_OutRad Frame_Wid)))
 (command "extrude" (entlast) "" (rtos Frame_Thk) "0")
 (command "subtract" solid1 "" (entlast) "")
 (command "move" (entlast) "" (strcat "0,0," (rtos (* -0.5 Frame_Thk))) "")
 (setq solid1 (entlast))

; Create solid mass support - solid2
 (command "circle" "0,0" (rtos Mag_Rad))
 (command "extrude" (entlast) "" (rtos Spg_Thk) "0")
 (command "move" (entlast) "" (strcat "0,0," (rtos (* -0.5 Spg_Thk))) "")
 (setq solid2 (entlast))

; Create solid mass - solid3
 (command "box" "c" (strcat "0,0," (rtos (* 0.5 (+ Mag_Thk Spg_Thk)))) "l" (rtos Mag_Wid)
(rtos Mag_Wid) (rtos Mag_Thk))
 (setq solid3 (entlast))

; Create solid springs - solid4
 (setq n 0)                               ; Set index for SpgNum
 (setq solid4 '())
 (setq Outer_Spring_Length 0)             ; Outer length of one spring
 (setq Inner_Spring_Length 0)             ; Inner length of one spring
 (repeat SpgNum                           ; Repeat each spring
```

```
  (setq ti 0)                                   ; Set initial time index

  (command "pline")
  (while (>= (setq R (- (+ (- Frame_OutRad Frame_Wid) Spg_Wid) (/ (* ti (* SpgNum AngVel
(+ Spg_Wid Gap))) (* 2 pi)))) Spg_Wid)
    (setq ang (+ (* AngVel ti) (/ (* 2 n pi) SpgNum)))
    (setq x (* R (cos ang)))
    (setq y (* R (sin ang)))

; Calculate outer spring length
    (cond ((= n 0)
           (progn (cond ((and (> ti 0) (<= R (- Frame_OutRad Frame_Wid)) (>= R (+
Mag_Rad Spg_Wid)))
                        (progn (setq x_dis (- x x_pre))
                               (setq y_dis (- y y_pre))
                               (setq pt_dis (sqrt (+ (* x_dis x_dis) (* y_dis y_dis))))
                               (setq Outer_Spring_Length (+ Outer_Spring_Length
pt_dis))
                        )
                       )
                 )
                 (setq x_pre x)
                 (setq y_pre y)
           )
          )
    )

    (command (strcat (rtos x) "," (rtos y)))
    (setq ti (+ ti 1))
  )

  (setq ti (- ti 1))
  (while (>= ti 0)
    (setq ang (+ (* AngVel ti) (/ (* 2 n pi) SpgNum)))
    (setq R (- (- Frame_OutRad Frame_Wid) (/ (* ti (* SpgNum AngVel (+ Spg_Wid Gap))) (* 2
pi))))
    (setq x (* R (cos ang)))
    (setq y (* R (sin ang)))

; Calculate inner spring length
    (cond ((= n 0)
           (progn (cond ((and (> ti 0) (<= R (- Frame_OutRad Frame_Wid Spg_Wid)) (>= R
Mag_Rad))
                        (progn (setq x_dis (- x x_pre))
                               (setq y_dis (- y y_pre))
                               (setq pt_dis (sqrt (+ (* x_dis x_dis) (* y_dis y_dis))))
                               (setq Inner_Spring_Length (+ Inner_Spring_Length
pt_dis))
                        )
                       )
                 )
                 (setq x_pre x)
                 (setq y_pre y)
           )
          )
    )

    (command (strcat (rtos x) "," (rtos y)))
```

```
    (setq ti (- ti 1))
   )

   (command "c")

   (command "extrude" (entlast) "" (rtos Spg_Thk) "0")
   (command "move" (entlast) "" (strcat "0,0," (rtos (* -0.5 Spg_Thk))) "")
   (setq solid4 (append solid4 (list (entlast))))
   (setq n (+ n 1))
  )

  (command "union" solid1 solid2 solid3)     ; Union all solids
  (setq i 0)
  (repeat SpgNum
   (command (nth i solid4))
   (setq i (+ i 1))
  )
  (command "")

 ; Print output
  (print "Outer length of one spring:")
  (print Outer_Spring_Length)
  (print "Inner length of one spring:")
  (print Inner_Spring_Length)
  (print "Average length of one spring:")
  (print (setq Spring_Length (* 0.5 (+ Outer_Spring_Length Inner_Spring_Length))))
  (print "Total length of all springs:")
  (setq Total_Springs_Length (* SpgNum Spring_Length))

 )
```

APPENDIX D: *ANSYS* Program – FEA of Generator With Spiral Springs

```
! ANSYS 5.5 command file to draw a 3D spiral micro generator
! by Gordon Chan, 2000

/FILNAME, MicroGen                    ! Set jobname and title
/TITLE, Model of Micro Generator
/UNITS, SI                            ! Set SI unit
*AFUN, DEG                            ! Set unit for angular functions
/PLOPTS, LEG2, OFF

! ---------- System constants ----------

pi=3.14159265358979323846264338327795      ! Pi
K_Idx=20000                           ! Starting keypoint number - Can be any large
number. No effect on result
L_Idx=20000                           ! Starting line number - Can be any large number.
No effect on result

! ---------- Input parameters ----------

! Geometry
SpgNum=2                              ! Number of springs
Frm_InR=4.5E-3                        ! Inner radius of frame (mm)
Mass_Wid=3E-3                         ! Center mass width (mm)
Mass_Thk=3E-3                         ! Center mass thickness (mm)
Spg_Wid=0.1E-3                        ! Spring width (mm)
Spg_Thk=0.11E-3                       ! Spring thickness (mm)
Gap=0.5E-3                            ! Gap between springs (mm)
AngVel=2*pi/100                       ! Angular velocity (rad/time) - Small value gives
fine model

! Material properties
Mass_Ex=207E9                         ! Young's modulus of magnet (Pa)
Mass_Nu=0.28                          ! Poisson's ratio of magnet
Mass_Den=8120                         ! Density of magnet (kg/m^3)
Spg_Ex=110E9                          ! Young's modulus of springs (Pa)
Spg_Nu=0.35                           ! Poisson's ratio of springs
Spg_Den=8960                          ! Density of springs (kg/m^3)
Spg_ShrZ=1.2                          ! Shear deflection constant Z
Spg_ShrY=1.2                          ! shear deflection constant Y
Shl_EFS=0                             ! Elastic foundation stiffness of mass support
Shl_RMI=1                             ! Bending moment of inertia ratio of mass support

! Input parameters
! Either F_Max or Disp_Max is used only. F_Max=0 => Disp_Max is used. Disp_Max=0 =>
F_Max is used.
F_Max=0.1                             ! Magnitude of applied force (N)
Disp_Max=0                            ! Magnitude of applied displacement (m)
Damp_Rat=0.01                         ! Damping ratio
```

```
! Control parameters
Mode_Num=10                          ! Number of modes to expand in modal analysis
InFrqMin=0                           ! Starting value of input frequency (Hz) in
harmonic analysis
InFrqMax=350                         ! Ending value of input frequency (Hz) in harmonic
analysis
NSbMin=20                            ! Minimum number of frequency data sampled in
harmonic analysis
NSbMax=30                            ! Maximum number of frequency data sampled in
harmonic analysis

! ------------------------ Porgram start ------------------------

/PREP7

Mass_Rad=Mass_Wid/2**0.5             ! Center mass support radius
t_0=2*pi*Spg_Wid/(SpgNum*AngVel*(Spg_Wid+Gap))      ! Set initial time
t_End=2*pi*(Frm_InR-Mass_Rad)/(SpgNum*AngVel*(Spg_Wid+Gap)) ! Set end time
L_Num=NINT(t_End-t_0)                ! Total number of line segments in one spring
t_Period=(t_End-t_0)/L_Num           ! Length of one time period (time)

! ---------------------- Geometric Modeling ----------------------

! Geometric modeling of springs
*DO, i, 0, SpgNum-1, 1

 *DO, t, t_0, t_End, t_Period
  R=Frm_InR+0.5*Spg_Wid-t*SpgNum*AngVel*(Spg_Wid+Gap)/(2*pi) ! Distance between
spring and origin at time t
  ang=AngVel*t+2*i*pi/SpgNum
  x=R*COS(ang*180/pi)
  y=R*SIN(ang*180/pi)
  K,, x, y, 0                        ! Create keypoints of springs
 *ENDDO

 *DO, t, 1, L_Num, 1
  LSTR, t+i*(L_Num+1), t+1+i*(L_Num+1) ! Create lines of springs
 *ENDDO

*ENDDO

! Measure spring length
Spg_Leng=0                           ! Average length of one spring
*DO, i, 1, L_Num, 1
 *GET, L_Temp, LINE, i, LENG         ! Get length of one line segment in spring
 Spg_Leng=Spg_Leng+L_Temp
*ENDDO
T_Spg_L=Spg_Leng*SpgNum              ! Total length of all springs

NUMSTR, KP, K_Idx                    ! Set starting number of keypoints
K, K_Idx, 0, 0, 0                    ! Define center keypoint
NUMSTR, LINE, L_Idx                  ! Set starting number of lines

! Geometric modeling of mass support
*IF, SpgNum, EQ, 1, THEN             ! Case: One spring
 K, L_Num+2, -KX(L_Num+1), -KY(L_Num+1), 0
 K, K_Idx+1, KY(L_Num+1)-KY(L_Num+2), KX(L_Num+2)-KX(L_Num+1), 0 ! Create temp
reference keypoints
```

```
 K, K_Idx+2, KY(L_Num+2)-KY(L_Num+1), KX(L_Num+1)-KX(L_Num+2), 0
 LARC, L_Num+1, L_Num+2, K_Idx+1, Mass_Rad+0.5*Spg_Wid
 LARC, L_Num+1, L_Num+2, K_Idx+2, Mass_Rad+0.5*Spg_Wid
 KDELE, K_Idx+1                          ! Delete temp reference keypoints
 KDELE, K_Idx+2
 LSEL, S,,, L_Idx, L_Idx+1

*ELSEIF, SpgNum, EQ, 2, THEN             ! Case: Two springs
 K, K_Idx+1, KY(L_Num+1)-KY(2*L_Num+2), KX(2*L_Num+2)-KX(L_Num+1), 0 ! Create
temp reference keypoints
 K, K_Idx+2, KY(2*L_Num+2)-KY(L_Num+1), KX(L_Num+1)-KX(2*L_Num+2), 0
 LARC, L_Num+1, 2*L_Num+2, K_Idx+1, Mass_Rad+0.5*Spg_Wid
 LARC, 2*L_Num+2, L_Num+1, K_Idx+2, Mass_Rad+0.5*Spg_Wid
 KDELE, K_Idx+1                          ! Delete temp reference keypoints
 KDELE, K_Idx+2
 LSEL, S,,, L_Idx, L_Idx+1

*ELSE                                    ! Case: Three springs or more
 LSEL, NONE
 *DO, i, 0, SpgNum-1, 1
  *IF, i, EQ, SpgNum-1, THEN
   K_Temp=L_Num+1
  *ELSE
   K_Temp=(i+2)*(L_Num+1)
  *ENDIF
  LARC, (i+1)*(L_Num+1), K_Temp, K_Idx, Mass_Rad+0.5*Spg_Wid
 *ENDDO
*ENDIF

NUMSTR, AREA, 3                          ! Set starting number of areas
AL, ALL                                  ! Create area of mass support

! Geometric modeling of mass
NUMSTR, AREA, 2                          ! Set starting number of areas
BLC5, 0, 0, Mass_Wid, Mass_Wid
NUMSTR, AREA, 1                          ! Set starting number of areas
AOVLAP, ALL
VEXT, 2,,,,, Mass_Thk                    ! Create volume of mass

! Free memory
ang=
AngVel=
i=
K_Temp=
L_Idx=
L_Temp=
pi=
R=
t=
t_0=
t_End=
t_Period=
x=
y=

! ------------------- Finite Element Modeling --------------------

! Define elements, real constants and material properties
```

```
ET, 1, BEAM4, , 0, , , , 0, 0, , 0, 0          ! Define beam element for springs
ET, 2, SOLID73                                 ! Define solid element for magnet
ET, 3, SHELL63, 0, 0, 0, , 0, 2, 0, 0, 0       ! Define shell element for mass support

UIMP, 1, EX, NUXY, DENS, Spg_Ex, Spg_Nu, Spg_Den    ! Define material properties for
springs
UIMP, 2, EX, NUXY, DENS, Mass_Ex, Mass_Nu, Mass_Den      ! Define material properties
for magnet

! Define real constants for springs: AREA, IZZ, IYY, TKZ, TKY, THETA, , , , , , ADDMAS
Spg_Area=Spg_Wid*Spg_Thk                ! Cross section area of springs
Spg_Izz=Spg_Thk*(Spg_Wid**3)/12         ! Izz of springs
Spg_Iyy=Spg_Wid*(Spg_Thk**3)/12         ! Iyy of springs
R, 1, Spg_Area, Spg_Izz, Spg_Iyy, Spg_Thk, Spg_Wid, 0
RMORE, , Spg_Izz+Spg_Iyy, Spg_ShrZ, Spg_ShrY
! Define real constants for mass support
R, 3, Spg_Thk, Spg_Thk, Spg_Thk, Spg_Thk, Shl_EFS,0
RMORE, Shl_RMI

! Finite element modeling
MOPT, LSMO, ON                          ! Smooth line
MOPT, TIMP, 5                           ! Tet improvement in VMESH
MSHKEY, 0                               ! Free meshing
MSHAPE, 1, 3D                           ! Element shape to be used
MSHMID, 0                               ! Midside node
SMRTSIZE, 1                             ! Smart sizing

ALLSEL

! Mesh springs
ESIZE, 1E-2                             ! Set smaller element size
TYPE, 1
MAT, 1
REAL, 1
LMESH, 1, L_Num*SpgNum, 1
ESEL, S, MAT, , 1
CM, Springs, ELEM                       ! Create springs component
ALLSEL

! Mesh mass support
TYPE, 3
MAT, 1
REAL, 3
AMESH, 1, 1, 1
ESEL, S, TYPE, , 3
CM, Plane, ELEM                         ! Create mass support component
ALLSEL

! Mesh magnet
HPTCREATE, AREA, 3, , COORD, 0, 0, Mass_Thk    ! Create hard point on magnet
TYPE, 2
MAT, 2
VMESH, 1
ESEL, S, MAT, , 2
CM, Magnet, ELEM                        ! Create magnet component
ALLSEL

*GET, Node_Num, NODE, , COUNT           ! Total number of nodes
```

```
*GET, Ele_Num, ELEM, , COUNT          ! Total number of elements

KSEL, S, HPT, , K_Idx+9
NSLK, S
*GET, Node_Ct, NODE, , NUM, MIN       ! Store node number at top center of magnet
ALLSEL

FINISH
SAVE

! ------------------ Structural Static Analysis --------------------

/FILNAME, StatGen                     ! Set jobname and title
/TITLE, Structural Static Analysis of Micro Generator

! Begin solution
/SOLU
ANTYPE, STATIC, NEW                   ! Static analysis
EQSLV, ITER, 5,                       ! Equation solver

! Apply boundary conditions
*DO, i, 0, SpgNum-1, 1
 DK, (L_Num+1)*i+1, ALL, 0, , 0       ! Fix end points of springs
*ENDDO

! Apply load
*IF, Disp_Max, EQ, 0, THEN
 FK, K_Idx+9, FZ, -F_Max              ! Apply force on magnet
*ELSE
 DK, K_Idx+9, UZ, -Disp_Max           ! Apply displacement on magnet
*ENDIF

! Restrict bending at contact point between mass support and springs
*IF, SpgNum, EQ, 1, THEN              ! Case: One spring
 DK, L_Num+1, ROTX, 0, , , ROTY, ROTZ
*ELSEIF, SpgNum, EQ, 2, THEN         ! Case: Two springs
 DK, L_Num+1, ROTX, 0, , , ROTY, ROTZ
 DK, 2*L_Num+2, ROTX, 0, , , ROTY, ROTZ
*ELSE                                 ! Case: Three springs or more
 *DO, i, 1, SpgNum, 1
 DK, i*(L_Num+1), ROTX, 0, , , ROTY, ROTZ
 *ENDDO
*ENDIF

SOLCONTROL, ON
SOLVE                                 ! Begin solving

! Free memory
i=
L_Num=

! Review results
/POST1
SET, FIRST                            ! Read results

*IF, Disp_Max, EQ, 0, THEN
 *GET, CtNod_UZ, NODE, Node_Ct, U, Z  ! Store value of vertical displacement of magnet
(m)
```

```
 Spg_Con=-F_Max/CtNod_UZ                ! Calculate spring constant (N/m)
*ELSE
 *GET, CtNod_FZ, NODE, Node_Ct, RF, FZ      ! Store value of vertical reactive force at
magnet (N)
 Spg_Con=-CtNod_FZ/Disp_Max             ! Calculate spring constant (N/m)
*ENDIF

NSORT, U, Z, 1, 0                       ! Sort nodal data
/OUTPUT, Spiral_S, txt                  ! Redirect output to file
*STATUS
PRNSOL, U, Z                            ! Print vertical displacement
PRESOL, ELEM                            ! Print element results
/OUTPUT                                 ! Redirect output to screen

FINISH
SAVE
```

BIBLIOGRAPHY

[1] C. B. Williams and R. B. Yates, *Analysis of Micro-Electric Generator for Microsystems*, Sensors and Actuators A 52, pp. 8-11, 1996.

[2] C. B. Williams, R. C. Woods and R. B. Yates, *Feasibility Study of a Vibration Powered Micro-Electric Generator*, IEE, 1996.

[3] C. Shearwood and R. B. Yates, *Development of an Electromagnetic Micro-generator*, Electronics Letters, vol. 33, nos. 22, pp. 1883-1884, Oct. 1997.

[4] R. Amirtharajah and A. P. Chandrakasan, *Self-Powered Signal Processing Using Vibration-Based Power Generator*, IEEE Journal of Solid-State Circuits, vol. 33, no. 5, pp. 687-695, 1998.

[5] R. Amirtharajah and A. Chandrakasan, *Self-Powered Low Power Signal Processing*, Symposium on VLSI Circuits, Digest of Technical Papers, 1997.

[6] H. Matsuki *et al.*, Implantable Transformer for an Artificial Heart Utilizing Amorphous Magnetic Fibers, J. App. Phys., vol. 64, pp. 5859-5861, 1988.

[7] J. J. Kiely, D. V. Morgan, D. M. Rowe and J. M. Humphrey, *Low Cost Miniature Thermoelectric Generator*, Electron. Lett., vol. 27, no. 25, pp. 2332-2334, 1991.

[8] B. Rashidian and M. G. Allen, Electrothermal Microactuators Based on Dielectric Loss Heating, Proc. 6th IEEE Workshop on MEMS, Feb. 1993, pp. 24-29.

[9] J. B. Bates, G. R. Gruzalski and C. F. Luck, *Rechargeable Solid State Lithium Microbatteries*, Proc. 6th IEEE Workshop on MEMS, Feb. 1993, pp. 82-86.

[10] J. B. Lee, Z. Chen, M. G. Allen, A. Rohatgi and R. Arya, *A High Voltage Solar Cell Array As An Electrostatic MEMS Power Supply*, IEEE, 1994.

[11] J. B. Lee, Z. Chen, M. G. Allen, A. Rohatgi and R. Arya, *A Miniaturized High-Voltage Solar Cell Array As An Electrostatic MEMS Power Supply*, Journal of MEMS, vol. 4, no. 3, pp. 102-108, Sept. 1995.

[12] P. B. Koeneman, I. J. Busch-Vishniac and K. L. Wood, *Feasibility of Micro Power Supplies for MEMS*, J. of MEMS, vol. 6, no. 4, 1997.

[13] L. A. Geddes, *Historical Highlights in Cardiac Pacing*, IEEE Eng. Med. Biol., pp. 12-18, 1990.

[14] D. Friedman, H. Heinreich and D. W. Duan, *A Low-Power CMOS Integrated Circuit For Field-Powered Radio Frequency Identification Tags*, ISSCC 1997 Dig. Tech. Papers, pp. 294-295, 1997.

[15] J. Bouvier, Y. Thorigne, S. Abou Hassan, M. J. Revillet and P. Senn, *A Smart Card CMOS Circuit With Magnetic Power And Communications Interface*, ISSCC 1997 Dig. Tech. Papers, pp. 296-297, 1997.

[16] M. Hayakawa, *Electronic Wristwatch With Generator*, US Patent 5 001 685, Mar. 1991.

[17] T. Starner, *Human Powered Wearable Computing*, IBM Syst. J., vol. 35, nos. 3/4, pp. 618-629, 1996.

[18] Kozuka, T., *et al.*, *Acoustic Manipulation of Micro Objects Using an Ultrasonic Standing Wave*, Proc. Fifth Int. Symp. On Micro Machine and Human Science (MHS '94), pp. 83-97, 1994.

[19] P. Fung, P. Sun and K. Young, *Further Physics*, vol. 2, 2nd ed., Longman Group (Far East) Ltd., 1993.

[20] R. C. Dorf and R. H. Bishop, *Modern Control Systems*, 7th ed., Addison-Wesley Publishing Co., 1995.